Astron Astrophys Rev (2017) 25:5
https://doi.org/10.1007/s00159-017-0104-7

REVIEW ARTICLE

The Main Belt Comets and ice in the Solar System

Colin Snodgrass[1] · Jessica Agarwal[2] · Michael Combi[3] · Alan Fitzsimmons[4] · Aurelie Guilbert-Lepoutre[5] · Henry H. Hsieh[6,7] · Man-To Hui[8] · Emmanuel Jehin[9] · Michael S. P. Kelley[10] · Matthew M. Knight[10] · Cyrielle Opitom[11] · Roberto Orosei[12] · Miguel de Val-Borro[13] · Bin Yang[11]

Received: 19 June 2017 / Published online: 14 November 2017

Abstract We review the evidence for buried ice in the asteroid belt; specifically the questions around the so-called Main Belt Comets (MBCs). We summarise the evidence for water throughout the Solar System, and describe the various methods for detecting it, including remote sensing from ultraviolet to radio wavelengths. We review progress in the first decade of study of MBCs, including observations, modelling of ice survival, and discussion on their origins. We then look at which methods will likely be most effective for further progress, including the key challenge of direct detection of (escaping) water in these bodies.

✉ Colin Snodgrass
colin.snodgrass@open.ac.uk

1 School of Physical Sciences, The Open University, Milton Keynes MK7 6AA, UK

2 Max-Planck-Institut für Sonnensystemforschung, Göttingen, Germany

3 University of Michigan, Ann Arbor, USA

4 Queen's University Belfast, Belfast, UK

5 CNRS/UTINAM-UMR 6213 UBFC, Besançon, France

6 Planetary Science Institute, Tucson, USA

7 Academia Sinica, Taipei, Taiwan

8 University of California Los Angeles, Los Angeles, USA

9 Universite de Liege, Liège, Belgium

10 University of Maryland, College Park, USA

11 European Southern Observatory, Santiago, Chile

12 Istituto di Radioastronomia, Istituto Nazionale di Astrofisica, Bologna, Italy

13 NASA Goddard Space Flight Center, Greenbelt, USA

Keywords Comets: general · Minor planets · Asteroids: general · Methods: observational

1 Introduction

The traditional view of our Solar System neatly divides it into the inner part, home of the terrestrial planets and rocky asteroids, and the outer region of the gas giants and icy small bodies. These are separated by the 'snow line', which marks the distance from the Sun where the ambient temperature allows icy bodies to form and survive. In this picture, the terrestrial planets formed 'dry', as only rocky material condensed from the solar nebula in the inner regions, while the outer planets became giants due to the fast formation of icy cores, followed by the runaway accretion of the abundant gas further from the young Sun. Earth's water was then delivered by occasional impacts of comets, whose eccentric orbits brought ice from their distant parent regions to the terrestrial planet region.

Despite the pleasing simplicity of this model, there are a number of awkward problems: the samples of asteroids that we have on Earth, meteorites, show a variety of compositions, including aqueously altered minerals which must have formed in the presence of water, incompatible with asteroids being entirely dry rocks (e.g., Brearley and Jones 1998). On the other hand, results from the Stardust mission showed that comet dust contains minerals formed at high temperature, presumably near to the Sun (Brownlee et al. 2006). Meanwhile, many extrasolar systems with gas giant planets close to their stars have been discovered, presenting a challenge to formation models (e.g., Mayor and Queloz 1995; Winn and Fabrycky 2015). Finally, recent observations have uncovered evidence of ice in unexpected places in the inner Solar System, including the population of 'Main-Belt Comets' (MBCs) which have stable asteroid-like orbits, inside the snow line, but which demonstrate comet-like activity (Hsieh and Jewitt 2006).

The solution comes from the recognition that planetary systems are dynamic places, with the orbits of even the largest planets able to evolve and migrate, especially in the early period when interaction between forming planets and the protoplanetary disc is strong. Numerical models that trace how planetary orbits interact and change can explain the migration of planets to Hot Jupiter orbits (e.g., Trilling et al. 1998). More importantly, for studies of our own Solar System, these models also reveal the way that such planetary migrations stir up the population of small bodies. They can therefore be tested, by comparing their outcomes with the observed architecture of the Solar System—not only the present-day orbits of the planets, but also the orbits and different properties of various populations of comets and asteroids. For example, the 'Nice model' (Gomes et al. 2005) is able to reconstruct the architecture of the trans-Neptunian region, possibly implant trans-Neptunian objects in the main asteroid belt (Levison et al. 2009), and explain the increased impact rate on the Moon during the Late Heavy Bombardment period, via the gravitational effect of Uranus and Neptune interacting. The latest family of models, known as the 'Grand Tack' (Walsh et al. 2011), uses Jupiter and Saturn migrating first inwards and then 'tacking' outwards to

explain the relatively small size of Mars and also to scatter both rocky and icy small bodies throughout the Solar System.

A common criticism of these dynamical models is that they are highly tunable and therefore lack predictive power—the input parameters can be arbitrarily adjusted until they produce a simulated Solar System that looks like our own. Increasing the number of independent constraints on these models, thus reducing the amount of available free parameter space, is therefore an important way to refine and improve them. For example, a recent analysis of meteoritic evidence (Doyle et al. 2015) appears to rule out the possibility that the parent bodies of carbonaceous chondrite meteorites (i.e., C-type asteroids) were formed beyond Jupiter, as suggested in the Grand Tack model, indicating that at least this feature of the model, if not the whole model itself, is inconsistent with the physical evidence. Study of the present-day distribution of icy bodies, particularly those containing water ice, is another way to provide such constraints on these models, which generally predict that icy bodies will be found everywhere, but differ in details such as abundance, distribution, and ratios relative to other materials (e.g., rocky components or other volatiles).

In this review, we look at the MBCs as a population of icy bodies. We consider them in the context of water and ice detections throughout the Solar System (Sect. 2), reviewing what is known about this population in general (Sect. 3) before considering the specific problems of modelling ice survival in their interiors (Sect. 4) and of directly studying this ice observationally (Sect. 5), including predictions for activity levels (Sect. 6). We also consider what the lessons learned about comets in general from Rosetta tell us about MBCs (Sect. 7) before discussing what future observations and missions will further advance this field (Sect. 8).

Previous reviews on the subject of MBCs cover the more general topic of 'active asteroids', including considering how non-icy bodies can eject dust and therefore exhibit comet-like appearances (Bertini 2011; Jewitt et al. 2015c). We briefly discuss this below, but concentrate on questions related to MBCs and ice in the Solar System. The topic of water in small bodies, and in the Solar System more generally, is also the subject of earlier reviews by Jewitt et al. (2007) and Encrenaz (2008), while Hartmann et al. (2017) consider the topic of water in extrasolar protoplanetary discs. Dones et al. (2015) give a recent review of the various cometary reservoirs in our Solar System from a dynamical point of view.

2 Ice in the Solar System

Water, usually in the form of ice, is found throughout the Solar System. Beyond Earth, it has long been recognised in the outer planets and comets, and is now also observed throughout the terrestrial planet region. Evidence for water is found with now almost monotonous regularity on Mars, but more surprisingly, ice has also been identified in permanently shadowed craters of Mercury (Lawrence et al. 2013) and the Moon (Colaprete et al. 2010). While these deposits could plausibly have been delivered by comet impacts in the geologically recent past, evidence for ice in smaller bodies is more difficult to attribute to an exogenous source.

2.1 Water in the planets

Radar mapping of Mercury suggested the presence of polar ice in 1991 (Slade et al. 1992; Harmon and Slade 1992). Thermal models show that in permanently shadowed regions of high-latitude craters, water ice covered by a regolith layer can be stable to evaporation over billions of years (Paige et al. 1992; Vasavada et al. 1999). The ice is thought to have been implanted by either constant micrometeoritic, asteroidal and cometary influx (Killen et al. 1997), or to stem from a few large impacts by comets and/or asteroids (Moses et al. 1999; Barlow et al. 1999). The MESSENGER spacecraft observed areas of high and low near-infrared (NIR) reflectivity, which is interpreted as surface ice and ice buried under a layer of organic material (Neumann et al. 2013; Paige et al. 2013). The total amount of polar water ice on Mercury is estimated to 3×10^{15} kg (Eke et al. 2017), equivalent to 300 comets the size of 67P/Churyumov-Gerasimenko[1] (Pätzold et al. 2016).

Water ice has also been hypothesised to exist on the Moon in permanently shadowed craters near the poles (Spudis et al. 2013; Hayne et al. 2015), although a debate about alternative interpretations of data is on-going (Eke et al. 2014; Haruyama et al. 2013). Hydroxyl- and/or water-bearing materials are widely spread across the lunar surface (Pieters et al. 2009).

On Venus, water has been found only in the form of atmospheric vapour in spurious quantities of the order of a few parts per million in the nitrogen- and CO_2-dominated atmosphere (Encrenaz 2008). The high deuterium-to-hydrogen (D/H) ratio (de Bergh et al. 1991) in the Venusian atmosphere is interpreted as an indication for an earlier escape of water to space from the upper atmosphere, which would be more efficient for the lighter isotope. The absence of water from the Venusian atmosphere has been connected to the strong greenhouse effect that makes the existence of ice or liquid water on Venus unlikely (Ingersoll 1969; Mueller 1970). The water vapour present in the current atmosphere may be re-supplied by chemical interaction with water-containing rocks (Mueller 1970) or could be provided by meteoritic and cometary infall (Lewis 1974).

The present-day Earth hosts abundant water in all three states of matter—solid (ice), liquid, and gas—due to a fortuitous combination of surface temperature and pressure. The origin and evolution of water on Earth (and on the other terrestrial planets) is a subject of ongoing research. Two key questions are (1) whether Earth incorporated a sufficient amount of water at the time of accretion to explain its present day water content ('wet accretion') or if the accreted material was depleted in volatiles due to the high temperature in the inner solar nebula ('dry accretion'), and (2) what fraction of the Earth's water was delivered later by exogenous sources, e.g., comet and asteroid impacts (Drake and Righter 2002). Comparing isotope ratios of volatiles in Earth, comets, asteroids, and meteorites, especially of the D/H ratio, can give us clues to answering these questions. However, it is not clear to what extent the D/H ratio in Vienna Standard Mean Ocean Water (VSMOW; the most commonly used standard isotopic reference for 'Earth water'—Balsiger et al. 1995) represents that of the early

[1] Hereafter 67P. We will give the name of comets only when they are first mentioned.

Earth. An increase of D/H by a factor 2–9 over the lifetime of the Earth due to mass fractionation during atmospheric loss is possible (Genda and Ikoma 2008), and the Earth's lower mantle (supposedly least affected by atmospheric processes) has a D/H ratio lower by up to 20% than VSMOW (Hallis et al. 2015). This places the Earth's D/H ratio between that of the protosolar nebula and that of comets from the outer Solar System (see, e.g., Saal et al. 2013; Altwegg et al. 2015 and references therein, and Sect. 4.1 below).

On Mars, water currently is present in the form of ice at the polar caps (Bibring et al. 2004; Langevin et al. 2005) and in craters (Armstrong et al. 2005; Brown et al. 2008), in a small amount of vapour in the atmosphere (Clancy et al. 1992), and embedded in hydrated minerals (Bibring et al. 2006). Liquid water may exist under specific conditions (Malin et al. 2006; Martín-Torres et al. 2015). There is strong geologic and mineralogic evidence that liquid water was more abundant on Mars in the past, when the atmosphere was thicker (Sagan et al. 1973; Lasue et al. 2013). Like on Venus, an elevated D/H ratio indicates that a significant amount of water vapour escaped to space from the atmosphere, affecting H_2O more than D_2O (Encrenaz et al. 2016). The original water content of Mars may have been sufficient to cover the planet with a layer of up to 1 km depth (Lasue et al. 2013). There is currently no evidence for the existence of water on the Martian moons, Phobos and Deimos (Rivkin et al. 2002).

Saturn and Jupiter contain water in liquid and solid form in their lower cloud layers (Niemann et al. 1998; Baines et al. 2009), but its abundance in these gas giants is not well known (Atreya and Wong 2005). Uranus and Neptune are thought to contain a large layer of ices, including H_2O, above a rocky core. Also their atmospheres contain H_2O (Podolak et al. 1995). The rings of the giant planets contain water ice at various fractions. While Saturn's rings consist mainly of water ice with a small admixture of organics and other contaminants (Nicholson et al. 2008), the rings of Jupiter, Uranus and Neptune contain at best a small fraction of water ice (Lane et al. 1989; Wong et al. 2006; de Kleer et al. 2013). Many of the moons of the outer planets and Pluto contain a significant fraction of water, with Tethys possibly consisting almost entirely of water ice (Thomas et al. 2007). Some, such as Jupiter's Europa and Saturn's Enceladus, are thought to contain a tidally heated global or local subsurface ocean of liquid water beneath the outer shell of ice (Carr et al. 1998; Manga and Wang 2007; Nimmo et al. 2007; Hansen et al. 2008).

2.2 Kuiper Belt objects, Centaurs and comets

Compared to the major planets in the Solar System, small icy bodies have experienced much less thermal evolution and their physical properties are well preserved. The Kuiper Belt objects (KBOs) are numerous small icy bodies beyond Neptune, which are thought to be the most primitive remnants from the early Solar System. As these objects were formed far beyond the 'snow line', volatile ices (especially water ice) are believed to be a principle constituent in KBOs. Optical and near-infrared spectroscopy is a widely used method to investigate surface properties as well as the chemical compositions of small bodies, although it is technically challenging to obtain spectral data on KBOs because of their great distance from the Sun and thus faintness. For

atmosphere-less bodies, evidence for water comes from solid-state absorption features in the spectrum of sunlight reflected from their surfaces (see Sect. 5). So far, spectra of KBOs fall into three categories, namely water-rich, methane-dominated and featureless ones (Trujillo et al. 2011). For example, water ice was detected on KBOs Quaoar and Haumea (including its satellites) with two strong absorption bands at 1.5 and 2.0 μm, respectively (Jewitt et al. 2004; Trujillo et al. 2007; Schaller and Brown 2008). Other large KBOs exhibit these bands as well as the absorption feature of crystalline ice at 1.65 μm, for example: Charon (Brown and Calvin 2000; Grundy et al. 2016), and Orcus (Barucci et al. 2008). Haumea's satellite Hi'iaka and collisional family members are also known to be covered by crystalline ice (Dumas et al. 2011; Schaller and Brown 2008; Snodgrass et al. 2010a; Carry et al. 2012). The spectra of Pluto, Eris and Makemake show a series of distinct bands of methane in the NIR (Grundy et al. 2016; Brown et al. 2005; Licandro et al. 2006). Some trace elements, i.e., ammonia and methanol, have been detected on mid-sized KBOs (Brown and Calvin 2000; Barucci et al. 2008, 2011). Compared to spectroscopic observations, Trujillo et al. (2011) showed that a new near-infrared photometric system is sensitive to water ice and methane ice while reducing telescope observing time by a factor of ~ 3. This system is particularly useful for surveying a large number of objects with moderate amount of telescope time.

According to Jewitt and Kalas (1998), Centaurs are defined as objects with perihelia $q > a_J$ ($a_J = 5.2$ au) and semimajor axes $a < a_N$ ($a_N = 30$ au). These objects are widely believed to be 'refugees' from the Kuiper belt (Levison and Duncan 1997), located on unstable orbits between Jupiter and Neptune with short dynamical lifetimes of about 10^6–10^7 years (Dones et al. 1999; Horner et al. 2004). Both optically blue and red members have been found among Centaurs (Tegler et al. 2008; Peixinho et al. 2012; Fraser and Brown 2012). (5145) Pholus is found to be one of the reddest objects observed to date in the Solar System (Fink et al. 1992; Davies et al. 1993), whose spectrum shows not only strong water ice bands, but also an absorption complex at 2.27 μm (Cruikshank et al. 1998). Dalle Ore et al. (2015) studied seven KBOs and three Centaurs that are among the reddest known. They conclude that these 'ultra-red' objects in general might contain methanol/hydrocarbon ices and their organic materials could have been produced by irradiation of the volatile ices. Jewitt et al. (2009) reported observations of a sample of 23 Centaurs and found nine to be active. They found that 'active Centaurs' in their sample have perihelia systematically smaller than the inactive ones. Centaurs have their perihelia beyond the water ice sublimation critical distance of ~ 5 au, which suggests that the comet-like activity of Centaurs is driven by a mechanism different from water ice sublimation. Therefore, the cometary activity might be powered by conversion of amorphous ice into the crystalline phase and the subsequent release of trapped gases, such as carbon monoxide and carbon dioxide (Jewitt et al. 2009). Thermal evolution models have been used to study the occurrence of crystallisation, the depth that the front would reach, and how it can contribute to Centaurs' activity for various orbits and obliquities (Fig. 1; Guilbert-Lepoutre 2012).

Comets generally have small, irregularly shaped nuclei that are composed of refractory materials (such as carbon, silicates, etc.) and icy grains (e.g., water ice, carbon dioxide ice and methanol ice). These objects may have experienced very little alter-

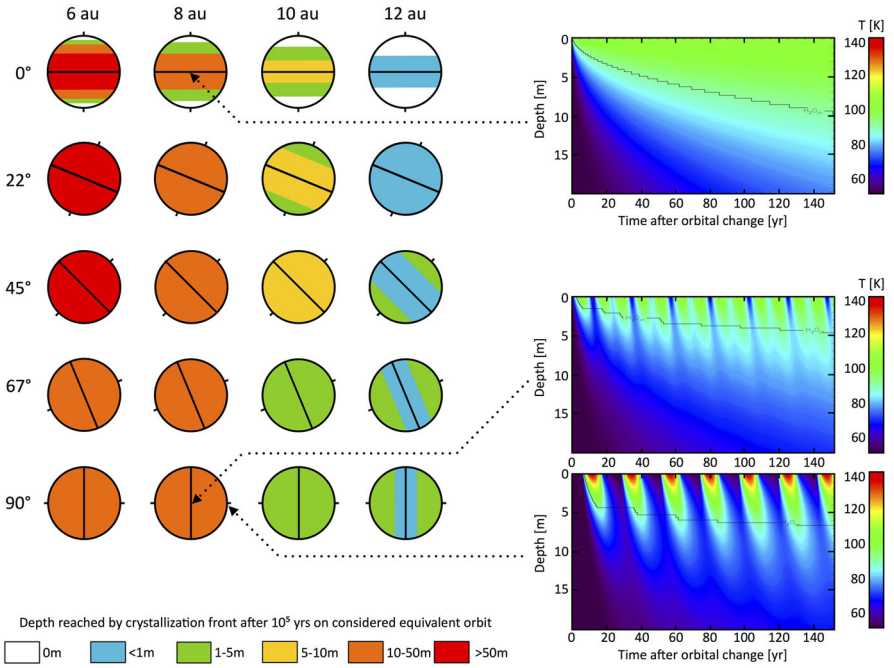

Fig. 1 Left: The depths where the crystallisation front stops for different (a_c = equivalent semimajor axis, obliquity) configurations, after 10^5 years. Note that crystallisation may not be complete above, in the subsurface layer. The rotation period is very small compared to all other time scales involved. Right: How the heat wave and crystallisation front progress in the subsurface layer for three cases (at 8 au and from top to bottom, under the equator at 0° obliquity, under the equator at 90° obliquity and under the pole at 90° obliquity), during the time the objects may be active ($\sim$ few 10^2 years after an orbital change labelled time = 0). Black line shows the crystallisation fronts. Image reproduced with permission from Guilbert-Lepoutre (2012), copyright by AAS

ation since their formation in the coldest regions of the young Solar System. As such, comets serve as the best probe for studying the physical conditions (e.g., temperature, pressure and composition) of the outer Solar nebula. However, direct detection of water ice in comets is surprisingly scarce. To date, solid ice features have only been observed in a handful of comets via ground-based facilities (Davies et al. 1997; Kawakita et al. 2004; Yang et al. 2009, 2014) and in situ observations (Sunshine et al. 2006; A'Hearn et al. 2012; Protopapa et al. 2014; De Sanctis et al. 2015). Knowledge of ices in comets mainly comes from spectroscopic observations of emission lines and bands from the gas coma, which are discussed in more detail in Sect. 5.

2.3 Evidence for water in asteroids

Although the asteroid belt could be an important source for Earth's water (Morbidelli et al. 2000), thermal models have shown that surfaces of most asteroids are too hot for water ice to remain stable against sublimation (see Schorghofer 2008 and Sect. 4). To

date, only a few detections of surface ice in asteroids have been reported. On the other hand, hydrated minerals have been widely observed in asteroids (Rivkin et al. 2015).

The largest body in the asteroid belt, (1) Ceres, contains significant water ice. Although its surface does not show signatures of water ice, the shape of Ceres was explained with a significant ice mantle (Thomas et al. 2005). Observations in the UV hinting at escaping water (A'Hearn and Feldman 1992) were confirmed in the sub-mm with detections with the Herschel space telescope (Küppers et al. 2014). Using nuclear spectroscopy data acquired by NASA's Dawn mission, Prettyman et al. (2017) analysed the elemental abundances of hydrogen, iron, and potassium on Ceres. They found that the regolith, at mid-to-high latitudes, contains high concentrations of hydrogen, consistent with broad expanses of water ice. The presence of ice in the largest asteroid has inspired debate about its origin, including suggestions that Ceres could have formed in the KBO region (McKinnon 2012), but there is growing evidence that it is not the only icy asteroid, and that smaller bodies also have ice.

In the $\sim$ 100 km diameter range, asteroid (24) Themis bears some significance in the debate of whether ice can originate from and survive in the Main Belt (MB), as water ice may have been detected at its surface (Campins et al. 2010; Rivkin and Emery 2010) via an absorption feature near 3 μm. We note that Themis was not found to be active by Jewitt and Guilbert-Lepoutre (2012), who suggested that if indeed present at its surface, water ice should be relatively clean and confined to a limited spatial extent, which was then confirmed by McKay et al. (2017). Jewitt and Guilbert-Lepoutre (2012) observed Themis far from perihelion, however, which as discussed in Sect. 6.1, may mean that the sublimation strength at the time was several orders of magnitude weaker than might be expected for Themis closer to perihelion. Many members of the Themis family show evidence for hydration (Florczak et al. 1999; Takir and Emery 2012), and the second largest member of the family after Themis itself—(90) Antiope—might have some surface water ice (Hargrove et al. 2015).

In a wider survey of large asteroids, Takir and Emery (2012) identified four 3 μm spectral and orbital groups, each of which is presumably linked to distinct surface mineralogy. Searches for water and OH features in near-Earth objects (NEOs) were upended by the discovery of OH in the lunar regolith by three spacecraft (Sunshine et al. 2009; Pieters et al. 2009; Clark 2009). Detections of water and/or hydroxyl on large asteroids have been reported for (175706) 1996 FG3 (Rivkin et al. 2015), (16) Psyche (Takir et al. 2017), and (433) Eros and (1036) Ganymede (Rivkin et al. 2017). Although smaller (km-scale) asteroids are generally too faint for spectroscopy in the 3 μm region, the activity of MBCs offers evidence that water is also present in at least some smaller asteroids.

3 The Main Belt Comets

3.1 Definitions: active asteroids and Main Belt Comets

An 'active' asteroid can be thought of as any body in an asteroidal (rather than cometary) orbit which is observed to lose mass, normally through the observation of a dust tail or trail. 'Asteroidal' orbits have Tisserand parameters (Kresak 1982;

Kosai 1992) with respect to Jupiter,

$$T_{\mathrm{J}} = \frac{a_{\mathrm{J}}}{a} + 2\sqrt{\frac{a(1-e^2)}{a_{\mathrm{J}}}}\cos(i) \geq 3.05, \quad (1)$$

and semimajor axes a less than that of Jupiter ($a_{\mathrm{J}} = 5.2$ au). Here a, e, and i are the semimajor axes (in au), eccentricity, and inclination (in degrees) of the orbit, respectively. Such orbits are distinct from comets (which have $T_{\mathrm{J}} < 3.0$; cf. Levison 1996). We use $T_{\mathrm{J}} = 3.05$ instead of $T_{\mathrm{J}} = 3.00$ because small drifts in T_{J} beyond 3.0 are possible due to non-gravitational forces or terrestrial planet interactions (e.g., Levison et al. 2006; Hsieh and Haghighipour 2016). Other authors (e.g., Jewitt et al. 2015c) have used $T_{\mathrm{J}} = 3.08$ as the boundary for similar reasons; the resulting list of MBC candidates is the same.

For the purposes of this paper, we use the term MBC to refer to an active asteroid that exhibits activity determined to likely be due to sublimation (e.g., from dust modelling results, or confirmation of recurrent activity near perihelion with intervening periods of inactivity). Various processes can be the source of mass loss for active asteroids in general, but repeated mass loss over several perihelion passages is most plausibly explained by sublimation. In addition, mass loss sustained over a prolonged period, although not unique to sublimation, can also be suggestive of ice sublimation since it is difficult to explain by a single impact, for example.

We are specifically not considering objects in the main asteroid belt whose cometary appearance has been shown to be due to mechanisms other than sublimation. These include debris released by impacts (either cratering events or catastrophic disruption)—e.g., (596) Scheila (Bodewits et al. 2011; Jewitt et al. 2011; Ishiguro et al. 2011a, b; Moreno et al. 2011b) and P/2012 F5 (Gibbs) (Stevenson et al. 2012; Moreno et al. 2012)—and rotational disruption—e.g., 311P (Jewitt et al. 2015b)—thought to be an outcome of YORP spin-up for small asteroids (Scheeres 2015). There are other hypothesised effects that have yet to be conclusively demonstrated to explain observed 'activity', such as thermal cracking, electrostatic levitation of dust, or radiation pressure accelerating dust away from the surface (Jewitt et al. 2015c). We also exclude dynamically asteroidal objects (i.e., with $T_{\mathrm{J}} > 3.05$) outside of the asteroid belt for which activity has been detected, e.g., (3200) Phaethon (Jewitt and Li 2010; Li and Jewitt 2013; Hui and Li 2017) and 107P/(4015) Wilson-Harrington (Fernandez et al. 1997). See Jewitt et al. (2015c) and references therein for more extensive discussion of active asteroids beyond our definition of 'MBC'. MBCs are of special interest within the broader class of active asteroids as they indicate the possible presence of water in bodies of a size that are very common in the asteroid belt, implying that there is potentially a large population of icy bodies there.

3.2 Discovery of MBCs

Since the discovery of 133P/Elst–Pizarro in 1996, the first recognised MBC, as of September 2017 ten more members have been detected. We summarise discovery circumstances of the currently known MBCs in Table 1. The discovery rate has increased

Table 1 MBC discovery circumstances

Object	Discovery date	Tel.[a]	m_V [b]	ν[c] (°)
133P/Elst–Pizarro	1996 Jul 14	ESO 1.0 m	18.3	21.6
238P/Read	2005 Oct 24	SW 0.9 m	20.2	26.4
176P/LINEAR	2005 Nov 26	GN 8.1 m	19.5	10.1
259P/Garradd	2008 Sep 2	SS 0.5 m	18.5	18.5
324P/La Sagra	2010 Sep 14	LS 0.45 m	18.3	20.1
288P/2006 VW_{139}	2011 Nov 5	PS1 1.8 m	18.7	30.7
P/2012 T1 (PANSTARRS)	2012 Oct 6	PS1 1.8 m	19.6	7.4
P/2013 R3 (Catalina-PANSTARRS)	2013 Sep 15	PS1 1.8 m	20.5	14.0
313P/Gibbs	2014 Sep 24	CSS 0.68 m	19.3	8.0
P/2015 X6 (PANSTARRS)	2015 Dec 7	PS1 1.8 m	20.7	328.9
P/2016 J1-A/B (PANSTARRS)	2016 May 5	PS1 1.8 m	21.4	345.9

[a] Discovery telescope: CSS 0.68 m: Catalina Sky Survey 0.68 m; ESO 1.0 m: European Southern Observatory 1.0 m; GN 8.1 m: Gemini-North 8.1 m; LS 0.45 m: La Sagra 0.45 m; PS1: Pan-STARRS1 1.8 m; SS 0.5 m: Siding Spring 0.5 m; SW 0.9 m: Spacewatch 0.9 m
[b] Approximate mean reported V-band magnitude at time of discovery
[c] True anomaly in degrees at time of discovery

significantly since 133P was discovered, thanks to wide-field sky surveys, especially those designed to find transients or NEOs. Two new MBCs have been added to the list since the review by Jewitt et al. (2015c): P/2015 X6 (PANSTARRS), and P/2016 J1 (PANSTARRS), both discovered by the Pan-STARRS survey at Haleakala, Hawaii. P/2016 J1 is particularly interesting as it was observed to split into two pieces (Hui et al. 2017; Moreno et al. 2017), and its current activity perhaps was triggered by a small impact, whereby formerly buried ice started sublimating and the torque rapidly drove the parent to fragment (Hui et al. 2017). It reinforces the idea that rotational instability is one of the important fates that comets may suffer, especially for those sub-kilometre sized. In addition to sky surveys such as Pan-STARRS, there have been attempts to search for MBCs with targeted observations of known asteroids in main-belt orbits to search for activity (Hsieh 2009), and in archival data from the Canada–France–Hawaii Telescope (Gilbert and Wiegert 2009, 2010; Sonnett et al. 2011) and the Palomar Transient Factory (Waszczak et al. 2013). Recently, a citizen science project[2] to crowd source the visual identification of MBCs has been employed in the search (Hsieh et al. 2016; Schwamb et al. 2017). To date none of these targeted searches have discovered any MBCs.

3.3 Population estimates

Based on Pan-STARRS1 discovery statistics, on the order of ∼ 50–150 currently active MBCs comparable in brightness to the known MBCs are expected to exist (Hsieh et al.

[2] http://www.comethunters.org.

2015a), where their respective individual activity strengths will depend on their orbit positions at the time of observation. We have not yet found them all as they need to be both active (which they are for only a few months of a 5–6 years orbit) and well placed for observations by surveys at the same time. While the pace of MBC discoveries has accelerated somewhat relative to the past to roughly one per year since the start of the Pan-STARRS1 survey (Table 1), an even higher rate of discoveries will be necessary to increase the known population to the point at which it can be meaningfully statistically analysed.

Assuming that we have mostly been discovering the brightest members of the MBC population, increasing the discovery rate will most likely require increasing the sensitivity of search efforts, to find similar MBCs at less optimal observing geometries, or to sample the population of intrinsically fainter targets with lower activity levels, which are presumably more numerous. To date, nearly all of the known MBCs have been discovered by telescopes with apertures smaller than 2 m. The use of larger telescopes for conducting surveys (e.g., the Dark Energy Survey's 4 m Blanco telescope or the 8.4 m Large Synoptic Survey Telescope) immediately allows for more sensitive searches for MBCs, but their respective observing efforts must also be coupled with at least reasonably capable search algorithms like that used by Pan-STARRS1 (cf. Hsieh et al. 2012b).

Other than the direct confirmation of sublimation products from a MBC, the next most critical priority for advancing MBC research is the discovery of more objects. A larger population of known objects (perhaps an order of magnitude larger than the currently known population) will allow us to achieve a more meaningful understanding of the abundance and distribution of MBCs in the asteroid belt as well as their typical physical and dynamical properties.

3.4 Outgassing from MBCs

The gas comae of comets are generally observed through fluorescence emission bands of various species, across a wide range of wavelengths from the UV to radio. The CN radical has strong emissions in the optical range, especially between 3590 and 4220 Å. The (0–0) band at 3883 Å is one of the most prominent feature of comet optical spectra. It has been detected at up to almost 10 au for comet Hale–Bopp (Rauer et al. 2003) and it is usually one of the first gas emissions detected in comets from the ground. The CN radical can also be used as a proxy of water production. The ratio of water production rates to CN production rates in the coma of a typical Jupiter-family comet is around $Q(H_2O)/Q(CN) = 350$, even though variations of the ratio have been observed along the orbit of a comet as well as from one comet to another (A'Hearn et al. 1995).

Upper limits of the CN production rate have been determined for several MBCs using spectroscopic observations on large telescopes: the Very Large Telescope (VLT), Gemini, the Gran Telescopio Canarias (GTC), and Keck. Hsieh et al. (2012b) and Licandro et al. (2013), respectively, determined upper limits of $Q(CN) = 1.3 \times 10^{24}$ and $Q(CN) = 3.76 \times 10^{23}$ mol s^{-1} for 288P, Hsieh et al. (2013) report an upper limit of $Q(CN) = 1.5 \times 10^{23}$ mol s^{-1} for P/2012 T1 (PANSTARRS), and Licandro et al. (2011) measure an upper limit of $Q(CN) = 1.3 \times 10^{21}$ mol s^{-1} for 133P. For

Table 2 Upper limits on MBC gas production Adapted from Snodgrass et al. 2017b

MBC	Tel.	r (au)	Q(CN) mol s^{-1}	$Q(H_2O)$[a] mol s^{-1}	References
133P	VLT	2.64	1.3×10^{21}	1.5×10^{24}	Licandro et al. (2011)
176P[b]	Herschel	2.58	–	4×10^{25}	de Val-Borro et al. (2012)
324P	Keck	2.66	3×10^{23}	1×10^{26}	Hsieh et al. (2012c)
259P	Keck	1.86	1.4×10^{23}	5×10^{25}	Jewitt et al. (2009)
288P	Gemini	2.52	1.3×10^{24}	1×10^{26}	Hsieh et al. (2012b)
	GTC	2.52	1.1×10^{24}	–	Licandro et al. (2013)
596[c]	Keck	3.10	9×10^{23}	1×10^{27}	Hsieh et al. (2012a)
P/2013 R3	Keck	2.23	1.2×23	4.3×10^{25}	Jewitt et al. (2014a)
313P	Keck	2.41	1.8×10^{23}	6×10^{25}	Jewitt et al. (2015a)
P/2012 T1	Keck	2.42	1.5×10^{23}	5×10^{25}	Hsieh et al. (2013)
	Herschel	2.50	–	7.6×10^{25}	O'Rourke et al. (2013)
	VLT	2.47	–	8×10^{25}	Snodgrass et al. (2017b)

[a] Where both Q(CN) and $Q(H_2O)$ are given, the latter is derived from the former. Values quoted in the original reference are given

[b] 176P was not visibly active (no dust release) at the time of the Herschel observations

[c] The dust ejected from (596) Scheila was almost certainly due to a collision, rather than cometary activity (e.g., Bodewits et al. 2011; Ishiguro et al. 2011a, b; Yang and Hsieh 2011)

comparison, we note that these upper limits are in line with the lowest recorded production rates for 'normal' comets near 1 au; one of the lowest successfully measured was 209P/LINEAR with $Q(\mathrm{CN}) = 5.8 \times 10^{22}$ mol s^{-1} (Schleicher and Knight 2016), while more commonly measured CN production rates are at least a few times 10^{23} (A'Hearn et al. 1995). The derived water production rates from these measurements, assuming a 'typical' water/CN ratio for comets, are around $Q(H_2O) = 10^{25} - 10^{26}$ mol s^{-1}, which would be low for a typical Jupiter-family comet (JFC) at MB distances (e.g., Rosetta measurements for 67P inbound agree at $Q(H_2O) \sim 10^{26}$ mol s^{-1} at 3 au, and a few times this at around 2.5 au, where most of the MBC measurements were made; Hansen et al. 2016). Attempts to detect CN in MBCs to date are summarised by Snodgrass et al. (2017b) and listed in Table 2.

These upper limits on water production all rely on the assumption that MBCs have a similar water/CN ratio to other comets, which is unlikely to be the case (see detailed discussion in following sections). Attempts have also been made to directly detect outgassing water using the Herschel space telescope (de Val-Borro et al. 2012; O'Rourke et al. 2013), and to detect the photo-dissociation products of water (OH and O) with the VLT (Snodgrass et al. 2017b; Jehin 2015). These are discussed in more detail in Sect. 5. A second implicit assumption in any upper limit measurement is that gas is still present at the time of the observation (i.e., that activity is ongoing). In most cases these observations were performed when there was dust visible around the MBC, and ongoing activity is a reasonable assumption, but it is also possible that an initial period of activity lifted dust and then shut off, leaving slow moving dust coma and tail visible after faster moving gas already dispersed. Models of dust coma

morphology can be used to differentiate between ongoing activity and remnant dust from short impulsive events (e.g., Moreno et al. 2011a).

4 MBC origins and survival of ice

Constraining the origin of MBCs is particularly important in the context of understanding whether these objects can be representative of ice-rich asteroids native to the MB, or have been implanted from outer regions of the Solar System during its complex dynamical evolution (cf. Hsieh 2014a). MBCs could be representative of the source of the terrestrial planets' volatiles and of the Earth's oceans in particular, and can therefore be extremely astrobiologically significant. It is also important to understand to what degree MBCs can be expected to have compositions which are comparable to traditional comets, e.g., their H_2O/CN ratio.

4.1 Isotopic ratios

Isotopic ratios, and particularly the D/H ratio in water, are used to trace the formation location of Solar System ices. In the protoplanetary disc, reactions in the vapour phase meant that D/H varied with temperature, but when the ice froze out, the ratio became fixed, meaning that the D/H ratio observed now records, in some way, the temperature and therefore location at which the ice originally formed. D/H is expected to increase with the heliocentric distance at which a body formed (Robert et al. 2000; Robert 2006). As mentioned in Sect. 2, the Earth's oceans have a mean D/H value that is lower than that measured in most comets, including the most recent measurement by Rosetta for 67P (Mumma and Charnley 2011; Altwegg et al. 2015). As the D/H values measured in meteorites are closer to VSMOW, it is possible that asteroids are instead the dominant source of Earth's water. Therefore, ice-rich asteroids such as MBCs are potentially remnants of the population that supplied our oceans. However, no D/H ratio has yet been measured for an MBC, and a space mission to visit one would be required to do this (see Sect. 8). This is seen as a priority for future measurements, both to confirm the match between ice in MBCs and Earth's water, but also to better understand the original source region where MBCs formed. In addition to D/H, isotopic ratios in other volatile elements (O, C, N, S) are measured in comets (Jehin et al. 2009; Bockelée-Morvan et al. 2015). Combining information from different elements can place stronger constraints on source location within the protoplanetary disc, but these measurements are even more challenging than D/H, given the relatively low abundance of other volatile species relative to water.

4.2 Dynamical evolution

Studying the dynamical stability and evolution of MBCs is a key component in efforts to identify their likely source regions in the Solar System. Most MBCs have been found to be mostly stable over 10^8 years or more (Jewitt et al. 2009; Haghighipour 2009; Hsieh et al. 2012b, c, 2013), suggesting that they formed in situ where we see them

today in the asteroid belt. These results were corroborated by Hsieh and Haghighipour (2016) who studied synthetic test particles rather than real objects, concluding that objects on orbits with both low eccentricities and low inclinations are unlikely to have been recently implanted outer Solar System objects.

Despite the fact that most MBCs appear to occupy long-term stable orbits, some MBCs like 238P/Read and 259P/Garradd are rather unstable on timescales of the order of 10^7 years (Jewitt et al. 2009; Haghighipour 2009), suggesting that they may be recently emplaced. Though the architecture of the modern Solar System appears to largely lack reliable pathways by which outer Solar System objects can evolve onto MBC-like orbits (e.g., Fernández et al. 2002), such interlopers cannot be completely excluded. Considering only the dynamical influence of major planets and the Sun, Hsieh and Haghighipour (2016) showed that pathways exist that are capable of temporarily implanting JFCs in the MB, largely shaped by the effects of close encounters with the terrestrial planets. However, they also showed that such implanted objects would not be stable for more than 100 Myr. These dynamical pathways appear to work both ways, with a non-negligible possibility that some JFCs could originate from the MB (Fernández and Sosa 2015).

A final scenario to consider is whether planet migrations during the early stages of Solar System evolution, as described by the Grand Tack and Nice models, could have resulted in the emplacement of icy outer Solar System objects in the MB (Levison et al. 2009; Walsh et al. 2011). In this case, ice formed in the outer regions of the Solar System could have been implanted in the MB, and would have experienced a different thermal history from ice that remained in the outer Solar System, thus allowing us to probe processes related to the thermophysical evolution of icy bodies in general. As discussed earlier in this paper though, much work remains in developing and performing observational tests for these models as well as refining them to the point where predictions (e.g., the distribution in orbital element space of implanted objects in the MB) can be made and tested.

Hui and Jewitt (2017) is the first work which systematically examines nongravitational effects of the MBCs. The authors report statistically significant detections of nongravitational effects for 313P/Gibbs and 324P/La Sagra. Intriguingly, the nongravitational effect on 324P is found to be large (composite nongravitational parameter $\sim 10^{-7}$ au day^{-2}; Hui and Jewitt 2017), which may be correlated with the fact that it is one of the most active MBCs (Hsieh 2014b), and may support the argument that some MBCs may have originated as JFCs (Hsieh and Haghighipour 2016). For the rest of the MBCs, Hui and Jewitt (2017) fail to obtain meaningful detections on nongravitational effects, which is consistent with the fact that the activity of the MBCs is normally orders-of-magnitude weaker than typical comets. Given this, conclusions about dynamical evolutionary paths of the MBCs by previous authors without consideration of the nongravitational effects are likely unaffected.

4.3 Family origins

In addition to the dynamical considerations discussed above, we need to account for the formation of asteroid families by catastrophic disruption of large parent bodies

when trying to constrain the origins of MBCs. MBCs P/2012 T1 and 313P have for example been linked to the Lixiaohua family (Hsieh et al. 2013, 2015b), while 133P, 176P/LINEAR, 238P and 288P/2006 VW_{139} have been linked to the Themis family (Toth 2000; Hsieh 2009; Hsieh et al. 2009b, 2012b). MBC 324P has also been dynamically linked with a small cluster of six objects (including 324P itself), but due to the small number of cluster members identified to date, this grouping does not yet formally satisfy the criteria for being classified as a family or clump as defined by Novaković et al. (2011).

The link between several MBCs and the Themis family is interesting, not only because of the water ice detection on Themis itself, but because spectra that have been obtained for Themis asteroids are best matched by carbonaceous chondrites meteorites with different degrees of aqueous alteration (Fornasier et al. 2016; Marsset et al. 2016). These observations are consistent with a large parent body made of significant amounts of water ice, which differentiated (hence the hydration of minerals) but maintained layers of pristine/unheated material (Castillo-Rogez and Schmidt 2010). The layering of composition, or internal heterogeneity, could in this case explain the spectral variability observed among Themis family members, which cannot be completely explained by space weathering processes (Fornasier et al. 2016). Among the Themis family lie much younger sub-families: the Beagle family, aged less than 10 Myr (Nesvorný et al. 2008), and the 288P cluster, estimated to be 7.5 Myr old (Novaković et al. 2012). It is possible that MBCs 133P and 288P may be members of those young sub-families rather than primordial members of the Themis family, increasing the possibility that water ice—if initially present in the various precursors—could have survived in both objects until today.

We note that while young families similar to those found for 133P and 288P have not yet been formally identified for the other known MBCs, the small sizes of other MBC nuclei suggests that they too may be fragments of recent catastrophic disruption events. Smaller objects are collisionally destroyed on statistically shorter timescales relative to larger objects (Cheng 2004; Bottke et al. 2005), meaning that currently existing smaller objects are statistically more likely to have been recently formed (e.g., in the fragmentation of a larger parent body) than larger bodies. The young families resulting from those fragmentation events may perhaps simply have not yet been identified because an insufficient number of members have been discovered to date, preventing the identification of the families by standard clustering analyses. As more asteroids are discovered by ongoing and future surveys, it will therefore be useful to periodically re-run clustering analyses for all MBCs to check if any new young families can be identified.

4.4 Thermal processing and ice survival

Hsieh et al. (2015a) noted that MBC activity patterns are predominantly modulated by variations in heliocentric distance. This observation implies that such activity is the result of ice being present on a global scale, buried under a slowly growing dust mantle, allowing for activity to be sustained over multiple perihelion passages, rather than the result of isolated local active sites containing exposed ice being seasonally

illuminated (which would tend to produce activity more randomly distributed along object orbits). However, given the small number of MBCs and the different individual cases, both scenarios have to be taken into account. Schorghofer (2008) studied the survival of water ice inside asteroids, assumed to be spherical icy objects on orbits ranging from 2 to 3.3 au from the Sun. They introduced the concept of the 'buried snowline', i.e., the limit beyond which subsurface water ice can be sustained for the age of the Solar System inside asteroids. Due to the very low thermal conductivities observed for such objects, they found that ice could have survived for billions of years in the top few metres from the surface, provided the mean temperature of the surface remains below 145 K: this is achievable in the polar regions of most objects in the outer MB with low obliquity.

Individual studies have mainly focused on 133P, since it has been active for four consecutive perihelion passages. Prialnik and Rosenberg (2009) studied two aspects of the survival of ices in 133P, both during the long-term thermophysical evolution of the object since its formation, and after an impact in the recent history of the object. For the 4.6 Gyr evolution, they used a one-dimensional thermophysical model able to compute both the thermal history of the object and the retreat of various volatiles, in particular, water, CO, and CO_2. They assumed that 133P was formed in the outer Solar System and then implanted in the MB, where the larger equilibrium temperature would have caused ices to sublimate, causing the sublimation front to penetrate deeper below the surface. They found that only water ice would have been able to survive inside 133P, 50–150 m below its surface. Other minor species would have all been lost, and would not have been sustained even in the case of an extremely low thermal conductivity. From these results, they infer that in order for 133P to be active today, an impact must have occurred, by which material was removed from the surface to expose ice-rich layers. This idea is consistent with the study of Capria et al. (2012) who found that impact rates in the MB are consistent with MBC activity being the result of impacts able to expose water ice at the surface of asteroids.

With this scenario in mind, Prialnik and Rosenberg (2009) then studied the thermal processing of 133P with a fully three-dimensional model which allows the assessment of the latitudinal variations of sublimation and dust mantling. Their results show that a dust mantle is being slowly built after repeated perihelion passages, with a thickness that is not uniform across the surface due to latitudinal variations of ice evolution. It is interesting to note that their analysis includes results consistent with the main features observed in 133P's secular lightcurve as studied by Ferrín (2006), in particular an increase in brightness of ~ 2 mag above the bare nucleus at peak activity, and a time lag of ~ 150 days after perihelion passage for peak activity. Prialnik and Rosenberg (2009) were able to reproduce these features when considering large tilt angles in their simulations. A large obliquity was suggested for 133P (Toth 2006), but has not been confirmed (Hsieh et al. 2010). This would indicate that the behaviour expected from water ice evolving in the MB can reproduce the activity pattern of this MBC: this implies that although no signatures of gaseous species have been detected, ice can be the origin of MBC activity, at least for 133P.

Using a different modelling approach, namely an asynchronous model coupling the simulation of accurate diurnal variations of the temperature with the simulation of ice sublimation over long timescales, Schorghofer (2016) revisited the thermo-physical

evolution of 133P. In particular, Prialnik and Rosenberg (2009) focused on 133P having spent billions of years in the MB, when we know from dynamical studies that it belongs to the Themis family (aged 2.5 Gyr) and perhaps to the Beagle family (aged 10 Myr) and thus has only been a discrete object since breaking up from the parent body at those times. Assuming that 133P is a direct member of the Themis family, Schorghofer (2016) found that water ice could indeed be found at depths consistent with those of Prialnik and Rosenberg (2009), but only for large grain sizes in the polar regions of 133P, i.e., ice can be found 2.4 to 39 m below the surface for 1 cm grains. When considering smaller grain sizes, Schorghofer (2016)'s results suggest that ice could be expected to be found much closer to the surface, and as close as 0.2 m for 100 μm grains. Assuming that 133P is a member of the much younger Beagle family, they suggest that ice could be found as close as a few cm below the surface (0.07–0.16 m for 100 μm grains) and within the top few metres in all cases (above 3.9 m for 1 cm grains).

Such different results between the two studies can in part be due to the different modelling approaches, or the initial thermo-physical properties assumed in the models. A better understanding of the internal structure of MBCs is crucial, however, for assessing the expected production rates, whether minor volatiles could have survived, and therefore to prepare for ground or space-based observations which might confirm the presence of ice on MBCs. Although an in-depth study of the survival of water ice and other volatiles is beyond the scope of this paper, we choose to provide an additional input given the discrepancy between the main studies of 133P's internal structure and evolution.

To further explore the stability of water ice in the interior of MBCs, we used the method described in Guilbert-Lepoutre (2014) who studied the survival of water ice on Jupiter Trojans. Below the orbital skin depth (∼a few to tens of metres), the material is not sensitive to variations of the surface temperature, but to the mean annual temperature. We therefore assumed equivalent circular orbits which receive the same amount of energy per orbit as asteroids, including MBCs, using $a_c = a(1 - e^2)$ as orbital input in a numerical model of three-dimensional heat transport to constrain the temperature distribution over the range of heliocentric distances spanned by MBCs (see Table 3). We have also considered a tilt angle between the rotation axis and the MBC orbit plane of 0°, 45° and 90° to obtain a limit on the dust layer thickness required for ice to survive underneath. For the main thermo-physical parameters, we have used a 2% albedo and a low thermal inertia of 3 J K^{-1} m^{-2} $s^{-1/2}$, which is consistent with values measured for comets, though among the lowest in the range of possible inertias (further details can be found in Guilbert-Lepoutre 2014 and Guilbert-Lepoutre et al. 2011). In Fig. 2, we show the depth at which water ice can be found after 1 Myr for the different orbital configurations considered, as preliminary results for a dedicated study of ice survival in the MB. The water ice depth ranges from a few centimetres to about 30 m for objects as close to the Sun as $a_c = 2.4$ au. It is worth noting that already after 1 Myr, highly volatile species such as CO or CH_4 would have already been lost. However, less volatile species such as CO_2, HCN or CH_3OH could still be present within the top 30–100 m, especially at large heliocentric distances. Although these results cannot be directly compared with existing works in meaningful way, given the different timescales simulated by the different approaches, they appear more

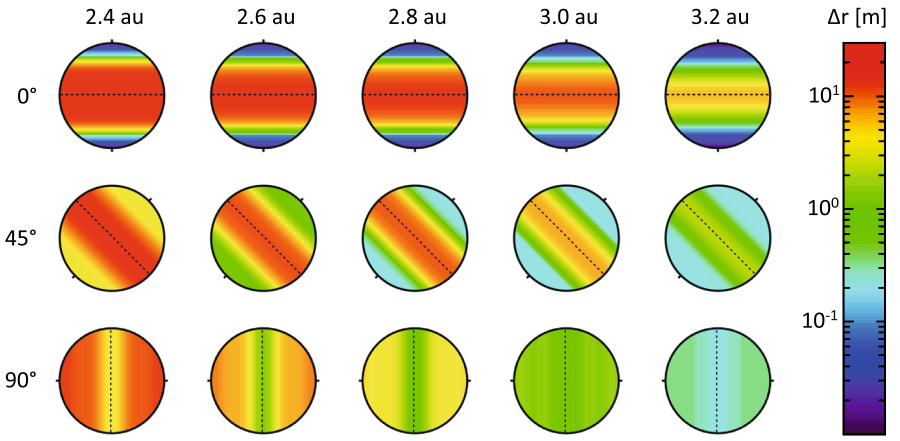

Fig. 2 Thickness of the porous dusty crust at the surface of MBCs required for water ice to be thermodynamically stable underneath after 1 Myr on equivalent orbits $a_c = a(1 - e^2)$ displayed as columns. Each row corresponds to a tilt angle between the object's rotation axis and its orbital plan. The Bond albedo is 2% and the thermal inertia at the surface is 3 J K^{-1} m^{-2} s$^{-1/2}$

Table 3 MBC properties relevant for thermal models

Object	a [a]	e [b]	a_c [c]	E[d]	T_q [e]
133P	3.166	0.159	3.08	4.65×10^{15}	160
238P	3.165	0.252	2.96	4.74×10^{15}	163
176P	3.196	0.193	3.07	4.66×10^{15}	161
259P	2.726	0.342	2.40	5.27×10^{15}	175
324P	3.096	0.154	3.02	4.69×10^{15}	162
288P	3.049	0.201	2.92	4.78×10^{15}	164
P/2012 T1	3.154	0.236	2.98	4.73×10^{15}	163
P/2013 R3	3.033	0.273	2.80	4.88×10^{15}	167
313P	3.156	0.242	2.97	4.74×10^{15}	163
P/2015 X6	2.755	0.170	2.67	4.99×10^{15}	170
P/2016 J1	3.172	0.228	3.00	4.71×10^{15}	162

[a] Semimajor axis, in au
[b] Eccentricity
[c] Semimajor axis, in au, of the equivalent circular orbit, i.e., the circular orbit receiving the same amount of energy per orbit
[d] Insolation per orbit, in W m^{-2}
[e] Theoretical equilibrium surface temperature at semimajor axis of equivalent circular orbit, assuming a sublimating isothermal grey-body (see Sect. 6.1 for description of calculations)

consistent with the results obtained by Schorghofer (2008) on the survival of water ice, and suggest that a detailed analysis needs to be performed for constraining the survival of minor volatile species.

5 Detecting water

As discussed in Sect. 3.4 above, CN has been used to search for outgassing around MBCs, but without success. To use MBCs as probes of the water content of the MB, we need to directly detect water (or its daughter/grand-daughter species). In this section we discuss the various means by which this is achieved in comets, and the prospects for applying these techniques to MBCs.

There are several techniques and wavelength ranges where water production rates in comets are determined. Water molecules themselves can be detected in their vibrational fluorescence transition in the NIR at 2.7 μm; however, the main band emission cannot be detected from the ground because of strong absorption by telluric water in the atmosphere. There are some weaker hot bands in the IR that can be detected and are routinely observed in medium-to-bright comets and at heliocentric distances much smaller than those of MBCs (Bockelée-Morvan et al. 2004). Rotational lines of water for the same reason also cannot be observed from the ground, but have been observed from space-borne platforms like ISO (Crovisier et al. 1997) and SWAS (Chiu et al. 2001). This is also how the most sensitive detection of water was made on approach by the Rosetta spacecraft to comet 67P by the MIRO instrument, a small radio telescope (Biver et al. 2015).

Otherwise water production is normally determined with greater sensitivity by observing water dissociation fragments such as OH, H and O(^{1}D). The OH radical is the primary product of the photodissociation of water at the level of about 82%. Its UV emission in the (0–0) band at 3080 Å is observed both from ground-based and space-based telescopes (Feldman et al. 2004). The fluorescence of the UV emissions produces a population inversion of rotational levels that are observed with radio telescopes at 18 cm (Despois et al. 1981; Schleicher and A'Hearn 1988). Space-based observations of atomic hydrogen have also been used as a proxy for determining water production rates. The chain of H_2O and OH photodissociation produces two H atoms per water molecule with nascent velocities of ~ 18 and ~ 8 km s^{-1}, respectively (Keller 1976); measurements of the Lyman-α emission at 1216 Å can be analysed to determine water production. Oxygen can be used via the forbidden lines of O(^{1}D) at 6300 Å (Fink 2009) in the inner coma, but the lowest production rates determined this way have been only a little lower than those from H Lyman-α, on the order of a few $\times 10^{27}$ mol s^{-1} (Fink 2009), also for comets near a heliocentric distance of about 1 au and very small geocentric distances.

In Table 4 we list the various emission features of water (and selected other key cometary species, for reference), along with example observations of these species in comets. We have tried to select the weakest detection, i.e., lowest $Q(H_2O)$, to show the limits of current technology, but of course the possibilities with very different facilities vary over orders of magnitude. Further examples of observations in different wavelength regimes are given in more detail in the following sub-sections. We give the diameter of the telescope used and the signal-to-noise per second achieved in order to allow some comparison to be made—we use this and the geometry of each observation to approximately scale the different capabilities to the expected MBC case in Sect. 6. It is worth noting that comet 67P is often the example chosen, as this otherwise faint comet was observed with all possible techniques as part of the

Table 4 Examples of detection of water and other key species in cometary comae

Wavelength	Species, line	Comet	Tel./inst.	Ø (m)	SNR/s	Q (mol s^{-1})	r (au)	Δ (au)	References
1216 Å	H, Ly-α	67P/C-G	PROCYON/LAICA	0.0415	7.07	1.24E+27	1.298	1.836	[1]
1304 Å	[OI]	note (a)							
1356 Å	[OI]	note (a)							
3080 Å	OH	73P-R/S-W 3 R	Lowell 1.1m/Phot.	1.1	0.46	1.30E+25	1.029	0.074	[2]
3080 Å	OH	88P/Howell	TRAPPIST	0.6	0.14	2.20E+27	2	1.44	[3]
5577 Å	[OI]	67P/C-G	VLT/UVES	8.2	0.07	5.00E+27	1.36	1.94	[4]
6300 Å	[OI]	67P/C-G	VLT/UVES	8.2	0.47	5.00E+27	1.36	1.94	[4]
6364 Å	[OI]	67P/C-G	VLT/UVES	8.2	1.41	5.00E+27	1.36	1.94	[4]
6563 Å	Hα	C/1996 B2 (Hyakutake)	McDonald	2.7	0.24	3.00E+29	0.9	0.2	[5]
2.66 μm	H_2O, ν_3	22P/Kopff	Akari/IRC	0.69	2.48	1.20E+27	2.4	2.4	[6]
2.9 μm	H_2O, hot bands	C/2014 Q2 (Lovejoy)	Keck/NIRSPEC	10	0.75	5.90E+29	1.29	0.83	[7]
6.3 μm	H_2O, ν_2	C/2004 B1 (LINEAR)	Spitzer/IRS	0.85	3.17	1.00E+28	2.2	2.0	[8]
1665 GHz	H_2O, 212–101	C/1995 O1 (Hale–Bopp)	ISO/LWS	0.60	0.17[a]	3.30E+29	2.8	3.0	[9]
1113 GHz	H_2O	81P/Wild 2	Herschel/HIFI	3.5	2.03	8.60E+27	1.61	0.93	[10]
557 GHz	H_2O	81P/Wild 2	Herschel/HIFI	3.5	4.75	1.13E+28	1.61	0.93	[10]
183 GHz	H_2O	103P/Hartley 2	IRAM	30	0.10	1.70E+25	1.06	0.15	[11]
18 cm	OH	103P/Hartley 2	Nançay	100	0.10	1.70E+28	1.1	0.15	[12]

Table 4 continued

Wavelength	Species, line	Comet	Tel./inst.	Ø (m)	SNR/s	Q (mol s^{-1})	r (au)	Δ (au)	References
1400–1640 Å	CO, 4th+ (A-X)	C/2000 WM1 (LINEAR)	HST/STIS	2.4	0.25	3.56E+26	1.084	0.358	[13]
1850–2300 Å	CO, Cameron	103P/Hartley 2	HST/FOS	2.4	0.06	2.60E+27	0.96	0.92	[14]
3883 Å	CN	67P/C-G	VLT/FORS2	8.2	0.12	1.40E+24	2.9	2.2	[15]
3883 Å	CN	C/2012 S1 (ISON)	Lowell 1.1m/Phot.	1.1	0.07	1.29E+24	4.554	4.039	[16]
4.26 μm	CO_2, ν_3	22P/Kopff	Akari/IRC	0.69	2.32	1.30E+26	2.4	2.4	[6]
4.67 μm	CO, $0 \rightarrow 1$	29P/S-W 1	VLT/CRIRES	8.2	0.09	2.64E+28	6.3	5.5	[17]
265 GHz	HCN	10P/Tempel 2	JCMT	15	0.08	9.00E+24	1.5	0.98	[18]

[a] Estimated, no SNR or exposure time quoted in reference

(a) [OI] lines in the UV were detected in C/1995 O1 (Hale–Bopp) via sounding rocket observations (McPhate et al. 1999) and in 67P via Rosetta/Alice (Feldman et al. 2015), but production rates are not given as the parent(s) and excitation process is model dependent (see Sect. 7)

References: [1] = Shinnaka et al. (2017); [2] = Schleicher and Bair (2011) ; [3] = Opitom et al. 2017, in prep.; [4] = Jehin (2015); [5] = Combi et al. (1999); [6] = Ootsubo et al. (2012); [7] = Paganini et al. (2017); [8] = Bockelée-Morvan et al. (2009); [9] = Crovisier et al. (1997); [10] = de Val-Borro et al. (2010); [11] = Drahus et al. (2012); [12] = Crovisier et al. (2013); [13] = Lupu et al. (2007); [14] = Weaver et al. (1994); [15] = Opitom et al. (2017); [16] = Knight and Schleicher (2015); [17] = Paganini et al. (2013); [18] = Biver et al. (2012)

campaign of observations supporting the Rosetta mission (Snodgrass et al. 2017), while for many species observations were only possible for very bright or very nearby comets (e.g., Hale–Bopp or 103P/Hartley 2; the latter was also a popular target due to the flyby of the NASA EPOXI mission close to perihelion—Meech et al. 2011).

5.1 UV/visible emission features

Photodissociation of water produces a lot of hydrogen in cometary comae, both directly and via further dissociation of OH, and the Lyman-α transition is one of the strongest emission features. However, it can only be observed from space, and even in Earth-orbit is difficult to detect in comets due to the overwhelming background from geocoronal emission. For the exceptionally bright and nearby comet C/1996 B2 (Hyakutake) Hubble Space Telescope (HST) spectroscopy detected the Ly-α emission, as the relative velocity (54 km s^{-1}) of the comet was sufficient to Doppler shift it away from the background (Combi et al. 1998). Observations with small field-of-view (FOV), like HST, are difficult to interpret directly because the innermost coma is optically thick to Lyman-α (Combi et al. 1998), so most observations have been very wide field like sounding rockets and the SOHO SWAN all-sky Lyman-α camera (Bertaux et al. 1998; Mäkinen et al. 2001; Combi et al. 2011b). Because the H coma can cover 10 or more degrees of the sky, background stars can become a serious limitation, especially for fainter comets. The lowest water production rates determined from SOHO SWAN measurements have been $\sim 10^{27}$ mol s^{-1}, and these were only for comets very close to SOHO, e.g., comet 103P (Combi et al. 2011a), which was at a heliocentric distance of only slightly more than 1 au. In Table 4 we give an example from a Ly-α imager on another spacecraft, the 2° FOV LAICA camera on the experimental Japanese PROCYON micro-satellite, which was designed to test deep-space navigation of a 50 kg satellite. The LAICA camera was designed to study the geocorona, but was also successfully employed to measure water production rates in 67P near perihelion (Shinnaka et al. 2017). The small sizes of these telescopes (2.7 and 4.2 cm diameter for SWAN and LAICA, respectively) implies that more sensitive instruments could be built relatively easily, but background noise will remain a limiting factor for Ly-α observations.

There are also emission lines from atomic oxygen in the UV, at 1304 and 1356 Å, which we list in Table 4 for completeness, but note that these are weak and have not been used to derive production rates. Also only observable from space, they were detected in C/1995 O1 (Hale–Bopp) from sounding rocket observations (McPhate et al. 1999), and from close range in 67P by Rosetta/ALICE (Feldman et al. 2015), but the excitation process (photons vs electrons), and therefore the production rate, is highly model dependent (see Sect. 7). There is no realistic prospect of remote detection of these lines in an MBC.

Emission bands of OH, the direct product of water photo-dissociation, can be detected at optical wavelengths. The strongest group of OH lines visible in this wavelength range is in the 3070–3105 Å region (Swings et al. 1941). This OH emission is often used to estimate the water production rate of comets, via spectroscopy or photometry. Low-resolution spectroscopy gives total production rates (e.g., Cochran et al.

2012), while higher resolution with either large telescopes or from space can improve signal-to-noise (S/N) for bright comets and reveal the structure within the band (e.g., Weaver et al. 2003; Jehin et al. 2006). Using narrow-band filters that isolate the region around the OH emission can give production rates and can be used to image the 2D structure of the gas coma, with OH production rates as low as 2.2×10^{27} mol s^{-1} detected for comet 88P/Howell at 2 au from the Sun using the 60 cm TRAPPIST telescope (Opitom et al. 2017, in prep.), but the most sensitive production rates come from photometry with a traditional photomultiplier (e.g., Schleicher and Bair 2011). However, at these wavelengths atmospheric extinction is high and the efficiency of most optical telescope detectors and optics is low, so OH emission is difficult to detect for faint comets. One attempt at detecting OH emission from an MBC was made, using the medium-resolution X-shooter spectrograph on the 8 m VLT, but only upper limits were obtained, at $8 - 9 \times 10^{25}$ mol s^{-1}, in 2.5 h of integration (Snodgrass et al. 2017b). A search for OH emission from Ceres using VLT/UVES produced a similar upper limit (Rousselot et al. 2011), which is below the production rate found by Herschel observations (Küppers et al. 2014), suggesting some variability in the outgassing rate from Ceres.

Atomic oxygen emissions are detected in the optical range through three forbidden oxygen lines at 5577.339 Å for the green line and 6300.304 and 6363.776 Å for the red doublet. Those lines are produced by prompt emission following the photodissociation of various parent molecules (H_2O, CO_2, CO, but also O_2) into a short-lived excited oxygen atoms (Festou and Feldman 1981; Cessateur et al. 2016). The combination of measurements of two forbidden lines O^1D and O^1S shows that is possible to even estimate the CO_2/H_2O ratio (McKay et al. 2012; Decock et al. 2013; Cessateur et al. 2016). The 6300.304 Å line, which is the brightest of the three forbidden oxygen lines has been successfully used to derive water production rates (e.g., Spinrad 1982; McKay et al. 2012). Observation of the forbidden oxygen lines require high-resolution spectroscopy and a sufficient Doppler shift of the comet emission lines to be distinguished from telluric oxygen lines. Those observations are challenging and cannot be done for all comets. However, they may be a very sensitive way to detect water (or CO and CO_2) on faint comets, as observations of the Rosetta target 67P showed that those oxygen lines were among the first emissions to be detected from Earth (Jehin 2015). Such observations have been attempted on the MBC 133P with the UVES instrument at the VLT, but none of the forbidden oxygen lines were detected (Bodewits, Private Communication, 2017). Observations of Ceres and Themis also produced only upper limits of 4.6×10^{28} and 4.5×10^{27} mol s^{-1}, respectively (McKay et al. 2017).

Finally, for the UV/visible range, there is the emission line of Hα at 6563 Å. Despite its common use in astronomical observations, it has been detected in relatively few comets, and the best example of which we are aware was for Hyakutake, a very bright comet with $Q = 3 \times 10^{29}$ mol s^{-1}, in spectroscopy with the 2.7 m telescope at McDonald observatory (Combi et al. 1999). Hα does not appear promising for detection of outgassing from an MBC.

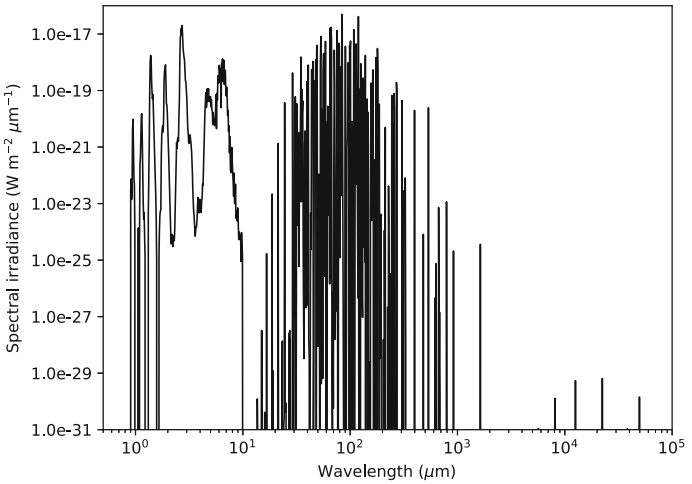

Fig. 3 Spectrum of water emission features in the NIR–radio (1 μm to 10 cm) at R=100, generated for an MBC with $Q = 10^{24}$ mol s^{-1}, r = 3 au, Δ = 2 au, and an atmospheric temperature of 80 K. The beam width is 1° at all wavelengths

5.2 Infrared and sub-mm/radio emission features

Molecular species in the gas comae of comets, including water, produce a large number of emission features in the infrared (Crovisier 1984; Mumma et al. 2003; Bockelée-Morvan et al. 2004; Cernicharo and Crovisier 2005) and sub-millimetre (Biver et al. 2007; Bockelée-Morvan 2008), which are caused by the vibrational and rotational modes. We show the NIR–radio spectrum of a model MBC atmosphere that comprised water, generated using the Goddard Planetary Spectrum Generator[3] (Villanueva et al. 2015), in Fig. 3. Water itself is difficult to observe from Earth due to its presence in the atmosphere, but at high resolution and with sufficient Doppler shift comet lines can be separated from telluric ones. Sufficiently high spectral resolution also allows the structure of vibrational bands to be resolved, or even isotopic measurements to be made for bright comets (e.g., Paganini et al. 2017). The advantage of observing in this region is that water is directly detected, rather than production rates being derived via daughter species. For fainter comets, where high-resolution spectroscopy is impossible, or where there is too low radial velocity with respect to Earth, observations from space telescopes are necessary. Some of the most sensitive observations were made with the Akari satellite, with detections of the 2.7 μm ν_3 band of water at $Q = 1.2 \times 10^{27}$ mol s^{-1} made in comet 22P/Kopff when it was at 2.4 au from the Sun (Ootsubo et al. 2012). This band was also observed in bright comets in both imaging and spectroscopy by the International Space Observatory (ISO) satellite (Colangeli et al. 1999; Crovisier et al. 1997) and the Deep Impact spacecraft (Feaga et al. 2014). At longer wavelengths, the ν_2 band at 6.3 μm was observed by ISO and Spitzer, again for relatively bright comets with $Q \sim 10^{28} - 10^{29}$ mol s^{-1} (Crovisier et al. 1997;

[3] https://sed.gsfc.nasa.gov/psg/index.php

Bockelée-Morvan et al. 2009). None of these space telescopes are still operating at these wavelengths, but the James Webb Space Telescope (JWST) will (see Sect. 8).

At sub-mm and radio wavelengths very high resolution spectroscopy is possible, enabling detection of spectrally resolved individual rotational lines used to determine the kinematics of gas flows and excitation conditions in the coma, although mostly these observations are sensitive to larger molecules. With large dishes or arrays on Earth a large number of molecules have been identified in comets (e.g., Biver et al. 2002, 2014), especially hydrocarbons, with methanol and HCN being most regularly observed, and abundances normally measured relative to HCN. Water is generally not identified from the ground, although Drahus et al. (2012) were able to detect the 183 GHz band with the 30 m IRAM telescope during the close approach of comet 103P, at $Q = 1.7 \times 10^{25}$ mol s^{-1}. The launch of sub-mm space telescopes, in particular Odin and Herschel, allowed observations of several ortho- and para-water lines (e.g., at 557 and 1113 GHz; de Val-Borro et al. 2010, 2014; Hartogh et al. 2010; Biver et al. 2012). The 3.5 m mirror of Herschel gave it excellent sensitivity, and the high-resolution Heterodyne Instrument for the Far Infrared (HIFI; de Graauw et al. 2010) instrument meant that D/H could be measured for the first time in a bright enough JFC (103P; Hartogh et al. 2011).

Direct detection of H_2O emission from MBCs has been attempted using Herschel. Based on the visibility and anticipated gas emission activity during the Herschel mission lifetime (2009–2013), two MBCs, 176P and P/2012 T1, were observed by HIFI (de Val-Borro et al. 2012; O'Rourke et al. 2013). 176P passed its perihelion on 2011 June 30 and was observed by Herschel/HIFI on UT 2011 August 8.78 when it was at a heliocentric distance of 2.58 au and a distance of 2.55 au from the spacecraft. At the end of the mission, the newly discovered P/2012 T1 was observed as part of director's discretionary time on UT 2013 January 16.31, about 3 months after its perihelion passage, when the object was at a heliocentric distance of 2.50 au and a distance of 2.06 au from Herschel. The line emission of the fundamental 1_{10}–1_{01} rotational transition of ortho-H_2O at 557GHz was searched for in both objects. There was no detection of H_2O line emission in either of the targets. However, sensitive 3-σ upper limits were inferred for the H_2O production rate of $< 4 \times 10^{25}$mol.s^{-1} and $< 7.6 \times 10^{25}$mol.s^{-1} for 176P and P/2012 T1, respectively. While 176P was shown to be inactive during its 2011 passage from ground-based observations, dust emission activity was clearly observed in P/2012 T1 at the time of the Herschel observation suggesting that the gas production was lower than the derived upper limit (O'Rourke et al. 2013).

Finally, at very long (radio) wavelengths, there is OH emission at 18 cm. There are two lines (1.665 and 1.667 GHz) that are regularly observed in comets, especially using the Nançay array (Crovisier et al. 2013). The (at the time) largest single dish telescope in the world, the 300 m Arecibo radio telescope, has also targeted comets at 18 cm (Lovell et al. 2002), but even using these facilities only the brightest comets are detectable, with the most sensitive detection again coming from the close approach of 103P to Earth in 2010. Detection of MBC-level outgassing at 18 cm does not appear likely.

5.3 Absorption features from surface ice or coma ice grains

It is also possible to detect water ice directly on surfaces of small bodies, or on grains in the comae of comets, through absorption features in the reflected solar continuum. Water ice may take many forms, depending on the temperature and pressure at the time of formation (Petrenko and Whitworth 1999). If temperatures were low ($T < 50K$), water would have frozen out into its amorphous phase, but had they been higher (120–180 K), water molecules would have been able to arrange themselves into a crystalline structure (Mukai 1986). Observationally, amorphous ice and crystalline ice are recognisable through infrared spectroscopy. The position, shape, intensity and width of absorption bands in an ice spectrum are indicators of the structure, temperature and thermal history of the ice (Newman et al. 2008). For ground-based observations, there are two key bands for recognising crystalline (as opposed to amorphous) water ice. One is the 3.1 μm Fresnel reflection peak, which is caused by a stretching mode of the water molecule, and another one is a temperature-sensitive absorption band at 1.65 μm that is only seen in crystalline ice (Grundy and Schmitt 1998). The 1.65 μm feature is absent in most available NIR spectra of the observed comets, except for the outbursting comet P/2010 H2 (Yang and Sarid 2010). On the other hand, several thermodynamical models have proposed that the heat, generated through crystallisation of amorphous ice, is an important energy source thought to trigger distant cometary activity even when comets are beyond the critical sublimation heliocentric distance (Prialnik 1992; Prialnik et al. 2004). Given the current observational constraints on water ice in comets, it remains uncertain whether the ice in comets is amorphous even before their entry to the hot, inner region of the Solar System.

Most direct evidence of the presence of water-bearing minerals on asteroids comes from infrared observations, particularly in the so-called 3 μm region, where the hydroxyl fundamental absorption and the strong first overtone of water are both present. Characteristics of absorption features in this region, such as wavelength position of the band centres, the shape of the absorption bands and their relative intensities are diagnostics of mineralogy as well as abundance. However, the 3 μm region is notoriously difficult for ground-based observations because of intense atmospheric absorptions and faint solar radiation in this wavelength regime. Nevertheless, spectral surveys of large asteroids in the 3 μm region have flowered, mostly using the SpeX instrument at the IRTF telescope (Takir and Emery 2012; Rivkin et al. 2015).

Compared with the NIR observations, visible spectroscopy is relatively easy to obtain using small-to-moderate-sized telescopes. Therefore, numerous efforts have been made to search for diagnostic features in MB asteroids between 0.4 and 0.9 μm (Vilas and Smith 1985; Luu and Jewitt 1990; Sawyer 1991; Xu 1994; Bus and Binzel 2002). A shallow but fairly broad (width $\sim$ 0.25 μm) absorption feature centred near 0.7 μm is found to be very common among the low-albedo asteroids (Sawyer 1991). This feature is attributed to an $Fe^{2+} \rightarrow Fe^{3+}$ charge transfer transition in hydrated minerals (Vilas and Gaffey 1989). Consistently, a 0.7 μm feature is also seen in the laboratory spectra of CM2 carbonaceous chondrite meteorites and terrestrial phyllosilicates (a hydrated mineral), which is similar to the asteroidal feature both in band centre and strength (Vilas and Gaffey 1989). Although King and Clark (1997) warned that a feature near 0.7 μm has been seen in many different minerals, and so

this feature alone is not sufficient for identifying aqueous alteration, the majority of minerals that show an absorption centred at 0.7 μm are iron- and OH-bearing silicates (Rivkin et al. 2002).

Additionally, 13 C-, P-, and G-class asteroids were observed in the UV/blue spectral regions and they exhibit an absorption feature near 0.43 μm (Vilas et al. 1993; Cochran and Vilas 1997). The blue/UV drop-off observed in these low-albedo asteroids is thought to be attributed to a ferric spin-forbidden absorption in aqueously altered iron-containing minerals (Burns 1981). Among low-albedo asteroids, the UV drop-off is found to be correlated with the 3 μm absorption due to hydrated mineral components (Feierberg et al. 1985). Similarly, the same correlation is observed in carbonaceous chondrites, which contain a significant fraction of hydrated silicates, such as phyllosilicates. Therefore, it has been suggested that the (U-B) colour might be also useful as an indicator of the presence hydrated materials (Gaffey and McCord 1978). These UV/visible wavelength features have not yet been observed in MBCs.

5.4 In situ detection of water

The last set of techniques for detecting water are those that can be applied by visiting the target with a spacecraft. Various cometary missions have done so, with the recent Rosetta mission combining mass spectroscopy with remote sensing instruments that were sensitive to water via the various emission and absorption features described in previous sections. The mass spectrometer and pressure gauge instrument ROSINA on Rosetta first detected water in August 2014, at a distance of ~ 100 km from the comet and 3.5 au from the Sun, at $Q \approx 5 \times 10^{25}$ mol s^{-1} (Hansen et al. 2016), although earlier detection was possible from the remote sensing instruments (see Sect. 7). Mass spectroscopy can measure both precise relative abundances of water and other volatiles, and isotopic ratios (Altwegg et al. 2015).

Suitably equipped spacecraft can also search for evidence of buried ice, in addition to identifying surface ice or outgassing water. Radar detection of subsurface water relies on the marked difference in dielectric properties between liquid water and other common geo-materials such as rocks and water ice. Whereas the relative dielectric permittivity of ice is 3.1, and that of rocks ranges between 4 and 10, liquid water has a permittivity of 80 (Ulaby et al. 1986, Appendix E). The marked dielectric contrast between a layer of liquid water and the surrounding rocks results in a high radar reflection coefficient, and thus in a strong radar echo. On Earth, this feature is routinely used in the identification of subglacial lakes (see e.g., Palmer et al. 2013). While liquid water is not expected to be present on an MBC, radar would be useful in identifying rock and ice layers. The radar reflection coefficient of a surface is determined both by dielectric properties and by geometry. Rough surfaces diffuse the impinging radar pulse and weaken the backscatter towards the radar (Ogilvy 1991), thus making the identification of water more and more ambiguous as the water/rock interface becomes rougher or more curved.

The depth at which radar can detect echoes from a subsurface interface is affected by the properties of the material between the surface and the interface. Electromagnetic waves are absorbed in a dielectric medium, such as rocks and ices, and can be scat-

tered by cracks, voids and other irregularities at scales comparable to the wavelength. However, assuming the results of the CONSERT experiment on board Rosetta can be used to predict the expected bulk dielectric properties of MBCs, then both dielectric attenuation and volume scattering should be low (Kofman et al. 2015).

At this moment, there are no useful precedents for the detection of water within an MBC. The CONSERT experiment is based on the transmission of a radar signal through the cometary material, rather than on its reflection at a dielectric interface. If used on an MBC, CONSERT would probably be unable to identify a ice layer, although it would likely measure a significant signal attenuation. The measurements at Phobos of the MARSIS experiment on board Mars Express (Picardi et al. 2005) are of limited value in predicting the expected performance of radar in detecting water within an MBC. MARSIS was originally designed solely for the observation of Mars, and Phobos is smaller than the MARSIS footprint (Safaeinili et al. 2009).

A higher-frequency radar, such as SHARAD on board NASA's Mars Reconnaissance Orbiter (Seu et al. 2007), could be used to acquire full coverage of an MBC and produce its three-dimensional radar tomography. This is a well-known technique on Earth (see e.g., Knaell and Cardillo 1995), but the irregular shape of an MBC will require some developments. In spite of the difficulties in deconvolving of the effects of geometric and dielectric interface properties on the echo, the detection of water pockets could then be demonstrated based on their greater radar backscatter cross section, compared to similar structures elsewhere in the subsurface, their relation to the surrounding stratigraphy, and the general geologic context.

6 Expected activity levels for MBCs

When considering how best to detect evidence of sublimation from MBCs, it is important to consider what levels of activity can be reasonably expected, as well as which MBCs are most likely to exhibit detectable levels of activity.

6.1 Predictions from energy balance

As described in Hsieh et al. (2015a) and elsewhere, the equilibrium temperature and unit-area water sublimation rate for a sublimating grey-body at a given heliocentric distance can be computed iteratively from the energy balance equation for a sublimating grey-body (neglecting heat conduction),

$$\frac{F_{\odot}}{r^2}(1-A) = \chi\left[\varepsilon\sigma T_{\mathrm{eq}}^4 + Lf_{\mathrm{D}}\dot{m}_w(T)\right], \tag{2}$$

the sublimation rate of ice into a vacuum,

$$\dot{m}_w = P_{\mathrm{v}}(T)\sqrt{\frac{\mu}{2\pi kT}}, \tag{3}$$

and the Clausius–Clapeyron relation,

$$P_{\rm v}(T) = 611 \times \exp\left[\frac{\Delta H_{\rm subl}}{R_{\rm g}}\left(\frac{1}{273.16} - \frac{1}{T}\right)\right]. \quad (4)$$

In the energy balance equation, $T_{\rm eq}$ is the equilibrium surface temperature, $F_\odot = 1360$ W m^{-2} is the solar constant, r is the heliocentric distance of the object in au, $A = 0.05$ is the assumed Bond albedo of the body, χ describes the distribution of solar heating over an object's surface ($\chi = 1$ for a flat slab facing the Sun where this so-called subsolar approximation produces the maximum attainable temperature for an object, $\chi = \pi$ for the equator of a rapidly rotating body with zero axis tilt, and $\chi = 4$ for an isothermal sphere, as in the limiting approximation of an extremely fast rotator and strong meridional heat flux), $\varepsilon = 0.9$ is the assumed effective infrared emissivity, and σ is the Stefan–Boltzmann constant. In the sublimation rate equation, $L = 2.83$ MJ kg^{-1} is the latent heat of sublimation of water ice, which is nearly independent of temperature, $f_{\rm D}$ describes the reduction in sublimation efficiency caused by the diffusion barrier presented by a rubble mantle, where $f_{\rm D} = 1$ in the absence of a mantle, $\dot{m}_w(T)$ is the water mass loss rate due to sublimation of surface ice, $\mu = 2.991 \times 10^{-26}$ kg is the mass of one water molecule, k is the Boltzmann constant. The equivalent ice recession rate, $\dot{\ell}_i$, corresponding to $\dot{m}_w$ is given by $\dot{\ell}_i = \dot{m}_w/\rho$, where ρ is the bulk density of the object. Lastly, in the Clausius–Clapeyron relation, $P_{\rm v}(T)$ is the vapour pressure of water in Pa, $\Delta H_{\rm subl} = 51.06$ MJ kmol^{-1} is the heat of sublimation for ice to vapour, and $R_{\rm g} = 8314$ J kmol^{-1} K^{-1} is the ideal gas constant.

We use these equations to compute the peak expected sublimation rate using the isothermal approximation for the known MBCs, and also convert unit-area sublimation rates from the above equations to a total surface-wide sublimation rate for each object assuming spherical bodies and active areas of 100% (Table 5). We can see from these results that there is a range of expected maximum water sublimation rates expected from various MBCs, and two important factors influencing these maximum rates are perihelion distance and nucleus size. Hsieh et al. (2015a) noted that, on average, the currently known MBCs have higher eccentricities (and therefore smaller perihelion distances) than the overall outer main-belt asteroid population, suggesting that the activity of those particular objects could be at least partly due to the fact that they reach higher peak temperatures than other asteroids with similar semimajor axes. The significance of having larger-than-average eccentricities and therefore smaller perihelion distances is further illustrated by Fig. 4, which illustrates water ice sublimation rates as a function of heliocentric distance, computed using Eqs. 2, 3, and 4 as well as the positions of the perihelion, aphelion, and semimajor axes of seven of the known MBCs. It is interesting to note that over the ranges of heliocentric distances traversed by these MBCs over the course of their orbits, the theoretical water ice sublimation rate varies by as much as four orders of magnitude in the isothermal case. This suggests that the fact that all are seen to be active near perihelion is not just a coincidence or observational bias.

Meanwhile, we see that larger maximum total water sublimation rates are expected for larger objects than smaller objects due to the simple fact that larger objects have

Table 5 MBC activity properties

Object	q [a]	R_N [b]	v_{esc} [c]	$Q(H_2O)_q$ [d]		dM/dt [e]	Active range[f]	References[g]
133P	2.664	1.9	2.2	3.5×10^{16}	1.6×10^{24}	1.4	350°–109°	[1-4]
238P	2.366	0.4	0.5	1.1×10^{17}	2.2×10^{23}	0.2	306°–123°	[5,6]
176P	2.580	2.0	2.4	4.9×10^{16}	2.5×10^{24}	0.1	1°–19°	[1,7]
259P	1.794	0.3	0.4	5.0×10^{17}	5.7×10^{23}	–	315°–49°	[8-10]
324P	2.620	0.6	0.7	4.2×10^{16}	1.9×10^{23}	4.0	300°–96°	[11-13]
288P	2.436	1.3	1.5	8.4×10^{16}	1.8×10^{24}	0.5	338°–47°	[14-16]
P/2012 T1	2.411	–	–	9.3×10^{16}	–	~1	7°–48°	[17-18]
P/2013 R3	2.204	–	–	1.8×10^{17}	–	–	14°–43°	[19]
313P	2.391	0.5	1.2	1.0×10^{17}	1.3×10^{24}	0.4	354°–53°	[20–23]
P/2015 X6	2.287	–	–	1.4×10^{17}	–	1.6	329°–344°	[24]
P/2016 J1-A	2.448	<0.9	<1.1	8.1×10^{16}	–	0.7	346°–12°	[25,26]
P/2016 J1-B	2.448	<0.4	<0.5	8.1×10^{16}	–	0.5	346°–12°	[25,26]

[a] Perihelion distance, in au
[b] Effective nucleus radius, in km
[c] Theoretical escape velocity, m s^{-1}, in assuming spherical, non-rotating nuclei with bulk densities of $\rho \sim 2500$ kg m^{-3}
[d] Unit-area and total (assuming 100% active area) theoretical water sublimation rates, in mol m^{-2} s^{-1} and mol s^{-1}, at perihelion, assuming a spherical sublimating isothermal grey-body.
[e] Peak reported observed dust mass production rate in kg s^{-1}
[f] True anomaly range over which activity has been reported. Listed ranges are incomplete, sometimes reflecting limitations in observational coverage rather than the confirmed absence of activity over orbit arcs not included in the listed true anomaly ranges
[g] References: [1] Hsieh et al. (2009a); [2] Jewitt et al. (2014b); [3] Hsieh et al. (2010); [4] Kaluna and Meech (2011); [5] Hsieh et al. (2009b); [6] Hsieh et al. (2011b); [7] Hsieh et al. (2011a); [8] Jewitt et al. (2009); [9] MacLennan and Hsieh (2012); [10] Hsieh and Chavez (2017); [11] Moreno et al. (2011a); [12] Hsieh et al. (2012c); [13] Hsieh (2014b); [14] Hsieh et al. (2012b); [15] Licandro et al. (2013); [16] Agarwal et al. (2016); [17] Hsieh et al. (2013); [18] Moreno et al. (2013); [19] Jewitt et al. (2014a); [20] Hsieh et al. (2015b); [21] Jewitt et al. (2015a); [22] Jewitt et al. (2015c); [23] Pozuelos et al. (2015); [24] Moreno et al. (2016); [25] Hui et al. (2017); [26] Moreno et al. (2017)

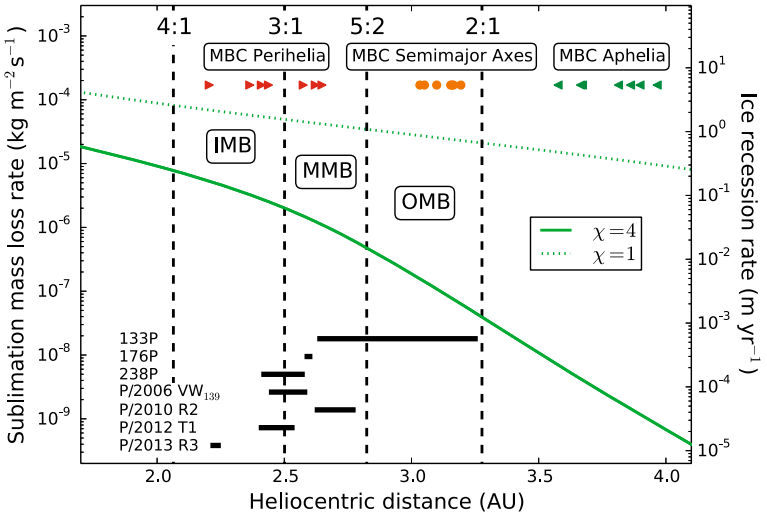

Fig. 4 Mass loss rate due to water ice sublimation from a sublimating grey body as a function of heliocentric distance over the range of the main asteroid belt, where the semimajor axis ranges of the inner, middle, and outer MB are labelled IMB, MMB, and OMB, respectively, and mass loss rates calculated using the isothermal approximation ($\chi = 4$) and subsolar approximation ($\chi = 1$) are marked with solid and dashed green lines, respectively. The positions of the major mean-motion resonances with Jupiter (4:1, 3:1, 5:2, and 2:1) that delineate the various regions of the main asteroid belt are shown with vertical dashed black lines. Also plotted are the perihelion distances (red, right-facing triangles), semimajor axis distances (orange circles), and aphelion distances (green, left-facing triangles) of the known outer main-belt MBCs, as well as the range of heliocentric distances over which they have been observed to exhibit activity (thick black horizontal lines) Image reproduced with permission from Hsieh et al. (2015a), copyright by Elsevier

greater surface areas over which sublimation can occur. This presents an interesting dilemma since larger (and therefore more massive) objects also have larger escape velocities (cf. Table 5) that ejected dust grains must reach in order to overcome the gravity of the active body and escape into space where they can be observed as comet-like dust emission. Ejection velocities for dust emission from many MBCs tend to be relatively low compared to ejection velocities for classical comets, yet they are often comparable to the escape velocities of the corresponding nuclei (cf. Hsieh et al. 2004). This competition between size preferences may be a highly consequential effect, meaning that there may be an 'ideal' size or size range for detectable MBCs where they are large enough to produce observable amounts of gas or dust emission but small enough that ejected dust can actually escape into space to become observable in the first place. Hsieh (2009) also noted that if MBC ice must be preserved in subsurface layers in order to survive to the present day and only excavated recently (cf. Hsieh et al. 2004), currently active MBCs must also tend to somewhat larger sizes so that they have the surface area to experience impacts capable of excavating subsurface ice on timescales consistent with their discovery rates in the asteroid belt, but still must be small enough for ejected dust to reach the escape velocity of the emitting body.

Interestingly, we see that measures of activity strength such as the peak inferred dust production rate or total activity duration listed in Table 5 are not strongly correlated to either the theoretical unit-area or total expected water sublimation rates at perihelion.

This discrepancy could be due to a number of factors, including differences in initial ice content or distribution, devolatilisation progression of active sites, overall fractions of active surface area on each body, or thermal properties of each object. In particular, rotation rates are not known for most MBC nuclei, yet may be significant factors in whether it is most appropriate to model their thermal behaviour using either the subsolar or isothermal approximations.

Notably, the total maximum predicted water sublimation rates listed in Table 5 are smaller than most of the detection limits for various sublimation detection techniques discussed elsewhere in this paper, and also assume 100% active areas, which are almost certainly not the case for most or all MBCs (for comets active areas of a few percent or less are typical; A'Hearn et al. 1995). We note, however, that these values represent calculations based on the isothermal (or 'fast-rotator') approximation, which produces the lowest temperatures and lowest production rates. At the other extreme, the subsolar approximation gives production rates as much as two orders of magnitude larger, suggesting that we may be more likely to detect gas emission from slower-rotating MBC nuclei or those with higher thermal inertias. Additionally, the total maximum predicted water sublimation rates listed here are computed assuming the surface area of spherical nuclei, whose effective radii have been estimated from their scattering cross-sections. If MBC nuclei are irregularly shaped, like 67P, or perhaps even binary, like 288P (Agarwal et al. 2016), larger usable surface areas and therefore higher gas production rates could be possible.

6.2 Predictions from observed dust activity

Although no direct detection of gas in an MBC has been made to date, we can use the observed dust comae as indicators of the mass-loss rates from these bodies. One method is to model the observed dust distribution to find the probable grain size distribution, the dust mass ejected over time, and then use nominal gas to dust mass loss ratios to constrain the sublimation rate. Moreno et al. (2011a) derived a maximum sustained dust mass loss rate of $\sim 3-4$ kg s^{-1} at 324P. In similar studies, Moreno et al. (2013) found that P/2012 T1 emitted $6-25\times10^6$ kg of dust over 4–6 months, implying an average mass loss rate of ~ 2 kg s^{-1}, while Pozuelos et al. (2015) found dust mass loss rates of $\sim 0.2-0.8$ kg s^{-1} at 313P. Assuming a dust/gas mass ratio of $\sim$ 1:1, this would imply maximum water sublimation rates of $Q(\mathrm{H_2O}) \sim 10^{26}$ mol s^{-1}.

Another method is by direct comparison with observations of normal active comets. The standard method of estimating the dust content of the coma is through measurement of the $Af\rho$ parameter (units of cm) as defined by A'Hearn et al. (1984). Although transformation to a dust mass-loss rate requires further assumptions or modelling, $Af\rho$ has the advantage that it is calculated solely on the basis of the observed photometric brightness. At the same time, the production rate Q(gas) can be accurately constrained through narrow-band photometry or spectrophotometry. A'Hearn et al. (1995) reported photometric observations and analysis of tens of comets, finding that for a typical comet $\log[Af\rho/Q(\mathrm{OH})] = -25.8 \pm 0.4$. The most active MBCs discovered so far appear to have $Af\rho \simeq 10-20$ cm (P/2012 T1, Hsieh et al. 2013; 313P, Hui and Jewitt

2015). Using the above relationship would imply $Q(H_2O) \simeq (7^{+10}_{-4}) \times 10^{25}$ mol s^{-1} assuming $Q(OH) \simeq 0.9\ Q(H_2O)$.

Comparing these estimates of $Q(H_2O)$ with the upper limits in Table 2 implies that current observational efforts may be close to directly detecting gas in MBCs. But there are two important factors to take into account. First, many upper limits are based on the non-detection of the bright CN emission band and assuming normal CN/OH cometary ratios. As discussed in Sect. 4.2, modelling indicates that more volatile species in subsurface ices may be depleted due to thermal processing. If HCN is the photodissociation parent molecule of CN, then the CN/OH ratio in MBC comae may be lower than in a normal comet. This would imply that $Q(H_2O)$ is higher than expected from the measured upper limit to $Q(CN)$. Second, mantling of the source region could occur to due fallback of slowly moving dust grains back onto the surface of the MBC. This 'airfall' was readily apparent in images of 67P from the Rosetta spacecraft (Thomas et al. 2015). This could plausibly increase the dust/gas ratio over time as the airfall layer on the sublimation site increases and the thermally active ice surface diminishes. This would mean that $Q(H_2O)$ is less than anticipated from measurements of the dust coma.

6.3 Relative strength of water signatures

We now consider which of the various water detection methods listed in Sect. 5 is most promising to detect MBC-level outgassing, which, following the discussion in the previous subsections, we take as $Q(H_2O) = 10^{24}$ mol s^{-1}. Comparing the relative effectiveness of the listed techniques is not straightforward, due to the great differences in observation type, geometry, and activity level of the comets used as examples. Even observations of the same comet—C/2009 P1 (Garradd)—with different telescopes/techniques gave different production rates, which was attributed to a halo of icy grains and different FOVs (Combi et al. 2013). Nevertheless, we attempt to draw some approximate conclusions by scaling these observations with a number of simplifying assumptions. We discard the possibility of in situ investigation for now; although it would certainly be effective, it is a very different prospect to astronomical observation in terms of cost. We also leave detection of absorption features out of this comparison, as this appears to be only possible for larger bodies: even for much more active comets, surface ice features are not detected remotely, and even in situ exploration shows only relatively small and variable ice patches on surfaces (De Sanctis et al. 2015).

To compare the strength of emission features across a range of wavelengths, we scale the observations listed in Table 4 to give the exposure time required to achieve an S/N of 5 detection of $Q = 10^{24}$ mol s^{-1} at $r = 3$ au and $\Delta = 2$ au. We ignore velocity effects, both heliocentric (i.e., Swings effect) and geocentric (i.e., assuming that lines are detectable without telluric interference). We make the assumption that the aperture is of fixed angular size and that the coma distribution scales as ρ^{-1}, i.e., that the signal scales as Δ^{-1}, which is not necessarily the case. A better approximation could be made with scaled Haser models (Haser 1957) for each observation, taking into account the different slit or measurement aperture areas, but we judged this to be

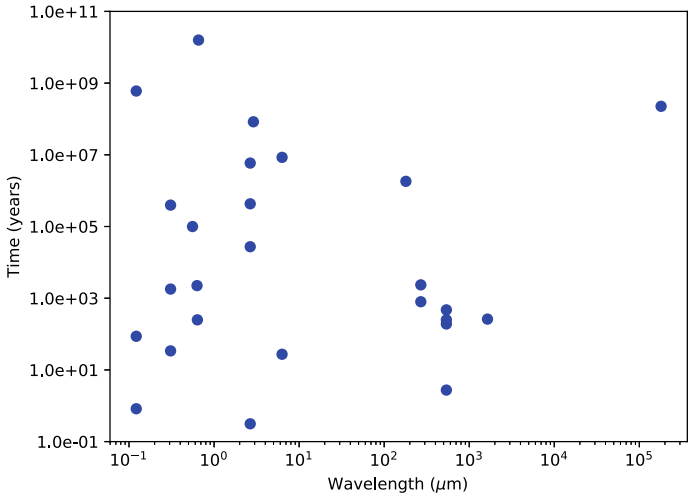

Fig. 5 Exposure time required to get 5σ detection of $Q = 10^{24}$ mol s^{-1} outgassing from an MBC, based on scaling the comet detections at various wavelengths in Table 4

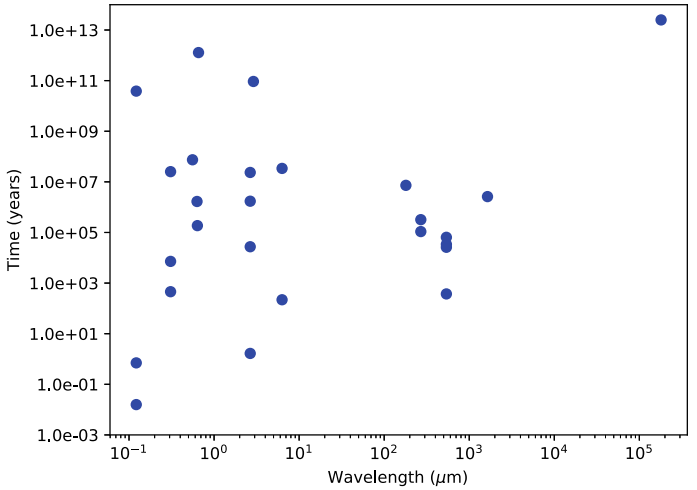

Fig. 6 Same as Fig. 5, but scaled to a telescope diameter of 30 cm in space

of secondary importance given the other uncertainties. We plot the scaled exposure times needed to make 5σ detections as a function of wavelength in Fig. 5. It is clear that the exposure times required with current technology are infeasible, and that there is a very large range (from $\sim$ 1 year to a Hubble time!). There are minima at Ly-α, the 2.66 μm water band, and at 557 GHz, indicating that these are the most promising places to try for future detections, although none of the space telescopes used to make the sensitive detections at these wavelengths (PROCYON/LAICA, Akari, Herschel) remain operational today. Of the ground-based observations, the most promising is the detection of the 3080 Å OH band with the photometer at the Lowell 1.1 m.

To enable a slightly fairer comparison between the different telescopes, we further scaled the exposure times to the same diameter of telescope. This also involves the significant assumption that telescope sensitivity can simply be scaled by collecting area, and obviously ignores the fact that a 10 m radio dish is a much cheaper instrument than a 10 m optical telescope. For comparison, we chose to scale the observations to a 30 cm diameter telescope (Fig. 6), as could be imagined in a relatively cheap space telescope in Earth orbit (e.g., the ESA S-class CHEOPS). Here the strong Lyα bands are clear winners, which is not surprising given the small size of current telescopes at this wavelength, but this ignores the significant background issues in these observations—S/N will not scale directly with telescope collecting area in this case. The NIR region continues to be promising, and a small-to-mid-sized space telescope covering 2.66 μm could be of use for a broad survey of weak outgassing. In the immediate future, the JWST will cover this range, but will not be used for broad surveys (see Sect. 8).

7 Rosetta

The recent ESA mission Rosetta has been transformative in cometary science, which includes implications for MBCs, at least by providing a very detailed source of information on a JFC for comparison. In this section, we briefly review some of the more relevant findings, in particular considering the early phase of the mission, when Rosetta first encountered comet 67P as its activity was only just starting. We are still in the early days of analysis of Rosetta data, but a review of some of the key results to date is presented by Taylor et al. (2017).

Rosetta entered orbit around 67P in August 2014, when the comet was at 3.6 au from the Sun, but was already able to study the beginning of activity while approaching using its remote sensing instruments, with the first detections of the comet and its dust in images taken as early as March 2014 (Tubiana et al. 2015). The first detection of the gas coma was through sub-mm observations of the 557 GHz water band by the MIRO instrument, in June 2014 at 3.9 au from the Sun, when the spacecraft was around half a million km from the comet (Gulkis et al. 2015). At this time the water production rate was slightly below the strongest limits on MBCs to date, at 1×10^{25} mol s^{-1}, and outgassing was not detectable from Earth (via sensitive searches for CN with large telescopes—Snodgrass et al. 2016; Opitom et al. 2017). This is the lowest activity comet environment ever visited by a spacecraft, with all previous mission performing fast flybys at $\sim$ 1 au, and there were some surprising results: the Rosetta Plasma Consortium instruments discovered oscillations in the magnetic field at around 40 mHz attributed to interactions with cometary ions and the solar wind (Richter et al. 2015), the so-called 'singing comet' based on the public release of an audio version of this interaction. Feldman et al. (2015) show that emission lines from atomic hydrogen and oxygen, observed by the Alice instrument in the UV, could only be explained by electron impact dissociation rather than the more typical photodissociation seen in cometary comae. This effect was also necessary to explain the morphology of the gas in the inner coma, as imaged by the OSIRIS cameras (Bodewits et al. 2016). Both of these effects were no longer detectable closer to perihelion, when the comet had a more typical activity.

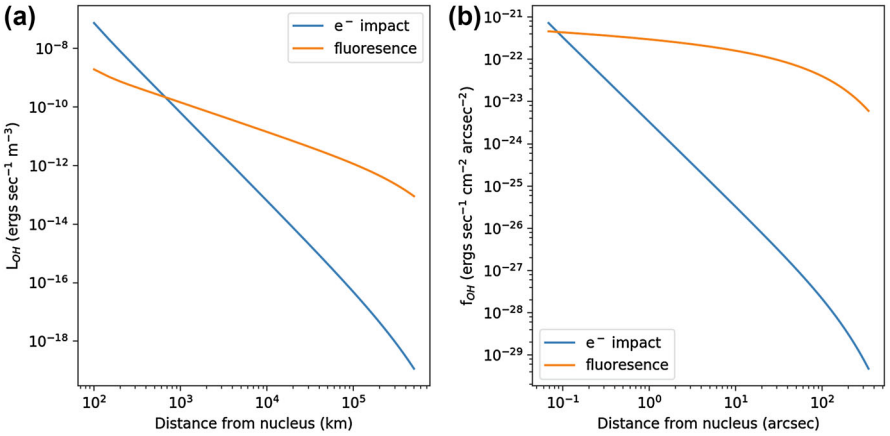

Fig. 7 **a** Calculated specific intensities of the OH(0–0) band at 3080 Å due to both fluorescence and prompt emission following electron impact dissociation of water, as a function of radial distance from the nucleus. The underlying H_2O and OH densities were calculated assuming a Haser model with $Q(H_2O) = 10^{24}$mol.s^{-1}. **b** Integrated surface brightness profiles observed at Earth derived from this model, assuming the MBC is at $r = 3$ au, $\Delta = 2$ au

An MBC with activity levels similar to, or even lower than, 67P at ~ 3.5 au, could be expected to show similar physics. While testing its interaction with the solar wind will require in situ probing with a spacecraft equipped with a magnetometer, it is probable that electron impacts would affect the observed emission in gas lines. To estimate the magnitude of this effect, we assume that electron impact dissociation of H_2O into the $A^2\Sigma^+$ state of OH takes place, followed by prompt emission to the ground state $X^2\Pi$. The increase in extra emission is extremely sensitive to the production rate of water, as the photoionisation of H_2O is expected to be the primary source of electrons in the inner coma. Scaling the conditions at 67P to an MBC at $\sim$ 3.0 au with a production rate of $Q(H_2O) = 10^{24}$ mol s^{-1}, the specific luminosity of the OH coma in ergs cm^{-2} s^{-1} is shown in Fig. 7. We model the density distribution using a simple Haser model, and scale the Rosetta measured electron density distribution to estimate the electron impact-induced emission using the technique described in Bodewits et al. (2016). A nearby spacecraft should be sensitive to this emission. However, integrating this luminosity distribution into potential surface brightnesses as seen from Earth shows that while a significant brightness enhancement exists, it is located within 1 arcsec of the MBC at low apparent flux levels.

Aside from exploring a very low activity comet environment, Rosetta is also important in the context of MBCs as it reveals a larger picture of comet formation. The full implications are likely to be debated for some time as further analysis of the Rosetta data is performed, but first attempts to model comet formation based on Rosetta results (e.g., Davidsson et al. 2016) point to the low density/high porosity of the comet (Sierks et al. 2015) and the presence of hyper-volatile species such as O_2 and N_2 (Bieler et al. 2015; Rubin et al. 2015) to show that it must have formed far from the Sun and avoided significant heating during its formation and subsequent evolution. This must be significantly different to the MBC case discussed in Sect. 4, and further points to

an expected difference in the observed composition of outgassing species between MBCs and JFCs.

8 Future prospects

In this section, we consider what options we will have for searching for water in MBCs in the coming years, both from ground- and space-based observatories, and from proposed dedicated space missions.

8.1 Ground-based telescopes

It is worth considering if a traditional photoelectric photometer mounted on a large telescope might allow successful detection of gas from an MBC. A photometer performs like a single large pixel, allowing it to achieve a particular signal-to-noise more efficiently than a CCD, where the noise associated with bias and readout becomes significant due to the large number of pixels in an aperture. Assuming a system could be scaled up directly, a photometer on a 10 m class telescope would provide a factor of $\sim$ 100 improvement over existing facilities, e.g., the 1.1 m telescope at Lowell Observatory used by D. Schleicher. Knight and Schleicher (2015) detected CN in 30 min on comet C/2012 S1 ISON at $r = 4.55$ au with a production rate of Q(CN) $\sim 10^{24}$ mol s^{-1}, near the limit for this instrument. This implies a hypothetical detection capability of $10^{21} - 10^{22}$ mol s^{-1} when accounting for the larger mirror, longer integrations, and an MBC at smaller r and Δ. Such production rates are near or somewhat below the most restrictive upper limits placed on MBC activity to date (as discussed in Sect. 5). Although the capabilities are promising, the lack of spatial context needed to definitively detect a very faint coma near a relatively bright nucleus likely makes a photometer a sub-optimal choice.

We briefly consider narrowband imaging with a CCD, which would have advantages over a photometer in providing spatial context, having generally higher quantum efficiency, and offering the possibility of selecting arbitrarily sized apertures. However, despite the very low read noise of modern CCDs, the small number of photons spread across a very large number of pixels makes the detection of faint gas emission via imaging relatively inefficient: with a blue optimised system and judicious binning, a CCD on a 10 m may be able to go 1–2 orders of magnitude fainter than a photometer on a 1 m with the same exposure times. However, this still likely underperforms the hypothetical photometer on a 10 m by about an order of magnitude.

With the start of scientific operations of the Atacama Large Millimetre/submillimetre Array (ALMA) interferometer in the second half of 2011, several observations of moderately bright Oort Cloud comets have been carried out with high sensitivity and high spatial resolution (e.g., observations of HNC, HCN, H_2CO and CH_3OH; Cordiner et al. 2014, 2017). As of 2017, ALMA consists of 43 12 m antennas and has unique capabilities to probe the physical and chemical structure of the innermost regions of the coma with great accuracy, providing new impetus to theoretical investigations of the coma. Spatially resolved observations allow for study of asymmetric outgassing, acceleration and cooling of the coma gases, and variations in gas kinetic temperature

resulting in greatly improved accuracy of the derived molecular abundances. In addition, the release site of a given cometary species, whether the nucleus or an extended source in the coma, can be constrained by measuring the spatial distribution in the inner coma on scales of the order of 1000 km from the nucleus for a compact array configuration.

Beginning in the second half of ALMA observing cycle 5 in early 2018, the newly installed Band 5 dual polarisations receivers, covering the frequency range 157–212 GHz, will become available creating exciting new observational possibilities. By providing a sensitive access to rotational transitions from H_2O and its isotopologues, ALMA has the capability to measure isotopic ratios in H_2O to test for the thermal and radiative processing history. These observations will contribute to our understanding of where and how cometary materials originated, as well as offering insight into the physical and chemical conditions of the solar nebula. Based on the upper limits on the H_2O of $< 4 \times 10^{25}$mol.s^{-1} and $< 7.6 \times 10^{25}$mol.s^{-1} for MBCs 176P and P/2012 T1 obtained by Herschel (de Val-Borro et al. 2012; O'Rourke et al. 2013), the total estimated time for a $< 4 \times 10^{25}$mol.s^{-1} detection of the H_2O 3_{13}–2_{20} emission line at 183.310 GHz with ALMA is 80 h including calibration overheads. These observations require excellent weather conditions with precipitable water vapour in the atmosphere < 0.4mm. Therefore, ALMA does not offer a promising way to detect water in MBCs for sensitivity reasons, unless a new MBC is discovered that is 10 times brighter than the ones observed by Herschel.

The next generation of extremely large telescopes (ELTs) are primarily designed to work at red optical and NIR wavelengths. For the 39 m ESO ELT, currently scheduled to be commissioned in 2024, the low- and intermediate-dispersion HARMONI spectrograph will have a wavelength coverage of $0.47 - 2.45$ μm, missing the primary fluorescence bands of OH(0–0) and CN(0–0). The 30 m Giant Magellan Telescope, scheduled for commissioning in 2022, will have the low/intermediate resolution spectrograph GMACS and the high-resolution spectrograph G-CLEF, both of which will operate at $0.35 - 0.95$ μm and will be sensitive to CN(0–0). The proposed thirty meter telescope would have the wide field optical spectrometer (WFOS) as a first light instrument, operating at $0.31 - 1.0$ μm. Hence it would miss the primary OH(0–0) band, although it would allow detection of the OH(1-0) band which has a relative brightness of 5–10% depending on the distance and heliocentric velocity of the MBC.

8.2 Space telescopes

With sensitivity in the NIR region, the JWST, a 6.5 m telescope orbiting the Earth–Sun L2 point, may provide our most immediate opportunity to directly detect water in an MBC coma (Kelley et al. 2016). The two brightest fluorescence bands of water are the ν_3 band at 2.7 μm and the ν_2 band at 6.3 μm, with fluorescence band g-factors near 3.2×10^{-4} and 2.4×10^{-4} s^{-1}, respectively, when opacity effects are neglected (Crovisier and Encrenaz 1983; Bockelée-Morvan et al. 2009; Debout et al. 2016). JWST has spectral sensitivity at both bands: the NIRSpec instrument covers 2.7 μm at spectral resolving powers, $R = \Delta\lambda/\lambda$, of ~ 100, ~ 1000, or ~ 2700; and MIRI covers 6.3 μm with $R \sim 70$ and ~ 3500 (Kendrew et al. 2015; Wells et al. 2015).

In general for comets and dark asteroids, the 2–3 μm region has a lower continuum flux than the 6–7 μm region, due to the low albedos of dust and surfaces. In addition, the sky background is stronger at the longer wavelengths due to zodiacal dust. Thus, given the similarities in band g-factors, the ν_3 band should be easier to observe in a MBC coma. We ran a JWST exposure time simulation with a NIRSpec fixed-slit (0.4 arcsec wide) and a V=19 mag MBC at $r = 2.7$ au, producing water with a rate of 10^{25} mol s^{-1}. The continuum would be detected with an SNR of 45 in 1 h. Assuming the brightest water lines are about one-tenth the total band flux ($\sim 1 \times 10^{-17}$ erg s^{-1} cm^{-2} in a 0.2 arcsec radius aperture), they may be detected with a peak signal-to-noise ratio of about 3 above the continuum in 10^4 s of integration time. This is a challenging observation, but with the right target and production rate, a direct water detection should be possible.

A Far-Infrared (Far-IR) Surveyor mission concept for NASA's 2020 Astrophysics Decadal Survey has been proposed recently (Meixner et al. 2016). Originally envisaged in NASA's 2013 Roadmap, this mission intends to build upon previous successful space and airborne infrared astronomy observatories such as ISO, Spitzer, Herschel, SOFIA and JWST. The mission will have a single large aperture telescope or an interferometer with a large gain in sensitivity of about 10^3–10^4 over the Herschel Space Observatory, and better angular resolution. The Far-IR Surveyor will be able to detect both water vapour and water ice, using the 43 μm water–ice band and a large number of water bands, as well as other volatile molecules. In small bodies in the Solar System, the Far-IR Surveyor can be used to detect gas sublimation and accurately measure the water production rates. Direct detection of water in MBCs will be possible with sensitivity to production rates of 10^{22}mols^{-1} at a heliocentric distance of 2.5 au. Alternatively, preliminary work continues for a future large UV/optical space telescope, with a 10–15 m diameter. Variously known as HDST or LUVIOR, details are not yet well known, but this will be very sensitive to many gas emission features, and will certainly be useful in studying weakly active comets, but is many years from becoming reality (Dalcanton et al. 2015).

An alternative approach to building increasingly large space telescopes is to take a small space telescope closer to the MBCs. CASTAway was recently proposed (as an ESA medium class mission) to launch a 50 cm diameter telescope, equipped with a low-resolution spectrograph covering 0.6–5 μm and a CCD camera, into an orbit that loops through the asteroid belt (Bowles et al. 2017). This mission is primarily designed to map the diversity of bodies in the asteroid belt, by performing a spectroscopic survey of more than 10 000 asteroids of all sizes and close flybys of 10–20 diverse objects. Even if an MBC cannot be one of the flyby targets (the relatively small size of the population makes it unlikely that a suitable multi-asteroid tour can include one), the telescope is designed to search for ice or outgassing, in the NIR through spectroscopy or via OH emission in the UV through narrowband imaging. The advantage of a dedicated survey mission, compared with JWST or other major facilities, is that many more potentially ice bodies can be targeted. Placing a telescope in the asteroid belt has the advantage that all sizes of asteroid can be targeted, and also presents unique viewing geometries. For MBCs, such view points can be useful to characterise dust tails, as was demonstrated by imaging P/2010 A2 with the OSIRIS cameras on Rosetta

(Snodgrass et al. 2010b)—any camera on any mission passing through the asteroid belt can potentially contribute to MBC dust trail characterisation as a target of opportunity.

8.3 Missions to MBCs

These various planned and proposed telescope facilities show that, while challenging, the detection of water outgassing from MBCs may be achieved in the near future. However, further detailed exploration of the water content of these bodies, and especially more challenging observations such as measurement of isotopic ratios (e.g., D/H in water), will be beyond even the next generation of telescope facilities. Investigating D/H, and the associated constraints on where in the Solar System planetary disc the ice condensed, will require in situ measurement. Missions to visit MBCs have been proposed for this purpose, to both ESA and NASA.

The European proposal Castalia would follow on from ESA's success with Rosetta, and take copies of some of the same key instruments, including the sensitive ROSINA mass spectrometer, to 133P. The mission is described in detail by Snodgrass et al. (2017a), but in summary this would be a rendezvous mission launched in the late 2020s, to arrive before 133P's 2035 perihelion. Its instrument complement comprises visible, NIR, and thermal IR cameras; mass spectrometers sensitive to neutral and ionised gas; a dust instrument that combines the strengths of the Rosetta GIADA and COSIMA instruments to study flux and composition of grains; a sensitive magnetometer and plasma package; and two ground-penetrating radars. Castalia would perform a detailed characterisation of the nucleus, including quantifying the amount and depth of buried ice via the first sub-surface radar measurements at a small body, and directly 'sniff' the escaping gas, measuring its composition at an isotopic level. Combining results from the similar Castalia and Rosetta instruments would allow very direct comparison between an MBC and JFC. As a proposal for the M-class of ESA missions Castalia is necessarily a simpler spacecraft than Rosetta (it does not carry a lander, for example), but the low activity and more circular orbit of MBCs helps make the mission 'easier'. The proposal is under consideration in September 2017, with the shortlist for phase A study for the ESA M5 call expected to be announced in December 2017.

A similar, but even more bare-essentials approach is taken by the proposed NASA Discovery mission Proteus (Meech and Castillo-Rogez 2015). This mission concentrates on its ability to measure composition and isotopy at very high precision in the low activity MBC environment, with the only other instrument (apart from the sensitive mass spectrometer) being a camera for context and surface characterisation. The core scientific motivation is testing whether or not the water in MBCs has an isotopic match to Earth's oceans. It was proposed to visit 238P in the last NASA Discovery round, and although not selected on that occasion is expected to be reproposed in a future round.

Finally, a proposed mission to an earlier round of ESA M-class missions aimed to not only visit an MBC, but to return a sample of dust from it, capturing this in aerogel during a flyby in the same way the NASA Stardust mission did at comet 81P/Wild 2. Although this mission (Caroline—Jones et al. 2017) would not have been sensitive to the volatile component of the MBC, the opportunity to apply sensitive laboratory

techniques to grains would certainly be revealing about the origins of the parent body. Currently the in situ investigation of volatiles is seen as the priority, with many of the Caroline team working on the Castalia proposal instead, but this concept remains interesting to investigate further in the future.

9 Conclusions

The repeated activity of MBCs is strong evidence that there is buried ice in numerous small asteroids in the MB, despite surface temperatures being too high for it to be stable. Thermal models suggest that this ice is buried up to $\sim$ 30 m deep, but it is thought that impacts could excavate enough of the insulating layer to allow periods of activity. Outgassing from this activity will produce characteristic spectral features across a wide range of wavelengths, from the UV to radio, but attempts to detect these in MBCs have not yet succeeded. Given the low activity levels expected from MBCs, it appears that this detection is beyond the capabilities of current telescope technology, but may be achievable in the coming years with new facilities, in particular the JWST. The 2.7 μm and 557 GHz water bands, and possibly UV observations of hydrogen (Ly-α) and OH, appear to be the most promising regions of the spectrum to attempt detections. To get more detailed information, such as the isotopic ratios that can answer questions on the relevance of MBCs as a source of Earth's water, or their original formation location in the protoplanetary disc, will require *in situ* investigation via a spacecraft visit.

Acknowledgements This work is a direct result of support by the International Space Science Institute, Bern, Switzerland, through the hosting and provision of financial support for an international team to discuss the science of MBCs. CS is supported by the UK STFC as a Rutherford fellow. AF was supported by UK STFC grant ST/L000709/1. HHH and MMK were supported by NASA Solar System Observations grant NNX16AD68G. MTH is financially supported by David Jewitt. MdVB was supported by NASA's Planetary Astronomy Program. MC is supported by NASA Solar System Observations Grant NNX15AJ81G. We thank Dave Schleicher for useful discussions. We made use of the Planetary Spectrum Generator developed by Geronimo Villanueva at NASA's Goddard Space Flight Center, and thank Geronimo for making this useful service available to the community.

References

Agarwal J, Jewitt D, Weaver H, Mutchler M, Larson S (2016) Hubble and Keck telescope observations of active asteroid 288P/300163 (2006 VW139). Astron J 151:12. https://doi.org/10.3847/0004-6256/151/1/12. arXiv:1510.07629

A'Hearn MF, Feldman PD (1992) Water vaporization on Ceres. Icarus 98:54–60. https://doi.org/10.1016/0019-1035(92)90206-M

A'Hearn MF, Schleicher DG, Millis RL, Feldman PD, Thompson DT (1984) Comet bowell 1980b. Astron J 89:579–591. https://doi.org/10.1086/113552

A'Hearn MF, Millis RC, Schleicher DO, Osip DJ, Birch PV (1995) The ensemble properties of comets: results from narrowband photometry of 85 comets, 1976–1992. Icarus 118:223–270. https://doi.org/10.1006/icar.1995.1190

A'Hearn MF, Feaga LM, Keller HU, Kawakita H, Hampton DL, Kissel J, Klaasen KP, McFadden LA, Meech KJ, Schultz PH, Sunshine JM, Thomas PC, Veverka J, Yeomans DK, Besse S, Bodewits D, Farnham TL, Groussin O, Kelley MS, Lisse CM, Merlin F, Protopapa S, Wellnitz DD (2012) Cometary volatiles and the origin of comets. Astrophys J 758:29

Altwegg K, Balsiger H, Bar-Nun A, Berthelier JJ, Bieler A, Bochsler P, Briois C, Calmonte U, Combi M, De Keyser J, Eberhardt P, Fiethe B, Fuselier S, Gasc S, Gombosi TI, Hansen KC, Hässig M, Jäckel A, Kopp E, Korth A, LeRoy L, Mall U, Marty B, Mousis O, Neefs E, Owen T, Rème H, Rubin M, Sémon T, Tzou CY, Waite H, Wurz P (2015) 67P/Churyumov-Gerasimenko, a Jupiter family comet with a high D/H ratio. Science 347(27):1261952. https://doi.org/10.1126/science.1261952

Armstrong JC, Titus TN, Kieffer HH (2005) Evidence for subsurface water ice in Korolev crater, Mars. Icarus 174:360–372. https://doi.org/10.1016/j.icarus.2004.10.032

Atreya SK, Wong AS (2005) Coupled clouds and chemistry of the giant planets—a case for multiprobes. Space Sci Rev 116:121–136. https://doi.org/10.1007/s11214-005-1951-5

Baines KH, Delitsky ML, Momary TW, Brown RH, Buratti BJ, Clark RN, Nicholson PD (2009) Storm clouds on Saturn: lightning-induced chemistry and associated materials consistent with Cassini/VIMS spectra. Planet Space Sci 57:1650–1658. https://doi.org/10.1016/j.pss.2009.06.025

Balsiger H, Altwegg K, Geiss J (1995) D/H and O-18/O-16 ratio in the hydronium ion and in neutral water from in situ ion measurements in comet Halley. J Geophys Res 100:5827–5834. https://doi.org/10.1029/94JA02936

Barlow NG, Allen RA, Vilas F (1999) Mercurian impact craters: implications for polar ground ice. Icarus 141:194–204. https://doi.org/10.1006/icar.1999.6165

Barucci MA, Brown ME, Emery JP, Merlin F (2008) Composition and surface properties of trans-Neptunian objects and Centaurs. In: Barucci MA, Boehnhardt H, Cruikshank DP, Morbidelli A (eds) The solar system beyond Neptune. University of Arizona press, Tucson, pp 143–160

Barucci MA, Alvarez-Candal A, Merlin F, Belskaya IN, de Bergh C, Perna D, DeMeo F, Fornasier S (2011) New insights on ices in Centaur and transneptunian populations. Icarus 214:297–307

Bertaux JL, Costa J, Quémerais E, Lallement R, Berthé M, Kyrölä E, Schmidt W, Summanen T, Makinen T, Goukenleuque C (1998) Lyman-alpha observations of comet Hyakutake with SWAN on SOHO. Planet Space Sci 46:555–568. https://doi.org/10.1016/S0032-0633(97)00179-7

Bertini I (2011) Main Belt Comets: a new class of small bodies in the Solar System. Planet Space Sci 59(5–6):365–377. https://doi.org/10.1016/j.pss.2011.01.014

Bibring JP, Langevin Y, Poulet F, Gendrin A, Gondet B, Berthé M, Soufflot A, Drossart P, Combes M, Bellucci G, Moroz V, Mangold N, Schmitt B, Team OMEGA, Erard S, Forni O, Manaud N, Poulleau G, Encrenaz T, Fouchet T, Melchiorri R, Altieri F, Formisano V, Bonello G, Fonti S, Capaccioni F, Cerroni P, Coradini A, Kottsov V, Ignatiev N, Titov D, Zasova L, Pinet P, Sotin C, Hauber E, Hoffman H, Jaumann R, Keller U, Arvidson R, Mustard J, Duxbury T, Forget F (2004) Perennial water ice identified in the south polar cap of Mars. Nature 428:627–630. https://doi.org/10.1038/nature02461

Bibring JP, Langevin Y, Mustard JF, Poulet F, Arvidson R, Gendrin A, Gondet B, Mangold N, Pinet P, Forget F, Team OMEGA, Berthé M, Gomez C, Jouglet D, Soufflot A, Vincendon M, Combes M, Drossart P, Encrenaz T, Fouchet T, Merchiorri R, Belluci G, Altieri F, Formisano V, Capaccioni F, Cerroni P, Coradini A, Fonti S, Korablev O, Kottsov V, Ignatiev N, Moroz V, Titov D, Zasova L, Loiseau D, Pinet P, Doute S, Schmitt B, Sotin C, Hauber E, Hoffmann H, Jaumann R, Keller U, Arvidson R, Duxbury T, Neukum G (2006) Global mineralogical and aqueous mars history derived from OMEGA/Mars express data. Science 312:400–404. https://doi.org/10.1126/science.1122659

Bieler A, Altwegg K, Balsiger H, Bar-Nun A, Berthelier JJ, Bochsler P, Briois C, Calmonte U, Combi M, de Keyser J, van Dishoeck EF, Fiethe B, Fuselier SA, Gasc S, Gombosi TI, Hansen KC, Hässig M, Jäckel A, Kopp E, Korth A, Le Roy L, Mall U, Maggiolo R, Marty B, Mousis O, Owen T, Rème H, Rubin M, Sémon T, Tzou CY, Waite JH, Walsh C, Wurz P (2015) Abundant molecular oxygen in the coma of comet 67P/Churyumov-Gerasimenko. Nature 526:678–681. https://doi.org/10.1038/nature15707

Biver N, Bockelée-Morvan D, Crovisier J, Colom P, Henry F, Moreno R, Paubert G, Despois D, Lis DC (2002) Chemical composition diversity among 24 comets observed at radio wavelengths. Earth Moon Planets 90:323–333

Biver N, Bockelée-Morvan D, Crovisier J, Lecacheux A, Frisk U, Hjalmarson k, Olberg M, Florn HG, Sandqvist A, Kwok S (2007) Submillimetre observations of comets with odin: 2001–2005. Planet Space Sci 55:1058–1068

Biver N, Crovisier J, Bockelée-Morvan D, Szutowicz S, Lis DC, Hartogh P, de Val-Borro M, Moreno R, Boissier J, Kidger M, Küppers M, Paubert G, Dello Russo N, Vervack R, Weaver H (2012) Ammonia

and other parent molecules in comet 10P/Tempel 2 from Herschel/HIFI and ground-based radio observations. Astron Astrophys 539:A68. https://doi.org/10.1051/0004-6361/201118447. arXiv:1201.4318

Biver N, Bockelée-Morvan D, Debout V, Crovisier J, Boissier J, Lis DC, Dello Russo N, Moreno R, Colom P, Paubert G, Vervack R, Weaver HA (2014) Complex organic molecules in comets C/2012 F6 (Lemmon) and C/2013 R1 (Lovejoy): detection of ethylene glycol and formamide. Astron Astrophys 566:L5. https://doi.org/10.1051/0004-6361/201423890. arXiv:1405.6605

Biver N, Hofstadter M, Gulkis S, Bockelée-Morvan D, Choukroun M, Lellouch E, Schloerb FP, Rezac L, Ip WH, Jarchow C, Hartogh P, Lee S, von Allmen P, Crovisier J, Leyrat C, Encrenaz P (2015) Distribution of water around the nucleus of comet 67P/Churyumov-Gerasimenko at 3.4 AU from the Sun as seen by the MIRO instrument on Rosetta. Astron Astrophys 583:A3. https://doi.org/10.1051/0004-6361/201526094

Bockelée-Morvan D (2008) Cometary science with ALMA. Astrophys Space Sci 313:183–189

Bockelée-Morvan D, Crovisier J, Mumma MJ, Weaver HA (2004) The composition of cometary volatiles. In: Festou M, Keller H, Weaver H (eds) Comets II. University of Arizona Press, Tucson, pp 391–423

Bockelée-Morvan D, Woodward CE, Kelley MS, Wooden DH (2009) Water in comets 71P/Clark and C/2004 B1 (Linear) with Spitzer. Astrophys J 696:1075–1083. https://doi.org/10.1088/0004-637X/696/2/1075. arXiv:0902.0759

Bockelée-Morvan D, Calmonte U, Charnley S, Duprat J, Engrand C, Gicquel A, Hässig M, Jehin E, Kawakita H, Marty B, Milam S, Morse A, Rousselot P, Sheridan S, Wirström E (2015) Cometary isotopic measurements. Space Sci Rev 197:47–83. https://doi.org/10.1007/s11214-015-0156-9

Bodewits D, Kelley MS, Li JY, Landsman WB, Besse S, A'Hearn MF (2011) Collisional excavation of asteroid (596) Scheila. Astrophys J 733:L3. https://doi.org/10.1088/2041-8205/733/1/L3. arXiv:1104.5227

Bodewits D, Lara LM, A'Hearn MF, La Forgia F, Gicquel A, Kovacs G, Knollenberg J, Lazzarin M, Lin ZY, Shi X, Snodgrass C, Tubiana C, Sierks H, Barbieri C, Lamy PL, Rodrigo R, Koschny D, Rickman H, Keller HU, Barucci MA, Bertaux JL, Bertini I, Boudreault S, Cremonese G, Da Deppo V, Davidsson B, Debei S, De Cecco M, Fornasier S, Fulle M, Groussin O, Gutiérrez PJ, Güttler C, Hviid SF, Ip WH, Jorda L, Kramm JR, Kührt E, Küppers M, López-Moreno JJ, Marzari F, Naletto G, Oklay N, Thomas N, Toth I, Vincent JB (2016) Changes in the physical environment of the inner coma of 67P/Churyumov-Gerasimenko with decreasing heliocentric distance. Astron J 152:130. https://doi.org/10.3847/0004-6256/152/5/130. arXiv:1607.05632

Bottke WF, Durda DD, Nesvorný D, Jedicke R, Morbidelli A, Vokrouhlický D, Levison HF (2005) Linking the collisional history of the main asteroid belt to its dynamical excitation and depletion. Icarus 179:63–94. https://doi.org/10.1016/j.icarus.2005.05.017

Bowles N, Snodgrass C, Gibbings A, Sanchez JP, Arnold J, Eccleston P, Andert T, Probst A, Naletto G, Vandaele AC, de Leon J, Nathues A, Thomas I, Thomas N, Jorda L, Da Deppo V, Haack H, Green SF, Carry B, Donaldson Hanna KL, Jorgensen JL, Kereszturi A, Demeo FE, Patel M, Davies J, Clarke F, Kinch K, Guilbert-Lepoutre A, Agarwal J, Rivkin AS, Pravec P, Fornasier S, Granvik M, Jones R, Murdoch N, Joy K, Pascale E, Tecza M, Barnes JM, Licandro J, Greenhagen BT, Calcutt S, Marriner C, Warren T, Tosh I (2017) CASTAway: an asteroid main belt tour and survey. Adv Space Res (**submitted**)

Brearley AJ, Jones RH (1998) Chondritic meteorites, Reviews in Mineralogy, vol 36. Mineralogical Society of America, p C1

Brown AJ, Byrne S, Tornabene LL, Roush T (2008) Louth crater: evolution of a layered water ice mound. Icarus 196:433–445. https://doi.org/10.1016/j.icarus.2007.11.023. arXiv:1401.8024

Brown ME, Calvin WM (2000) Evidence for crystalline water and ammonia ices on Pluto's satellite charon. Science 287:107–109

Brown ME, Trujillo CA, Rabinowitz DL (2005) Discovery of a planetary-sized object in the scattered Kuiper Belt. Astrophys J 635:L97–L100

Brownlee D, Tsou P, Aléon J, Alexander CMO, Araki T, Bajt S, Baratta GA, Bastien R, Bland P, Bleuet P, Borg J, Bradley JP, Brearley A, Brenker F, Brennan S, Bridges JC, Browning ND, Brucato JR, Bullock E, Burchell MJ, Busemann H, Butterworth A, Chaussidon M, Cheuvront A, Chi M, Cintala MJ, Clark BC, Clemett SJ, Cody G, Colangeli L, Cooper G, Cordier P, Daghlian C, Dai Z, D'Hendecourt L, Djouadi Z, Dominguez G, Duxbury T, Dworkin JP, Ebel DS, Economou TE, Fakra S, Fairey SAJ, Fallon S, Ferrini G, Ferroir T, Fleckenstein H, Floss C, Flynn G, Franchi IA, Fries M, Gainsforth Z, Gallien JP, Genge M, Gilles MK, Gillet P, Gilmour J, Glavin DP, Gounelle M, Grady MM, Graham GA, Grant PG, Green SF, Grossemy F, Grossman L, Grossman JN, Guan Y, Hagiya K, Harvey R, Heck P, Herzog GF, Hoppe P, Hörz F, Huth J, Hutcheon ID, Ignatyev K, Ishii H, Ito M, Jacob D,

Jacobsen C, Jacobsen S, Jones S, Joswiak D, Jurewicz A, Kearsley AT, Keller LP, Khodja H, Kilcoyne ALD, Kissel J, Krot A, Langenhorst F, Lanzirotti A, Le L, Leshin LA, Leitner J, Lemelle L, Leroux H, Liu MC, Luening K, Lyon I, MacPherson G, Marcus MA, Marhas K, Marty B, Matrajt G, McKeegan K, Meibom A, Mennella V, Messenger K, Messenger S, Mikouchi T, Mostefaoui S, Nakamura T, Nakano T, Newville M, Nittler LR, Ohnishi I, Ohsumi K, Okudaira K, Papanastassiou DA, Palma R, Palumbo ME, Pepin RO, Perkins D, Perronnet M, Pianetta P, Rao W, Rietmeijer FJM, Robert F, Rost D, Rotundi A, Ryan R, Sandford SA, Schwandt CS, See TH, Schlutter D, Sheffield-Parker J, Simionovici A, Simon S, Sitnitsky I, Snead CJ, Spencer MK, Stadermann FJ, Steele A, Stephan T, Stroud R, Susini J, Sutton SR, Suzuki Y, Taheri M, Taylor S, Teslich N, Tomeoka K, Tomioka N, Toppani A, Trigo-Rodríguez JM, Troadec D, Tsuchiyama A, Tuzzolino AJ, Tyliszczak T, Uesugi K, Velbel M, Vellenga J, Vicenzi E, Vincze L, Warren J, Weber I, Weisberg M, Westphal AJ, Wirick S, Wooden D, Wopenka B, Wozniakiewicz P, Wright I, Yabuta H, Yano H, Young ED, Zare RN, Zega T, Ziegler K, Zimmerman L, Zinner E, Zolensky M (2006) Comet 81P/Wild 2 under a microscope. Science 314:1711. https://doi.org/10.1126/science.1135840

Burns RG (1981) Intervalence transitions in mixed-valence minerals of iron and titanium. Ann Rev Earth Planet Sci 9:345

Bus SJ, Binzel RP (2002) Phase II of the small main-belt asteroid spectroscopic survey: a feature-based taxonomy. Icarus 158:146–177

Campins H, Hargrove K, Pinilla-Alonso N, Howell ES, Kelley MS, Licandro J, Mothé-Diniz T, Fernández Y, Ziffer J (2010) Water ice and organics on the surface of the asteroid 24 Themis. Nature 464:1320–1321. https://doi.org/10.1038/nature09029

Capria MT, Marchi S, de Sanctis MC, Coradini A, Ammannito E (2012) The activity of Main Belt Comets. Astron Astrophys 537:A71. https://doi.org/10.1051/0004-6361/201117556. arXiv:1111.5699

Carr MH, Belton MJS, Chapman CR, Davies ME, Geissler P, Greenberg R, McEwen AS, Tufts BR, Greeley R, Sullivan R, Head JW, Pappalardo RT, Klaasen KP, Johnson TV, Kaufman J, Senske D, Moore J, Neukum G, Schubert G, Burns JA, Thomas P, Veverka J (1998) Evidence for a subsurface ocean on Europa. Nature 391:363. https://doi.org/10.1038/34857

Carry B, Snodgrass C, Lacerda P, Hainaut O, Dumas C (2012) Characterisation of candidate members of (136108) Haumea's family. II. Follow-up observations. Astron Astrophys 544:A137. https://doi.org/10.1051/0004-6361/201219044. arXiv:1207.6491

Castillo-Rogez JC, Schmidt BE (2010) Geophysical evolution of the Themis family parent body. Geophys Res Lett 37:L10202. https://doi.org/10.1029/2009GL042353

Cernicharo J, Crovisier J (2005) Water in space: the water world of ISO. Space Sci Rev 119:29–69

Cessateur G, Keyser JD, Maggiolo R, Gibbons A, Gronoff G, Gunell H, Dhooghe F, Loreau J, Vaeck N, Altwegg K, Bieler A, Briois C, Calmonte U, Combi MR, Fiethe B, Fuselier SA, Gombosi TI, Hässig M, Le Roy L, Neefs E, Rubin M, Sémon T (2016) Photochemistry of forbidden oxygen lines in the inner coma of 67P/Churyumov-Gerasimenko. J Geophys Res (Space Physics) 121:804–816. https://doi.org/10.1002/2015JA022013

Cheng AF (2004) Collisional evolution of the asteroid belt. Icarus 169:357–372. https://doi.org/10.1016/j.icarus.2004.02.002

Chiu K, Neufeld DA, Bergin EA, Melnick GJ, Patten BM, Wang Z, Bockelée-Morvan D (2001) Post-perihelion SWAS observations of water vapor in the coma of comet C/1999 H1 (Lee). Icarus 154:345–349. https://doi.org/10.1006/icar.2001.6706

Clancy RT, Grossman AW, Muhleman DO (1992) Mapping Mars water vapor with the very large array. Icarus 100:48–59. https://doi.org/10.1016/0019-1035(92)90017-2

Clark RN (2009) Detection of adsorbed water and hydroxyl on the moon. Science 326:562–564. https://doi.org/10.1126/science.1178105

Cochran A, Barker E, Gray C (2012) Thirty years of cometary spectroscopy from McDonald Observatory. Icarus 218(1):144–168

Cochran AL, Vilas F (1997) The McDonald observatory serendipitous UV/blue spectral survey of asteroids. Icarus 127:121–129

Colangeli L, Epifani E, Brucato JR, Bussoletti E, De Sanctis C, Fulle M, Mennella V, Palomba E, Palumbo P, Rotundi A (1999) Infrared spectral observations of comet 103P/Hartley 2 by ISOPHOT. Astron Astrophys 343:L87–L90

Colaprete A, Schultz P, Heldmann J, Wooden D, Shirley M, Ennico K, Hermalyn B, Marshall W, Ricco A, Elphic RC, Goldstein D, Summy D, Bart GD, Asphaug E, Korycansky D, Landis D, Sollitt L (2010)

Detection of water in the LCROSS ejecta plume. Science 330:463. https://doi.org/10.1126/science.1186986

Combi MR, Brown ME, Feldman PD, Keller HU, Meier RR, Smyth WH (1998) Hubble space telescope ultraviolet imaging and high-resolution spectroscopy of water photodissociation products in comet Hyakutake (C/1996 B2). Astrophys J 494:816–821. https://doi.org/10.1086/305228

Combi MR, Cochran AL, Cochran WD, Lambert DL, Johns-Krull CM (1999) Observation and analysis of high-resolution optical line profiles in comet Hyakutake (C/1996 B2). Astrophys J 512:961–968. https://doi.org/10.1086/306798

Combi MR, Bertaux JL, Quémerais E, Ferron S, Mäkinen JTT (2011a) Water production by comet 103P/Hartley 2 observed with the SWAN instrument on the SOHO spacecraft. Astrophys J 734:L6. https://doi.org/10.1088/2041-8205/734/1/L6. arXiv:1104.4906

Combi MR, Lee Y, Patel TS, Mäkinen JTT, Bertaux JL, Quémerais E (2011b) SOHO/SWAN observations of short-period spacecraft target comets. Astron J 141:128. https://doi.org/10.1088/0004-6256/141/4/128

Combi MR, Mäkinen JTT, Bertaux JL, Quémerais E, Ferron S, Fougere N (2013) Water production rate of comet C/2009 P1 (Garradd) throughout the 2011–2012 apparition: evidence for an icy grain halo. Icarus 225:740–748. https://doi.org/10.1016/j.icarus.2013.04.030

Cordiner MA, Remijan AJ, Boissier J, Milam SN, Mumma MJ, Charnley SB, Paganini L, Villanueva G, Bockelée-Morvan D, Kuan YJ, Chuang YL, Lis DC, Biver N, Crovisier J, Minniti D, Coulson IM (2014) Mapping the release of volatiles in the inner comae of comets C/2012 F6 (Lemmon) and C/2012 S1 (ISON) using the atacama large millimeter/submillimeter array. Astrophys J 792:L2. https://doi.org/10.1088/2041-8205/792/1/L2. arXiv:1408.2458

Cordiner MA, Biver N, Crovisier J, Bockelée-Morvan D, Mumma MJ, Charnley SB, Villanueva G, Paganini L, Lis DC, Milam SN, Remijan AJ, Coulson IM, Kuan YJ, Boissier J (2017) Thermal physics of the inner coma: ALMA studies of the methanol distribution and excitation in comet C/2012 K1 (PanSTARRS). Astrophys J 837:177. https://doi.org/10.3847/1538-4357/aa6211. arXiv:1701.08258

Crovisier J (1984) The water molecule in comets—fluorescence mechanisms and thermodynamics of the inner coma. Astron Astrophys 130:361–372

Crovisier J, Encrenaz T (1983) Infrared fluorescence of molecules in comets—the general synthetic spectrum. Astron Astrophys 126:170–182

Crovisier J, Leech K, Bockelée-Morvan D, Brooke TY, Hanner MS, Altieri B, Keller HU, Lellouch E (1997) The spectrum of comet Hale–Bopp (C/1995 01) observed with the infrared space observatory at 2.9 AU from the Sun. Science 275:1904–1907. https://doi.org/10.1126/science.275.5308.1904

Crovisier J, Colom P, Biver N, Bockelée-Morvan D, Boissier J (2013) Observations of the 18 cm OH lines of comet 103P/Hartley 2 at Nançay in support to the EPOXI and Herschel missions. Icarus 222:679–683. https://doi.org/10.1016/j.icarus.2012.03.033. arXiv:1203.6450

Cruikshank DP, Roush TL, Bartholomew MJ, Geballe TR, Pendleton YJ, White SM, Bell JF, Davies JK, Owen TC, de Bergh C, Tholen DJ, Bernstein MP, Brown RH, Tryka KA, Dalle Ore CM (1998) The composition of Centaur 5145 pholus. Icarus 135:389–407

Dalcanton J, Seager S, Aigrain S, Battel S, Brandt N, Conroy C, Feinberg L, Gezari S, Guyon O, Harris W, Hirata C, Mather J, Postman M, Redding D, Schiminovich D, Stahl HP, Tumlinson J (2015) From cosmic birth to living Earths: the future of UVOIR space astronomy. ArXiv e-prints arXiv:1507.04779

Dalle Ore CM, Barucci MA, Emery JP, Cruikshank DP, de Bergh C, Roush TL, Perna D, Merlin F, Dalle Ore LV (2015) The composition of "ultra-red" TNOS and Centaurs. Icarus 252:311–326

Davidsson BJR, Sierks H, Güttler C, Marzari F, Pajola M, Rickman H, A'Hearn MF, Auger AT, El-Maarry MR, Fornasier S, Gutiérrez PJ, Keller HU, Massironi M, Snodgrass C, Vincent JB, Barbieri C, Lamy PL, Rodrigo R, Koschny D, Barucci MA, Bertaux JL, Bertini I, Cremonese G, Da Deppo V, Debei S, De Cecco M, Feller C, Fulle M, Groussin O, Hviid SF, Höfner S, Ip WH, Jorda L, Knollenberg J, Kovacs G, Kramm JR, Kührt E, Küppers M, La Forgia F, Lara LM, Lazzarin M, Lopez Moreno JJ, Moissl-Fraund R, Mottola S, Naletto G, Oklay N, Thomas N, Tubiana C (2016) The primordial nucleus of comet 67P/Churyumov-Gerasimenko. Astron Astrophys 592:A63. https://doi.org/10.1051/0004-6361/201526968

Davies JK, Sykes MV, Cruikshank DP (1993) Near-infrared photometry and spectroscopy of the unusual minor planet 5145 pholus (1992ad). Icarus 102:166–169

Davies JK, Roush TL, Cruikshank DP, Bartholomew MJ, Geballe TR, Owen T, de Bergh C (1997) The detection of water ice in comet Hale–Bopp. Icarus 127:238–245

de Bergh C, Bezard B, Owen T, Crisp D, Maillard JP, Lutz BL (1991) Deuterium on Venus—observations from earth. Science 251:547–549. https://doi.org/10.1126/science.251.4993.547

de Graauw T, Helmich FP, Phillips TG, Stutzki J, Caux E, Whyborn ND, Dieleman P, Roelfsema PR, Aarts H, Assendorp R, Bachiller R, Baechtold W, Barcia A, Beintema DA, Belitsky V, Benz AO, Bieber R, Boogert A, Borys C, Bumble B, Caïs P, Caris M, Cerulli-Irelli P, Chattopadhyay G, Cherednichenko S, Ciechanowicz M, Coeur-Joly O, Comito C, Cros A, de Jonge A, de Lange G, Delforges B, Delorme Y, den Boggende T, Desbat JM, Diez-González C, di Giorgio AM, Dubbeldam L, Edwards K, Eggens M, Erickson N, Evers J, Fich M, Finn T, Franke B, Gaier T, Gal C, Gao JR, Gallego JD, Gauffre S, Gill JJ, Glenz S, Golstein H, Goulooze H, Gunsing T, Güsten R, Hartogh P, Hatch WA, Higgins R, Honingh EC, Huisman R, Jackson BD, Jacobs H, Jacobs K, Jarchow C, Javadi H, Jellema W, Justen M, Karpov A, Kasemann C, Kawamura J, Keizer G, Kester D, Klapwijk TM, Klein T, Kollberg E, Kooi J, Kooiman PP, Kopf B, Krause M, Krieg JM, Kramer C, Kruizenga B, Kuhn T, Laauwen W, Lai R, Larsson B, Leduc HG, Leinz C, Lin RH, Liseau R, Liu GS, Loose A, López-Fernandez I, Lord S, Luinge W, Marston A, Martín-Pintado J, Maestrini A, Maiwald FW, McCoey C, Mehdi I, Megej A, Melchior M, Meinsma L, Merkel H, Michalska M, Monstein C, Moratschke D, Morris P, Muller H, Murphy JA, Naber A, Natale E, Nowosielski W, Nuzzolo F, Olberg M, Olbrich M, Orfei R, Orleanski P, Ossenkopf V, Peacock T, Pearson JC, Peron I, Phillip-May S, Piazzo L, Planesas P, Rataj M, Ravera L, Risacher C, Salez M, Samoska LA, Saraceno P, Schieder R, Schlecht E, Schlöder F, Schmülling F, Schultz M, Schuster K, Siebertz O, Smit H, Szczerba R, Shipman R, Steinmetz E, Stern JA, Stokroos M, Teipen R, Teyssier D, Tils T, Trappe N, van Baaren C, van Leeuwen BJ, van de Stadt H, Visser H, Wildeman KJ, Wafelbakker CK, Ward JS, Wesselius P, Wild W, Wulff S, Wunsch HJ, Tielens X, Zaal P, Zirath H, Zmuidzinas J, Zwart F (2010) The Herschel-Heterodyne Instrument for the far-infrared (HIFI). Astron Astrophys 518:L6. https://doi.org/10.1051/0004-6361/201014698

de Kleer K, de Pater I, Ádámkovics M, Hammel H (2013) Near-infrared spectra of the Uranian ring system. Icarus 226:1038–1044. https://doi.org/10.1016/j.icarus.2013.07.016

De Sanctis MC, Capaccioni F, Ciarniello M, Filacchione G, Formisano M, Mottola S, Raponi A, Tosi F, Bockelée-Morvan D, Erard S, Leyrat C, Schmitt B, Ammannito E, Arnold G, Barucci MA, Combi M, Capria MT, Cerroni P, Ip WH, Kuehrt E, McCord TB, Palomba E, Beck P, Quirico E, Piccioni G, Bellucci G, Fulchignoni M, Jaumann R, Stephan K, Longobardo A, Mennella V, Migliorini A, Benkhoff J, Bibring JP, Blanco A, Blecka M, Carlson R, Carsenty U, Colangeli L, Combes M, Crovisier J, Drossart P, Encrenaz T, Federico C, Fink U, Fonti S, Irwin P, Langevin Y, Magni G, Moroz L, Orofino V, Schade U, Taylor F, Tiphene D, Tozzi GP, Biver N, Bonal L, Combe JP, Despan D, Flamini E, Fornasier S, Frigeri A, Grassi D, Gudipati MS, Mancarella F, Markus K, Merlin F, Orosei R, Rinaldi G, Cartacci M, Cicchetti A, Giuppi S, Hello Y, Henry F, Jacquinod S, Reess JM, Noschese R, Politi R, Peter G (2015) The diurnal cycle of water ice on comet 67P/Churyumov–Gerasimenko. Nature 525(7570):500–503. https://doi.org/10.1038/nature14869

de Val-Borro M, Hartogh P, Crovisier J, Bockelée-Morvan D, Biver N, Lis DC, Moreno R, Jarchow C, Rengel M, Szutowicz S, Banaszkiewicz M, Bensch F, Błęcka MI, Emprechtinger M, Encrenaz T, Jehin E, Küppers M, Lara LM, Lellouch E, Swinyard BM, Vandenbussche B, Bergin EA, Blake GA, Blommaert JADL, Cernicharo J, Decin L, Encrenaz P, de Graauw T, Hutsemékers D, Kidger M, Manfroid J, Medvedev AS, Naylor DA, Schieder R, Stam D, Thomas N, Waelkens C, Szczerba R, Saraceno P, di Giorgio AM, Philipp S, Klein T, Ossenkopf V, Zaal P, Shipman R (2010) Water production in comet 81P/Wild 2 as determined by Herschel/HIFI. Astron Astrophys 521:L50. https://doi.org/10.1051/0004-6361/201015161. arXiv:1007.0149

de Val-Borro M, Rezac L, Hartogh P, Biver N, Bockelée-Morvan D, Crovisier J, Küppers M, Lis DC, Szutowicz S, Blake GA, Emprechtinger M, Jarchow C, Jehin E, Kidger M, Lara LM, Lellouch E, Moreno R, Rengel M (2012) An upper limit for the water outgassing rate of the Main-Belt Comet 176P/LINEAR observed with Herschel/HIFI. Astron Astrophys 546:L4. https://doi.org/10.1051/0004-6361/201220169. arXiv:1208.5480

de Val-Borro M, Bockelée-Morvan D, Jehin E, Hartogh P, Opitom C, Szutowicz S, Biver N, Crovisier J, Lis DC, Rezac L, de Graauw T, Hutsemékers D, Jarchow C, Kidger M, Küppers M, Lara LM, Manfroid J, Rengel M, Swinyard BM, Teyssier D, Vandenbussche B, Waelkens C (2014) Herschel observations of gas and dust in comet C/2006 W3 (Christensen) at 5 AU from the Sun. Astron Astrophys 564:A124. https://doi.org/10.1051/0004-6361/201423427. arXiv:1404.4869

Debout V, Bockelée-Morvan D, Zakharov V (2016) A radiative transfer model to treat infrared molecular excitation in cometary atmospheres. Icarus 265:110–124. https://doi.org/10.1016/j.icarus.2015.10.013

Decock A, Jehin E, Hutsemékers D, Manfroid J (2013) Forbidden oxygen lines in comets at various heliocentric distances. Astron Astrophys 555:A34. https://doi.org/10.1051/0004-6361/201220414. arXiv:1210.0842

Despois D, Gerard E, Crovisier J, Kazes I (1981) The OH radical in comets—observation and analysis of the hyperfine microwave transitions at 1667 MHz and 1665 MHz. Astron Astrophys 99:320–340

Dones L, Gladman B, Melosh HJ, Tonks WB, Levison HF, Duncan M (1999) Dynamical lifetimes and final fates of small bodies: orbit integrations vs opik calculations. Icarus 142:509–524

Dones L, Brasser R, Kaib N, Rickman H (2015) Origin and evolution of the cometary reservoirs. Space Sci Rev 197:191–269. https://doi.org/10.1007/s11214-015-0223-2

Doyle PM, Jogo K, Nagashima K, Krot AN, Wakita S, Ciesla FJ, Hutcheon ID (2015) Early aqueous activity on the ordinary and carbonaceous chondrite parent bodies recorded by fayalite. Nat Commun 6:7444. https://doi.org/10.1038/ncomms8444

Drahus M, Jewitt D, Guilbert-Lepoutre A, Waniak W, Sievers A (2012) The sources of HCN and CH_3OH and the rotational temperature in comet 103P/Hartley 2 from time-resolved millimeter spectroscopy. Astrophys J 756:80. https://doi.org/10.1088/0004-637X/756/1/80. arXiv:1202.3194

Drake MJ, Righter K (2002) Determining the composition of the Earth. Nature 416:39–44. https://doi.org/10.1038/416039a

Dumas C, Carry B, Hestroffer D, Merlin F (2011) High-contrast observations of (136108) Haumea-A crystalline water–ice multiple system. Astron Astrophys 528:A105

Eke VR, Bartram SA, Lane DA, Smith D, Teodoro LFA (2014) Lunar polar craters—Icy, rough or just sloping? Icarus 241:66–78. https://doi.org/10.1016/j.icarus.2014.06.021. arXiv:1312.4749

Eke VR, Lawrence DJ, Teodoro LFA (2017) How thick are Mercury's polar water ice deposits? Icarus 284:407–415. https://doi.org/10.1016/j.icarus.2016.12.001. arXiv:1611.05395

Encrenaz T (2008) Water in the Solar System. Astron Astrophys Rev 46:57–87. https://doi.org/10.1146/annurev.astro.46.060407.145229

Encrenaz T, DeWitt C, Richter MJ, Greathouse TK, Fouchet T, Montmessin F, Lefèvre F, Forget F, Bézard B, Atreya SK, Case M, Ryde N (2016) A map of D/H on Mars in the thermal infrared using EXES aboard SOFIA. Astron Astrophys 586:A62. https://doi.org/10.1051/0004-6361/201527018

Feaga LM, A'Hearn MF, Farnham TL, Bodewits D, Sunshine JM, Gersch AM, Protopapa S, Yang B, Drahus M, Schleicher DG (2014) Uncorrelated volatile behavior during the 2011 apparition of comet C/2009 P1 Garradd. Astron J 147:24. https://doi.org/10.1088/0004-6256/147/1/24. arXiv:1311.4802

Feierberg MA, Lebofsky LA, Tholen DJ (1985) The nature of c-class asteroids from 3 micron spectrophotometry. Icarus 63:183–191

Feldman PD, Cochran AL, Combi MR (2004) Spectroscopic investigations of fragment species in the coma. In: Festou M, Keller H, Weaver H (eds) Comet II. University of Arizona Press, Tucson, pp 425–447

Feldman PD, A'Hearn MF, Bertaux JL, Feaga LM, Parker JW, Schindhelm E, Steffl AJ, Stern SA, Weaver HA, Sierks H, Vincent JB (2015) Measurements of the near-nucleus coma of comet 67P/Churyumov-Gerasimenko with the Alice far-ultraviolet spectrograph on Rosetta. Astron Astrophys 583:A8. https://doi.org/10.1051/0004-6361/201525925. arXiv:1506.01203

Fernández JA, Sosa A (2015) Jupiter family comets in near-Earth orbits: are some of them interlopers from the asteroid belt? Planet Space Sci 118:14–24. https://doi.org/10.1016/j.pss.2015.07.010

Fernández JA, Gallardo T, Brunini A (2002) Are there many inactive Jupiter-family comets among the near-Earth asteroid population? Icarus 159:358–368. https://doi.org/10.1006/icar.2002.6903

Fernandez YR, McFadden LA, Lisse CM, Helin EF, Chamberlin AB (1997) Analysis of POSS images of comet–asteroid transition object 107P/1949 W1 (Wilson-Harrington). Icarus 128:114–126. https://doi.org/10.1006/icar.1997.5728

Ferrín I (2006) Secular light curves of comets, II: 133P/Elst Pizarro, an asteroidal belt comet. Icarus 185:523–543. https://doi.org/10.1016/j.icarus.2006.07.005

Festou M, Feldman PD (1981) The forbidden oxygen lines in comets. Astron Astrophys 103:154–159

Fink U (2009) A taxonomic survey of comet composition 1985–2004 using CCD spectroscopy. Icarus 201:311–334. https://doi.org/10.1016/j.icarus.2008.12.044

Fink U, Hoffmann M, Grundy W, Hicks M, Sears W (1992) The steep red spectrum of 1992 ad—an asteroid covered with organic material? Icarus 97:145–149

Florczak M, Lazzaro D, Mothé-Diniz T, Angeli CA, Betzler AS (1999) A spectroscopic study of the Themis family. Astron Astrophys Suppl 134:463–471. https://doi.org/10.1051/aas:1999150

Fornasier S, Lantz C, Perna D, Campins H, Barucci MA, Nesvorny D (2016) Spectral variability on primitive asteroids of the Themis and Beagle families: space weathering effects or parent body heterogeneity? Icarus 269:1–14. https://doi.org/10.1016/j.icarus.2016.01.002. arXiv:1601.05277

Fraser WC, Brown ME (2012) The hubble wide field camera 3 test of surfaces in the outer solar system: the compositional classes of the Kuiper Belt. Astrophys J 749:33

Gaffey MJ, McCord TB (1978) Asteroid surface materials—mineralogical characterizations from reflectance spectra. Space Sci Rev 21:555–628

Genda H, Ikoma M (2008) Origin of the ocean on the earth: early evolution of water D/H in a hydrogen-rich atmosphere. Icarus 194:42–52. https://doi.org/10.1016/j.icarus.2007.09.007. arXiv:0709.2025

Gilbert AM, Wiegert PA (2009) Searching for main-belt comets using the Canada–France–Hawaii Telescope Legacy Survey. Icarus 201:714–718. https://doi.org/10.1016/j.icarus.2009.01.011. arXiv:0901.4511

Gilbert AM, Wiegert PA (2010) Updated results of a search for Main-Belt Comets using the Canada–France–Hawaii Telescope Legacy Survey. Icarus 210:998–999. https://doi.org/10.1016/j.icarus.2010.07.016

Gomes R, Levison HF, Tsiganis K, Morbidelli A (2005) Origin of the cataclysmic late Heavy Bombardment Period of the terrestrial planets. Nature 435:466–469. https://doi.org/10.1038/nature03676

Grundy WM, Schmitt B (1998) The temperature-dependent near-infrared absorption spectrum of hexagonal H_2O ice. J Geophys Res 103:25,809–25,822

Grundy WM, Binzel RP, Buratti BJ, Cook JC, Cruikshank DP, Dalle Ore CM, Earle AM, Ennico K, Howett CJA, Lunsford AW, Olkin CB, Parker AH, Philippe S, Protopapa S, Quirico E, Reuter DC, Schmitt B, Singer KN, Verbiscer AJ, Beyer RA, Buie MW, Cheng AF, Jennings DE, Linscott IR, Parker JW, Schenk PM, Spencer JR, Stansberry JA, Stern SA, Throop HB, Tsang CCC, Weaver HA, Weigle GE, Young LA (2016) Surface compositions across Pluto and Charon. Science 351:aad9189

Guilbert-Lepoutre A (2012) Survival of amorphous water ice on Centaurs. Astron J 144:97. https://doi.org/10.1088/0004-6256/144/4/97

Guilbert-Lepoutre A (2014) Survival of water ice in Jupiter Trojans. Icarus 231:232–238. https://doi.org/10.1016/j.icarus.2013.12.014. arXiv:1401.5196

Guilbert-Lepoutre A, Lasue J, Federico C, Coradini A, Orosei R, Rosenberg ED (2011) New 3D thermal evolution model for icy bodies application to trans-Neptunian objects. Astron Astrophys 529:A71. https://doi.org/10.1051/0004-6361/201014194

Gulkis S, Allen M, von Allmen P, Beaudin G, Biver N, Bockelée-Morvan D, Choukroun M, Crovisier J, Davidsson BJR, Encrenaz P, Encrenaz T, Frerking M, Hartogh P, Hofstadter M, Ip WH, Janssen M, Jarchow C, Keihm S, Lee S, Lellouch E, Leyrat C, Rezac L, Schloerb FP, Spilker T (2015) Subsurface properties and early activity of comet 67P/Churyumov-Gerasimenko. Science 347(6220):709. https://doi.org/10.1126/science.aaa0709

Haghighipour N (2009) Dynamical constraints on the origin of Main Belt Comets. Meteorit Planet Sci 44:1863–1869. https://doi.org/10.1111/j.1945-5100.2009.tb01995.x. arXiv:0910.5746

Hallis LJ, Huss GR, Nagashima K, Taylor GJ, Halldórsson SA, Hilton DR, Mottl MJ, Meech KJ (2015) Evidence for primordial water in Earth's deep mantle. Science 350:795–797. https://doi.org/10.1126/science.aac4834

Hansen CJ, Esposito LW, Stewart AIF, Meinke B, Wallis B, Colwell JE, Hendrix AR, Larsen K, Pryor W, Tian F (2008) Water vapour jets inside the plume of gas leaving Enceladus. Nature 456:477–479. https://doi.org/10.1038/nature07542

Hansen KC, Altwegg K, Berthelier JJ, Bieler A, Biver N, Bockelée-Morvan D, Calmonte U, Capaccioni F, Combi MR, Keyser JD, Fiethe B, Fougere N, Fuselier SA, Gasc S, Gombosi TI, Huang Z, Le Roy L, Lee S, Nilsson H, Rubin M, Shou Y, Snodgrass C, Tenishev V, Toth G, Tzou CY, Wedlund CS (2016) Evolution of water production of 67P/Churyumov-Gerasimenko: an empirical model and a multi-instrument study. Mon Not R Astron Soc 462:stw2413. https://doi.org/10.1093/mnras/stw2413

Hargrove KD, Emery JP, Campins H, Kelley MSP (2015) Asteroid (90) antiope: another icy member of the Themis family? Icarus 254:150–156. https://doi.org/10.1016/j.icarus.2015.03.008

Harmon JK, Slade MA (1992) Radar mapping of Mercury—full-disk images and polar anomalies. Science 258:640–643. https://doi.org/10.1126/science.258.5082.640

Hartmann L, Ciesla F, Gressel O, Alexander R (2017) Disk evolution and the Fate of Water. Space Sci Rev. https://doi.org/10.1007/s11214-017-0406-0 arXiv: 1708.03360

Hartogh P, Crovisier J, de Val-Borro M, Bockelée-Morvan D, Biver N, Lis DC, Moreno R, Jarchow C, Rengel M, Emprechtinger M, Szutowicz S, Banaszkiewicz M, Bensch F, Blecka MI, Cavalié T, Encrenaz T, Jehin E, Küppers M, Lara LM, Lellouch E, Swinyard BM, Vandenbussche B, Bergin EA, Blake

GA, Blommaert JADL, Cernicharo J, Decin L, Encrenaz P, de Graauw T, Hutsemekers D, Kidger M, Manfroid J, Medvedev AS, Naylor DA, Schieder R, Thomas N, Waelkens C, Roelfsema PR, Dieleman P, Güsten R, Klein T, Kasemann C, Caris M, Olberg M, Benz AO (2010) HIFI observations of water in the atmosphere of comet C/2008 Q3 (Garradd). Astron Astrophys 518:L150. https://doi.org/10.1051/0004-6361/201014665. arXiv:1005.2969

Hartogh P, Lis DC, Bockelée-Morvan D, de Val-Borro M, Biver N, Küppers M, Emprechtinger M, Bergin EA, Crovisier J, Rengel M, Moreno R, Szutowicz S, Blake GA (2011) Ocean-like water in the Jupiter-family comet 103P/Hartley 2. Nature 478:218–220. https://doi.org/10.1038/nature10519

Haruyama J, Yamamoto S, Yokota Y, Ohtake M, Matsunaga T (2013) An explanation of bright areas inside Shackleton Crater at the lunar south pole other than water–ice deposits. Geophys Res Lett 40:3814–3818. https://doi.org/10.1002/grl.50753

Haser L (1957) Distribution d'intensité dans la tête d'une comète. Bulletin de la Societe Royale des Sciences de Liege 43:740–750

Hayne PO, Hendrix A, Sefton-Nash E, Siegler MA, Lucey PG, Retherford KD, Williams JP, Greenhagen BT, Paige DA (2015) Evidence for exposed water ice in the Moon's south polar regions from Lunar Reconnaissance Orbiter ultraviolet albedo and temperature measurements. Icarus 255:58–69. https://doi.org/10.1016/j.icarus.2015.03.032

Horner J, Evans NW, Bailey ME (2004) Simulations of the population of centaurs. II. Individual objects. MNRAS 355:321–329

Hsieh HH (2009) The Hawaii trails project: comet-hunting in the main asteroid belt. Astron Astrophys 505:1297–1310. https://doi.org/10.1051/0004-6361/200912342. arXiv:0907.5505

Hsieh HH (2014a) Main-belt comets as tracers of ice in the inner solar system. In: Haghighipour N (ed) Formation, detection, and characterization of extrasolar habitable planets, IAU symposium, vol 293, pp 212–218. https://doi.org/10.1017/S1743921313012866 arXiv:1408.4868

Hsieh HH (2014) The nucleus of Main-Belt Comet P/2010 R2 (La Sagra). Icarus 243:16–26. https://doi.org/10.1016/j.icarus.2014.08.033. arXiv:1408.4860

Hsieh HH, Chavez J (2017) Comet 259P/Garradd. CBET 4388: 20170502, Central Bureau for Astronomical Telegrams

Hsieh HH, Haghighipour N (2016) Potential Jupiter-family comet contamination of the main asteroid belt. Icarus 277:19–38. https://doi.org/10.1016/j.icarus.2016.04.043. arXiv:1604.08557

Hsieh HH, Jewitt D (2006) A population of comets in the main asteroid belt. Science 312:561–563. https://doi.org/10.1126/science.1125150

Hsieh HH, Jewitt DC, Fernández YR (2004) The strange case of 133P/Elst-Pizarro: a comet among the asteroids. Astron J 127:2997–3017. https://doi.org/10.1086/383208

Hsieh HH, Jewitt D, Fernández YR (2009a) Albedos of Main-Belt Comets 133P/Elst-Pizarro and 176P/LINEAR. Astrophys J 694:L111–L114. https://doi.org/10.1088/0004-637X/694/2/L111. arXiv:0902.3682

Hsieh HH, Jewitt D, Ishiguro M (2009b) Physical properties of Main-Belt Comet P/2005 U1 (Read). Astron J 137:157–168. https://doi.org/10.1088/0004-6256/137/1/157. arXiv:0810.1351

Hsieh HH, Jewitt D, Lacerda P, Lowry SC, Snodgrass C (2010) The return of activity in Main-Belt Comet 133P/Elst-Pizarro. Mon Not R Astron Soc 403(1):363–377. https://doi.org/10.1111/j.1365-2966.2009.16120.x. arXiv:0911.5522

Hsieh HH, Ishiguro M, Lacerda P, Jewitt D (2011a) Physical properties of Main-Belt Comet 176P/LINEAR. Astron J 142:29. https://doi.org/10.1088/0004-6256/142/1/29. arXiv:1105.0944

Hsieh HH, Meech KJ, Pittichová J (2011b) Main-Belt Comet 238P/read revisited. Astrophys J 736:L18. https://doi.org/10.1088/2041-8205/736/1/L18. arXiv:1106.0045

Hsieh HH, Yang B, Haghighipour N (2012a) Optical and dynamical characterization of comet-like main-belt asteroid (596) Scheila. Astrophys J 744:9. https://doi.org/10.1088/0004-637X/744/1/9. arXiv:1109.3477

Hsieh HH, Yang B, Haghighipour N, Kaluna HM, Fitzsimmons A, Denneau L, Novaković B, Jedicke R, Wainscoat RJ, Armstrong JD, Duddy SR, Lowry SC, Trujillo CA, Micheli M, Keane JV, Urban L, Riesen T, Meech KJ, Abe S, Cheng YC, Chen WP, Granvik M, Grav T, Ip WH, Kinoshita D, Kleyna J, Lacerda P, Lister T, Milani A, Tholen DJ, Vereš P, Lisse CM, Kelley MS, Fernández YR, Bhatt BC, Sahu DK, Kaiser N, Chambers KC, Hodapp KW, Magnier EA, Price PA, Tonry JL (2012b) Discovery of Main-Belt Comet P/2006 VW_{139} by Pan-STARRS1. Astrophys J 748:L15. https://doi.org/10.1088/2041-8205/748/1/L15. arXiv:1202.2126

Hsieh HH, Yang B, Haghighipour N, Novaković B, Jedicke R, Wainscoat RJ, Denneau L, Abe S, Chen WP, Fitzsimmons A, Granvik M, Grav T, Ip W, Kaluna HM, Kinoshita D, Kleyna J, Knight MM, Lacerda P, Lisse CM, Maclennan E, Meech KJ, Micheli M, Milani A, Pittichová J, Schunova E, Tholen DJ, Wasserman LH, Burgett WS, Chambers KC, Heasley JN, Kaiser N, Magnier EA, Morgan JS, Price PA, Jørgensen UG, Dominik M, Hinse T, Sahu K, Snodgrass C (2012c) Observational and dynamical characterization of Main-Belt Comet P/2010 R2 (La Sagra). Astron J 143:104. https://doi.org/10.1088/0004-6256/143/5/104. arXiv:1109.6350

Hsieh HH, Kaluna HM, Novaković B, Yang B, Haghighipour N, Micheli M, Denneau L, Fitzsimmons A, Jedicke R, Kleyna J, Vereš P, Wainscoat RJ, Ansdell M, Elliott GT, Keane JV, Meech KJ, Moskovitz NA, Riesen TE, Sheppard SS, Sonnett S, Tholen DJ, Urban L, Kaiser N, Chambers KC, Burgett WS, Magnier EA, Morgan JS, Price PA (2013) Main-Belt Comet P/2012 T1 (PANSTARRS). Astrophys J 771:L1. https://doi.org/10.1088/2041-8205/771/1/L1. arXiv:1305.5558

Hsieh HH, Denneau L, Wainscoat RJ, Schörghofer N, Bolin B, Fitzsimmons A, Jedicke R, Kleyna J, Micheli M, Vereš P, Kaiser N, Chambers KC, Burgett WS, Flewelling H, Hodapp KW, Magnier EA, Morgan JS, Price PA, Tonry JL, Waters C (2015a) The Main-Belt Comets: the Pan-STARRS1 perspective. Icarus 248:289–312. https://doi.org/10.1016/j.icarus.2014.10.031. arXiv:1410.5084

Hsieh HH, Hainaut O, Novaković B, Bolin B, Denneau L, Fitzsimmons A, Haghighipour N, Kleyna J, Kokotanekova R, Lacerda P, Meech KJ, Micheli M, Moskovitz N, Schunova E, Snodgrass C, Wainscoat RJ, Wasserman L, Waszczak A (2015b) Sublimation-driven activity in Main-Belt Comet 313p/Gibbs. Astrophys J 800:L16. https://doi.org/10.1088/2041-8205/800/1/L16. arXiv:1501.03873

Hsieh HH, Schwamb ME, Zhang ZW, Chen YT, Wang SY, Lintott C (2016) Comet hunters: a citizen science project to search for comets in the main asteroid belt. In: AAS/Division for planetary sciences meeting abstracts, vol 48, p 406.03

Hui MT, Jewitt D (2015) Archival observations of active asteroid 313p/Gibbs. Astron J 149:134. https://doi.org/10.1088/0004-6256/149/4/134

Hui MT, Jewitt D (2017) Non-gravitational acceleration of the active asteroids. Astron J 153:80. https://doi.org/10.3847/1538-3881/153/2/80. arXiv:1612.06920

Hui MT, Li J (2017) Resurrection of (3200) Phaethon in 2016. Astron J 153:23. https://doi.org/10.3847/1538-3881/153/1/23. arXiv:1611.07061

Hui MT, Jewitt D, Du X (2017) Split active asteroid P/2016 J1 (PANSTARRS). Astron J 153:141. https://doi.org/10.3847/1538-3881/aa6039. arXiv:1702.02766

Ingersoll AP (1969) The runaway greenhouse: a history of water on Venus. J Atmos Sci 26:1191–1198. https://doi.org/10.1175/1520-0469(1969)026<1191:TRGAHO>2.0.CO;2

Ishiguro M, Hanayama H, Hasegawa S, Sarugaku Y, Watanabe Ji, Fujiwara H, Terada H, Hsieh HH, Vaubaillon JJ, Kawai N, Yanagisawa K, Kuroda D, Miyaji T, Fukushima H, Ohta K, Hamanowa H, Kim J, Pyo J, Nakamura AM (2011a) Observational evidence for an impact on the main-belt asteroid (596) Scheila. Astrophys J 740:L11. https://doi.org/10.1088/2041-8205/740/1/L11

Ishiguro M, Hanayama H, Hasegawa S, Sarugaku Y, Watanabe Ji, Fujiwara H, Terada H, Hsieh HH, Vaubaillon JJ, Kawai N, Yanagisawa K, Kuroda D, Miyaji T, Fukushima H, Ohta K, Hamanowa H, Kim J, Pyo J, Nakamura AM (2011b) Interpretation of (596) Scheila's triple dust tails. Astrophys J 741:L24. https://doi.org/10.1088/2041-8205/741/1/L24. arXiv:1110.1150

Jehin E (2015) Report on the ground-based observation campaign of 67P/Churyumov-Gerasimenko. In: AAS/Division for Planetary Sciences Meeting Abstracts, vol 47, p 413.12

Jehin E, Manfroid J, Hutsemékers D, Cochran AL, Arpigny C, Jackson WM, Rauer H, Schulz R, Zucconi JM (2006) Deep impact: high-resolution optical spectroscopy with the ESO VLT and the Keck I telescope. Astrophys J 641:L145–L148. https://doi.org/10.1086/504110. arXiv:astro-ph/0603306

Jehin E, Manfroid J, Hutsemékers D, Arpigny C, Zucconi JM (2009) Isotopic ratios in comets: status and perspectives. Earth Moon Planets 105:167–180. https://doi.org/10.1007/s11038-009-9322-y

Jewitt D, Guilbert-Lepoutre A (2012) Limits to ice on asteroids (24) Themis and (65) Cybele. Astron J 143:21. https://doi.org/10.1088/0004-6256/143/1/21. arXiv:1111.3292

Jewitt D, Kalas P (1998) Thermal observations of Centaur 1997 CU26. Astrophys J 499

Jewitt D, Li J (2010) Activity in geminid parent (3200) Phaethon. Astron J 140:1519–1527. https://doi.org/10.1088/0004-6256/140/5/1519. arXiv:1009.2710

Jewitt D, Chizmadia L, Grimm R, Prialnik D (2007) Water in the small bodies of the solar system. In: Reipurth B, Jewitt D, Keil K (eds) Protostars and planets V. University of Arizona Press, Tucson, V 863–878

Jewitt D, Yang B, Haghighipour N (2009) Main-Belt Comet P/2008 R1 (Garradd). Astron J 137:4313–4321. https://doi.org/10.1088/0004-6256/137/5/4313. arXiv:0902.4315

Jewitt D, Weaver H, Mutchler M, Larson S, Agarwal J (2011) Hubble space telescope observations of Main-Belt Comet (596) Scheila. Astrophys J 733:L4. https://doi.org/10.1088/2041-8205/733/1/L4. arXiv:1103.5456

Jewitt D, Agarwal J, Li J, Weaver H, Mutchler M, Larson S (2014a) Disintegrating asteroid P/2013 R3. Astrophys J 784:L8. https://doi.org/10.1088/2041-8205/784/1/L8. arXiv:1403.1237

Jewitt D, Ishiguro M, Weaver H, Agarwal J, Mutchler M, Larson S (2014b) Hubble space telescope investigation of Main-Belt Comet 133P/Elst-Pizarro. Astron J 147:117. https://doi.org/10.1088/0004-6256/147/5/117. arXiv:1402.5571

Jewitt D, Agarwal J, Peixinho N, Weaver H, Mutchler M, Hui MT, Li J, Larson S (2015a) New active asteroid 313P/Gibbs. Astron J 149(2):81. https://doi.org/10.1088/0004-6256/149/2/81. arXiv:1412.6582

Jewitt D, Agarwal J, Weaver H, Mutchler M, Larson S (2015b) Episodic ejection from active asteroid 311P/Panstarrs. Astrophys J 798(2):109. https://doi.org/10.1088/0004-637X/798/2/109

Jewitt D, Hsieh H, Agarwal J (2015c) The active asteroids. In: Michel P, Demeo F, Bottke W (eds) Asteroids III, University of Arizona Press, Tucson, 221–241. https://doi.org/10.2458/azu_uapress_9780816532131-ch012

Jewitt DC, Sheppard S, Porco C (2004) Jupiter's outer satellites and Trojans. In: Bagenal F, Dowling TE, McKinnon WB (eds) Jupiter. The planet, satellites and magnetosphere. Cambridge University Press, Cambridge, 263–280

Jones GH et al (2017) Caroline—a search for the source of earth's water (**unpublished**)

Kaluna H, Meech K (2011) Analysis of the activity on Main Belt Comet 133P/Elst-Pizarro. In: EPSC-DPS joint meeting 2011, p 1375

Kawakita H, Watanabe Ji, Ootsubo T, Nakamura R, Fuse T, Takato N, Sasaki S, Sasaki T (2004) Evidence of icy grains in comet C/2002 T7 (LINEAR) at 3.52 au. Astrophys J 601:L191–L194

Keller HU (1976) The interpretations of ultraviolet observations of comets. Space Sci Rev 18:641–684. https://doi.org/10.1007/BF00169520

Kelley MSP, Woodward CE, Bodewits D, Farnham TL, Gudipati MS, Harker DE, Hines DC, Knight MM, Kolokolova L, Li A, de Pater I, Protopapa S, Russell RW, Sitko ML, Wooden DH (2016) Cometary science with the James Webb space telescope. PASP 128(1):018,009. https://doi.org/10.1088/1538-3873/128/959/018009. arXiv:1510.05878

Kendrew S, Scheithauer S, Bouchet P, Amiaux J, Azzollini R, Bouwman J, Chen CH, Dubreuil D, Fischer S, Glasse A, Greene TP, Lagage PO, Lahuis F, Ronayette S, Wright D, Wright GS (2015) The mid-infrared instrument for the James Webb space telescope, IV: the low-resolution spectrometer. PASP 127:623. https://doi.org/10.1086/682255. arXiv:1512.03000

Killen RM, Benkhoff J, Morgan TH (1997) Mercury's polar caps and the generation of an OH exosphere. Icarus 125:195–211. https://doi.org/10.1006/icar.1996.5601

King TVV, Clark RN (1997) The presence of a single absorption feature—what it does and doesn't imply. In: Lunar and planetary science conference, vol 28, p 727

Knaell KK, Cardillo GP (1995) Radar tomography for the generation of three-dimensional images. IEE Proc Radar Sonar Navig 142(2):54–60. https://doi.org/10.1049/ip-rsn:19951791

Knight MM, Schleicher DG (2015) Observations of comet ISON (C/2012 S1) from Lowell Observatory. Astron J 149:19. https://doi.org/10.1088/0004-6256/149/1/19. arXiv:1410.0684

Kofman W, Herique A, Barbin Y, Barriot JP, Ciarletti V, Clifford S, Edenhofer P, Elachi C, Eyraud C, Goutail JP, Heggy E, Jorda L, Lasue J, Levasseur-Regourd AC, Nielsen E, Pasquero P, Preusker F, Puget P, Plettemeier D, Rogez Y, Sierks H, Statz C, Svedhem H, Williams I, Zine S, Van Zyl J (2015) Properties of the 67P/Churyumov-Gerasimenko interior revealed by CONSERT radar. Science 349:aab0639. https://doi.org/10.1126/science.aab0639

Kosai H (1992) Short-period comets and Apollo–Amor–Aten type asteroids in view of Tisserand invariant. Celest Mech Dyn Astron 54:237–240. https://doi.org/10.1007/BF00049556

Kresak L (1982) On the similarity of orbits of associated comets, asteroids and meteoroids. Bull Astron Inst Czechoslov 33:104–110

Küppers M, O'Rourke L, Bockelée-Morvan D, Zakharov V, Lee S, von Allmen P, Carry B, Teyssier D, Marston A, Müller T, Crovisier J, Barucci MA, Moreno R (2014) Localized sources of water vapour on the dwarf planet (1) Ceres. Nature 505:525–527. https://doi.org/10.1038/nature12918

Lane AL, West RA, Nelson RM, Horn LJ, Wallis BD, Buratti BJ, Hord CW, Simmons KE, Pryor WR, Esposito LW (1989) Photometry from Voyager 2—initial results from the Neptunian atmosphere, satellites, and rings. Science 246:1450–1454. https://doi.org/10.1126/science.246.4936.1450

Langevin Y, Poulet F, Bibring JP, Schmitt B, Douté S, Gondet B (2005) Summer evolution of the north polar cap of Mars as observed by OMEGA/Mars express. Science 307:1581–1584. https://doi.org/10.1126/science.1109438

Lasue J, Mangold N, Hauber E, Clifford S, Feldman W, Gasnault O, Grima C, Maurice S, Mousis O (2013) Quantitative assessments of the martian hydrosphere. Space Sci Rev 174:155–212. https://doi.org/10.1007/s11214-012-9946-5

Lawrence DJ, Feldman WC, Goldsten JO, Maurice S, Peplowski PN, Anderson BJ, Bazell D, McNutt RL, Nittler LR, Prettyman TH, Rodgers DJ, Solomon SC, Weider SZ (2013) Evidence for water ice near Mercury's north pole from MESSENGER neutron spectrometer measurements. Science 339:292. https://doi.org/10.1126/science.1229953

Levison HF (1996) Comet taxonomy. In: Rettig T, Hahn JM (eds) Completing the inventory of the Solar System. In: Astronomical society of the pacific conference series, vol 107, San Francisco, pp 173–191

Levison HF, Duncan MJ (1997) From the Kuiper belt to Jupiter-family comets: the spatial distribution of ecliptic comets. Icarus 127:13–32

Levison HF, Terrell D, Wiegert PA, Dones L, Duncan MJ (2006) On the origin of the unusual orbit of comet 2P/Encke. Icarus 182:161–168. https://doi.org/10.1016/j.icarus.2005.12.016

Levison HF, Bottke WF, Gounelle M, Morbidelli A, Nesvorný D, Tsiganis K (2009) Contamination of the asteroid belt by primordial trans-Neptunian objects. Nature 460:364–366. https://doi.org/10.1038/nature08094

Lewis JS (1974) Volatile element influx on Venus from cometary impacts. Earth Planet Sci Lett 22:239–244. https://doi.org/10.1016/0012-821X(74)90087-9

Li J, Jewitt D (2013) Recurrent perihelion activity in (3200) Phaethon. Astron J 145:154. https://doi.org/10.1088/0004-6256/145/6/154. arXiv:1304.1430

Licandro J, Pinilla-Alonso N, Pedani M, Oliva E, Tozzi GP, Grundy WM (2006) The methane ice rich surface of large TNO 2005 FY_9: a Pluto-twin in the trans-Neptunian belt? Astron Astrophys 445:L35–L38

Licandro J, Campins H, Tozzi GP, de León J, Pinilla-Alonso N, Boehnhardt H, Hainaut OR (2011) Testing the comet nature of Main Belt Comets. The spectra of 133P/Elst-Pizarro and 176P/LINEAR. Astron Astrophys 532:A65. https://doi.org/10.1051/0004-6361/201117018. arXiv:1104.0879

Licandro J, Moreno F, de León J, Tozzi GP, Lara LM, Cabrera-Lavers A (2013) Exploring the nature of new Main-Belt Comets with the 10.4 m GTC telescope: (300163) 2006 VW139. Astron Astrophys 550:A17. https://doi.org/10.1051/0004-6361/201220080. arXiv:1212.1022

Lovell AJ, Howell ES, Schloerb FP, Lewis BM, Hine AA (2002) Arecibo observations of the 18 cm OH lines of six comets. In: Warmbein B (ed) Asteroids, comets, and meteors: ACM 2002, ESA Special Publication, vol 500, pp 681–684

Lupu RE, Feldman PD, Weaver HA, Tozzi GP (2007) The fourth positive system of carbon monoxide in the hubble space telescope spectra of comets. Astrophys J 670:1473–1484. https://doi.org/10.1086/522328. arXiv:0708.3088

Luu JX, Jewitt DC (1990) Charge-coupled device spectra of asteroids. I-Near-earth and 3:1 resonance asteroids. Astron J 99:1985–2011

MacLennan EM, Hsieh HH (2012) The nucleus of Main-Belt Comet 259P/Garradd. Astrophys J 758:L3. https://doi.org/10.1088/2041-8205/758/1/L3. arXiv:1209.3065

Mäkinen JTT, Bertaux JL, Pulkkinen TI, Schmidt W, Kyrölä E, Summanen T, Quémerais E, Lallement R (2001) Comets in full sky L_α maps of the SWAN instrument. I. Survey from 1996 to 1998. Astron Astrophys 368:292–297. https://doi.org/10.1051/0004-6361:20000545

Malin MC, Edgett KS, Posiolova LV, McColley SM, Dobrea EZN (2006) Present-day impact cratering rate and contemporary gully activity on Mars. Science 314:1573. https://doi.org/10.1126/science.1135156

Manga M, Wang CY (2007) Pressurized oceans and the eruption of liquid water on Europa and Enceladus. GRL 34:L07202. https://doi.org/10.1029/2007GL029297

Marsset M, Vernazza P, Birlan M, DeMeo F, Binzel RP, Dumas C, Milli J, Popescu M (2016) Compositional characterisation of the Themis family. Astron Astrophys 586:A15. https://doi.org/10.1051/0004-6361/201526962. arXiv:1601.02405

Martín-Torres FJ, Zorzano MP, Valentín-Serrano P, Harri AM, Genzer M, Kemppinen O, Rivera-Valentin EG, Jun I, Wray J, Bo Madsen M, Goetz W, McEwen AS, Hardgrove C, Renno N, Chevrier VF, Mischna M, Navarro-González R, Martínez-Frías J, Conrad P, McConnochie T, Cockell C, Berger G,

Vasavada RA, Sumner D, Vaniman D (2015) Transient liquid water and water activity at gale crater on Mars. Nature Geosci 8:357–361. https://doi.org/10.1038/ngeo2412

Mayor M, Queloz D (1995) A Jupiter-mass companion to a solar-type star. Nature 378:355–359. https://doi.org/10.1038/378355a0

McKay AJ, Chanover NJ, Morgenthaler JP, Cochran AL, Harris WM, Russo ND (2012) Forbidden oxygen lines in comets C/2006 W3 Christensen and C/2007 Q3 siding spring at large heliocentric distance: implications for the sublimation of volatile ices. Icarus 220:277–285. https://doi.org/10.1016/j.icarus.2012.04.030

McKay AJ, Bodewits D, Li JY (2017) Observational constraints on water sublimation from 24 Themis and 1 Ceres. Icarus 286:308–313. https://doi.org/10.1016/j.icarus.2016.09.032. arXiv:1609.07156

McKinnon WB (2012) Where did Ceres accrete—in situ in the asteroid belt, among the giant planets, or in the primordial transneptunian belt? In: AAS/Division for Planetary Sciences Meeting Abstracts, vol 44, p 111.14

McPhate JB, Feldman PD, McCandliss SR, Burgh EB (1999) Rocket-borne long-slit ultraviolet spectroscopy of comet Hale–Bopp. Astrophys J 521:920–927. https://doi.org/10.1086/307561

Meech KJ, Castillo-Rogez JC (2015) Proteus–a mission to investigate the origins of Earth's water. In: IAU General Assembly, vol 22, p 2257859

Meech KJ, A'Hearn MF, Adams JA, Bacci P, Bai J, Barrera L, Battelino M, Bauer JM, Becklin E, Bhatt B, Biver N, Bockelée-Morvan D, Bodewits D, Böhnhardt H, Boissier J, Bonev BP, Borghini W, Brucato JR, Bryssinck E, Buie MW, Canovas H, Castellano D, Charnley SB, Chen WP, Chiang P, Choi YJ, Christian DJ, Chuang YL, Cochran AL, Colom P, Combi MR, Coulson IM, Crovisier J, Dello Russo N, Dennerl K, DeWahl K, DiSanti MA, Facchini M, Farnham TL, Fernández Y, Florén HG, Frisk U, Fujiyoshi T, Furusho R, Fuse T, Galli G, García-Hernández DA, Gersch A, Getu Z, Gibb EL, Gillon M, Guido E, Guillermo RA, Hadamcik E, Hainaut O, Hammel HB, Harker DE, Harmon JK, Harris WM, Hartogh P, Hashimoto M, Häusler B, Herter T, Hjalmarson A, Holland ST, Honda M, Hosseini S, Howell ES, Howes N, Hsieh HH, Hsiao HY, Hutsemékers D, Immler SM, Jackson WM, Jeffers SV, Jehin E, Jones TJ, de Juan Ovelar M, Kaluna HM, Karlsson T, Kawakita H, Keane JV, Keller LD, Kelley MS, Kinoshita D, Kiselev NN, Kleyna J, Knight MM, Kobayashi H, Kobulnicky HA, Kolokolova L, Kreiny M, Kuan YJ, Küppers M, Lacruz JM, Landsman WB, Lara LM, Lecacheux A, Levasseur-Regourd AC, Li B, Licandro J, Ligustri R, Lin ZY, Lippi M, Lis DC, Lisse CM, Lovell AJ, Lowry SC, Lu H, Lundin S, Magee-Sauer K, Magain P, Manfroid J, Mazzotta Epifani E, McKay A, Melita MD, Mikuz H, Milam SN, Milani G, Min M, Moreno R, Mueller BEA, Mumma MJ, Nicolini M, Nolan MC, Nordh HL, Nowajewski PB, Team Odin, Ootsubo T, Paganini L, Perrella C, Pittichová J, Prosperi E, Radeva YL, Reach WT, Remijan AJ, Rengel M, Riesen TE, Rodenhuis M, Rodríguez DP, Russell RW, Sahu DK, Samarasinha NH, Sánchez Caso A, Sandqvist A, Sarid G, Sato M, Schleicher DG, Schwieterman EW, Sen AK, Shenoy D, Shi JC, Shinnaka Y, Skvarc J, Snodgrass C, Sitko ML, Sonnett S, Sosseini S, Sostero G, Sugita S, Swinyard BM, Szutowicz S, Takato N, Tanga P, Taylor PA, Tozzi GP, Trabatti R, Trigo-Rodríguez JM, Tubiana C, de Val-Borro M, Vacca W, Vandenbussche B, Vaubaillion J, Velichko FP, Velichko SF, Vervack RJ Jr, Vidal-Nunez MJ, Villanueva GL, Vinante C, Vincent JB, Wang M, Wasserman LH, Watanabe J, Weaver HA, Weissman PR, Wolk S, Wooden DH, Woodward CE, Yamaguchi M, Yamashita T, Yanamandra-Fischer PA, Yang B, Yao JS, Yeomans DK, Zenn T, Zhao H, Ziffer JE (2011) EPOXI: comet 103P/Hartley 2 observations from a worldwide campaign. Astrophys J 734:L1. https://doi.org/10.1088/2041-8205/734/1/L1. arXiv: 1106.0367

Meixner M, Cooray A, Carter R, DiPirro M, Flores A, Leisawitz D, Armus L, Battersby C, Bergin E, Bradford CM, Ennico K, Melnick GJ, Milam S, Narayanan D, Pontoppidan K, Pope A, Roellig T, Sandstrom K, Su KYL, Vieira J, Wright E, Zmuidzinas J, Alato S, Carey S, Gerin M, Helmich F, Menten K, Scott D, Sakon I, Vavrek R (2016) The far-infrared surveyor mission study: paper I, the genesis. In: Space telescopes and instrumentation 2016: optical, infrared, and millimeter wave, Proceedings of SPIE, vol 9904, p 99040K. https://doi.org/10.1117/12.2240456. arXiv:1608.03909

Morbidelli A, Chambers J, Lunine JI, Petit JM, Robert F, Valsecchi GB, Cyr KE (2000) Source regions and time scales for the delivery of water to Earth. Meteorit Planet Sci 35:1309–1320

Moreno F, Lara LM, Licandro J, Ortiz JL, de León J, Alí-Lagoa V, Agís-González B, Molina A (2011a) The dust environment of Main-Belt Comet P/2010 R2 (La Sagra). Astrophys J 738:L16. https://doi.org/10.1088/2041-8205/738/1/L16

Moreno F, Licandro J, Ortiz JL, Lara LM, Alí-Lagoa V, Vaduvescu O, Morales N, Molina A, Lin ZY (2011b) (596) Scheila in outburst: a probable collision event in the main asteroid belt. Astrophys J 738:130. https://doi.org/10.1088/0004-637X/738/2/130

Moreno F, Licandro J, Cabrera-Lavers A (2012) A short-duration event as the cause of dust ejection from Main-Belt Comet P/2012 F5 (Gibbs). Astrophys J 761:L12. https://doi.org/10.1088/2041-8205/761/1/L12. arXiv:1211.2104

Moreno F, Cabrera-Lavers A, Vaduvescu O, Licandro J, Pozuelos F (2013) The dust environment of Main-Belt Comet P/2012 T1 (PANSTARRS). Astrophys J 770:L30. https://doi.org/10.1088/2041-8205/770/2/L30. arXiv:1305.4380

Moreno F, Licandro J, Cabrera-Lavers A, Pozuelos FJ (2016) Dust loss from activated asteroid P/2015 X6. Astrophys J 826:137. https://doi.org/10.3847/0004-637X/826/2/137. arXiv:1605.04802

Moreno F, Pozuelos FJ, Novaković B, Licandro J, Cabrera-Lavers A, Bolin B, Jedicke R, Gladman BJ, Bannister MT, Gwyn SDJ, Vereš P, Chambers K, Chastel S, Denneau L, Flewelling H, Huber M, Schunová-Lilly E, Magnier E, Wainscoat R, Waters C, Weryk R, Farnocchia D, Micheli M (2017) The splitting of double-component active asteroid P/2016 J1 (PANSTARRS). Astrophys J 837:L3. https://doi.org/10.3847/2041-8213/aa6036. arXiv:1702.03665

Moses JI, Rawlins K, Zahnle K, Dones L (1999) External sources of water for Mercury's putative ice deposits. Icarus 137:197–221. https://doi.org/10.1006/icar.1998.6036

Mueller RF (1970) Dehydrogenation of Venus. Nature 227:363–365. https://doi.org/10.1038/227363a0

Mukai T (1986) Analysis of a dirty water–ice model for cometary dust. Astron Astrophys 164:397–407

Mumma MJ, Charnley SB (2011) The chemical composition of comets—emerging taxonomies and natal heritage. Annu Rev Astron Astrophys 49:471–524. https://doi.org/10.1146/annurev-astro-081309-130811

Mumma MJ, Disanti MA, dello Russo N, Magee-Sauer K, Gibb E, Novak R (2003) Remote infrared observations of parent volatiles in comets: a window on the early Solar System. Adv Space Res 31:2563–2575

Nesvorný D, Bottke WF, Vokrouhlický D, Sykes M, Lien DJ, Stansberry J (2008) Origin of the near-ecliptic circumsolar dust band. Astrophys J 679:L143. https://doi.org/10.1086/588841

Neumann GA, Cavanaugh JF, Sun X, Mazarico EM, Smith DE, Zuber MT, Mao D, Paige DA, Solomon SC, Ernst CM, Barnouin OS (2013) Bright and dark polar deposits on Mercury: evidence for surface volatiles. Science 339:296. https://doi.org/10.1126/science.1229764

Newman SF, Buratti BJ, Brown RH, Jaumann R, Bauer J, Momary T (2008) Photometric and spectral analysis of the distribution of crystalline and amorphous ices on enceladus as seen by cassini. Icarus 193:397–406

Nicholson PD, Hedman MM, Clark RN, Showalter MR, Cruikshank DP, Cuzzi JN, Filacchione G, Capaccioni F, Cerroni P, Hansen GB, Sicardy B, Drossart P, Brown RH, Buratti BJ, Baines KH, Coradini A (2008) A close look at Saturn's rings with cassini VIMS. Icarus 193:182–212. https://doi.org/10.1016/j.icarus.2007.08.036

Niemann HB, Atreya SK, Carignan GR, Donahue TM, Haberman JA, Harpold DN, Hartle RE, Hunten DM, Kasprzak WT, Mahaffy PR, Owen TC, Way SH (1998) The composition of the Jovian atmosphere as determined by the Galileo probe mass spectrometer. J Geophys Res 103:22,831–22,846. https://doi.org/10.1029/98JE01050

Nimmo F, Spencer JR, Pappalardo RT, Mullen ME (2007) Shear heating as the origin of the plumes and heat flux on Enceladus. Nature 447:289–291. https://doi.org/10.1038/nature05783

Novaković B, Cellino A, Knežević Z (2011) Families among high-inclination asteroids. Icarus 216:69–81. https://doi.org/10.1016/j.icarus.2011.08.016. arXiv:1108.3740

Novaković B, Hsieh HH, Cellino A (2012) P/2006 VW_{139}: a Main-Belt Comet born in an asteroid collision? MNRAS 424:1432–1441. https://doi.org/10.1111/j.1365-2966.2012.21329.x. arXiv:1205.4949

Ogilvy JA (1991) Theory of wave scattering from random rough surfaces. Rep Prog Phys 50:1553. https://doi.org/10.1088/0034-4885/50/12/001

Ootsubo T, Kawakita H, Hamada S, Kobayashi H, Yamaguchi M, Usui F, Nakagawa T, Ueno M, Ishiguro M, Sekiguchi T, Watanabe Ji, Sakon I, Shimonishi T, Onaka T (2012) AKARI near-infrared spectroscopic survey for CO_2 in 18 comets. Astrophys J 752:15. https://doi.org/10.1088/0004-637X/752/1/15

Opitom C, Snodgrass C, Jehin E, Fitzsimmons A, Manfroid J, Tozzi GP, Faggi S, Gillon M (2017) Ground-based monitoring of comet 67p/churyumov-gerasimenko gas activity throughout the rosetta mission. Mon Not R Astron Soc 469:S222–S229. https://doi.org/10.1093/mnras/stx1591

O'Rourke L, Snodgrass C, de Val-Borro M, Biver N, Bockelée-Morvan D, Hsieh H, Teyssier D, Fernandez Y, Kueppers M, Micheli M, Hartogh P (2013) Determination of an upper limit for the water outgassing rate of Main-Belt Comet P/2012 T1 (PANSTARRS). Astrophys J 774:L13. https://doi.org/10.1088/2041-8205/774/1/L13

Paganini L, Mumma MJ, Boehnhardt H, DiSanti MA, Villanueva GL, Bonev BP, Lippi M, Käufl HU, Blake GA (2013) Ground-based infrared detections of CO in the Centaur-comet 29P/Schwassmann-Wachmann 1 at 6.26 AU from the Sun. Astrophys J 766:100. https://doi.org/10.1088/0004-637X/766/2/100

Paganini L, Mumma MJ, Gibb EL, Villanueva GL (2017) Ground-based Detection of Deuterated Water in Comet C/2014 Q2 (Lovejoy) at IR Wavelengths. Astrophys J 836(2):L25. https://doi.org/10.3847/2041-8213/aa5cb3

Paige DA, Wood SE, Vasavada AR (1992) The thermal stability of water ice at the poles of Mercury. Science 258:643–646. https://doi.org/10.1126/science.258.5082.643

Paige DA, Siegler MA, Harmon JK, Neumann GA, Mazarico EM, Smith DE, Zuber MT, Harju E, Delitsky ML, Solomon SC (2013) Thermal stability of volatiles in the north polar region of Mercury. Science 339:300. https://doi.org/10.1126/science.1231106

Palmer SJ, Dowdeswell JA, Christoffersen P, Young DA, Blankenship DD, Greenbaum JS, Benham T, Bamber J, Siegert MJ (2013) Greenland subglacial lakes detected by radar. Geophys Res Lett 40:6154–6159. https://doi.org/10.1002/2013GL058383

Pätzold M, Andert T, Hahn M, Asmar SW, Barriot JP, Bird MK, Häusler B, Peter K, Tellmann S, Grün E, Weissman PR, Sierks H, Jorda L, Gaskell R, Preusker F, Scholten F (2016) A homogeneous nucleus for comet 67P/Churyumov-Gerasimenko from its gravity field. Nature 530:63–65. https://doi.org/10.1038/nature16535

Peixinho N, Delsanti A, Guilbert-Lepoutre A, Gafeira R, Lacerda P (2012) The bimodal colors of centaurs and small Kuiper Belt objects. Astron Astrophys 546:A86

Petrenko VF, Whitworth RW (1999) Physics of ice. Oxford University Press, Oxford

Picardi G, Plaut JJ, Biccari D, Bombaci O, Calabrese D, Cartacci M, Cicchetti A, Clifford SM, Edenhofer P, Farrell WM, Federico C, Frigeri A, Gurnett DA, Hagfors T, Heggy E, Herique A, Huff RL, Ivanov AB, Johnson WTK, Jordan RL, Kirchner DL, Kofman W, Leuschen CJ, Nielsen E, Orosei R, Pettinelli E, Phillips RJ, Plettemeier D, Safaeinili A, Seu R, Stofan ER, Vannaroni G, Watters TR, Zampolini E (2005) Radar soundings of the subsurface of Mars. Science 310:1925–1928. https://doi.org/10.1126/science.1122165

Pieters CM, Goswami JN, Clark RN, Annadurai M, Boardman J, Buratti B, Combe JP, Dyar MD, Green R, Head JW, Hibbitts C, Hicks M, Isaacson P, Klima R, Kramer G, Kumar S, Livo E, Lundeen S, Malaret E, McCord T, Mustard J, Nettles J, Petro N, Runyon C, Staid M, Sunshine J, Taylor LA, Tompkins S, Varanasi P (2009) Character and spatial distribution of OH/H_2O on the surface of the moon seen by M3 on Chandrayaan-1. Science 326:568

Podolak M, Weizman A, Marley M (1995) Comparative models of Uranus and Neptune. PSS 43:1517–1522. https://doi.org/10.1016/0032-0633(95)00061-5

Pozuelos FJ, Cabrera-Lavers A, Licandro J, Moreno F (2015) On the dust environment of Main-Belt Comet 313P/Gibbs. Astrophys J 806:102. https://doi.org/10.1088/0004-637X/806/1/102. arXiv:1505.01479

Prettyman TH, Yamashita N, Toplis MJ, McSween HY, Schörghofer N, Marchi S, Feldman WC, Castillo-Rogez J, Forni O, Lawrence DJ, Ammannito E, Ehlmann BL, Sizemore HG, Joy SP, Polanskey CA, Rayman MD, Raymond CA, Russell CT (2017) Extensive water ice within Ceres' aqueously altered regolith: evidence from nuclear spectroscopy. Science 355:55–59

Prialnik D (1992) Crystallization, sublimation, and gas release in the interior of a porous comet nucleus. Astrophys J 388:196–202

Prialnik D, Rosenberg ED (2009) Can ice survive in Main-Belt Comets? Long-term evolution models of comet 133P/Elst-Pizarro. MNRAS 399:L79–L83. https://doi.org/10.1111/j.1745-3933.2009.00727.x

Prialnik D, Benkhoff J, Podolak M (2004) Modeling the structure and activity of comet nuclei. In: Festou M, Keller H, Weaver H (eds) Comets II. University of Arizona Press, Tucson, pp 359–387

Protopapa S, Sunshine JM, Feaga LM, Kelley MSP, A'Hearn MF, Farnham TL, Groussin O, Besse S, Merlin F, Li JY (2014) Water ice and dust in the innermost coma of comet 103P/Hartley 2. Icarus 238:191–204

Rauer H, Helbert J, Arpigny C, Benkhoff J, Bockelée-Morvan D, Boehnhardt H, Colas F, Crovisier J, Hainaut O, Jorda L, Kueppers M, Manfroid J, Thomas N (2003) Long-term optical spectrophotometric monitoring of comet C/1995 O1 (Hale-Bopp). Astron Astrophys 397:1109–1122. https://doi.org/10.1051/0004-6361:20021550

Richter I, Koenders C, Auster HU, Frühauff D, Götz C, Heinisch P, Perschke C, Motschmann U, Stoll B, Altwegg K, Burch J, Carr C, Cupido E, Eriksson A, Henri P, Goldstein R, Lebreton JP, Mokashi P, Nemeth Z, Nilsson H, Rubin M, Szegö K, Tsurutani BT, Vallat C, Volwerk M, Glassmeier KH (2015)

Observation of a new type of low-frequency waves at comet 67P/Churyumov-Gerasimenko. Annales Geophysicae 33(8):1031–1036. https://doi.org/10.5194/angeo-33-1031-2015
Rivkin AS, Emery JP (2010) Detection of ice and organics on an asteroidal surface. Nature 464:1322–1323. https://doi.org/10.1038/nature09028
Rivkin AS, Brown RH, Trilling DE, Bell JF, Plassmann JH (2002) Near-infrared spectrophotometry of Phobos and Deimos. Icarus 156:64–75. https://doi.org/10.1006/icar.2001.6767
Rivkin AS, Howell ES, Vilas F, Lebofsky LA (2002) Hydrated minerals on asteroids: the astronomical record. In: Michel P, Demeo F, Bottke W (eds) Asteroids III. University of Arizona Press, Tucson, pp 235–253
Rivkin AS, Campins H, Emery JP, Howell ES, Licandro J, Takir D, Vilas F (2015) Astronomical observations of volatiles on asteroids. 65–87. https://doi.org/10.2458/azu_uapress_9780816532131-ch004
Rivkin AS, Howell ES, Emery JP, Sunshine J (2017) Evidence for OH or H_2O on the surface of 433 Eros and 1036 Ganymed. Icarus. https://doi.org/10.1016/j.icarus.2017.04.006
Robert F (2006) Solar system deuterium/hydrogen ratio. In: Lauretta DS, McSween HY (eds) Meteorites and the Early Solar System II. University of Arizona Press, Tucson, pp 341–351
Robert F, Gautier D, Dubrulle B (2000) The solar system D/H ratio: observations and theories. Space Sci Rev 92:201–224. https://doi.org/10.1023/A:1005291127595
Rousselot P, Jehin E, Manfroid J, Mousis O, Dumas C, Carry B, Marboeuf U, Zucconi JM (2011) A search for water vaporization on Ceres. Astron J 142:125. https://doi.org/10.1088/0004-6256/142/4/125
Rubin M, Altwegg K, Balsiger H, Bar-Nun A, Berthelier JJ, Bieler A, Bochsler P, Briois C, Calmonte U, Combi M, De Keyser J, Dhooghe F, Eberhardt P, Fiethe B, Fuselier SA, Gasc S, Gombosi TI, Hansen KC, Hässig M, Jäckel A, Kopp E, Korth A, Le Roy L, Mall U, Marty B, Mousis O, Owen T, Rème H, Sémon T, Tzou CY, Waite JH, Wurz P (2015) Molecular nitrogen in comet 67P/Churyumov-Gerasimenko indicates a low formation temperature. Science 348:232–235. https://doi.org/10.1126/science.aaa6100
Saal AE, Hauri EH, Van Orman JA, Rutherford MJ (2013) Hydrogen Isotopes in lunar volcanic glasses and melt inclusions reveal a carbonaceous chondrite heritage. Science 340:1317–1320. https://doi.org/10.1126/science.1235142
Safaeinili A, Cicchetti A, Nenna C, Calabrese D, Plettemeier D, Orosei R, Duxbury T, Plaut JJ, Picardi G, Flamini E (2009) Radar sounder observations of Phobos. In: European planetary science congress 2009, p 717
Sagan C, Toon OB, Gierasch PJ (1973) Climatic change on Mars. Science 181:1045–1049. https://doi.org/10.1126/science.181.4104.1045
Sawyer SR (1991) A high-resolution CCD spectroscopic survey of low-albedo main belt asteroids. PhD Thesis, The University of Texas, Austin
Schaller EL, Brown ME (2008) Detection of additional members of the 2003 EL61 collisional family via near-infrared spectroscopy. Astrophys J 684:L107–L109
Scheeres DJ (2015) Landslides and Mass shedding on spinning spheroidal asteroids. Icarus 247:1–17. https://doi.org/10.1016/j.icarus.2014.09.017. arXiv:1409.4015
Schleicher DG, A'Hearn MF (1988) The fluorescence of cometary OH. Astrophys J 331:1058. https://doi.org/10.1086/166622
Schleicher DG, Bair AN (2011) The composition of the interior of comet 73P/Schwassmann-Wachmann 3: results from narrowband photometry of multiple components. Astron J 141:177. https://doi.org/10.1088/0004-6256/141/6/177
Schleicher DG, Knight MM (2016) The extremely low activity comet 209P/LINEAR during its extraordinary close approach in 2014. Astron J 152:89. https://doi.org/10.3847/0004-6256/152/4/89. arXiv:1605.01705
Schorghofer N (2008) The lifetime of ice on main belt asteroids. Astrophys J 682:697–705. https://doi.org/10.1086/588633
Schorghofer N (2016) Predictions of depth-to-ice on asteroids based on an asynchronous model of temperature, impact stirring, and ice loss. Icarus 276:88–95. https://doi.org/10.1016/j.icarus.2016.04.037
Schwamb ME, Hsieh HH, Zhang ZW, Chen YT, Lintott C, Wang SY, Mishra I (2017) Assessing the Main-Belt Comet population with comet hunters. In: American astronomical society meeting abstracts, vol 229, p 112.04
Seu R, Phillips RJ, Alberti G, Biccari D, Bonaventura F, Bortone M, Calabrese D, Campbell BA, Cartacci M, Carter LM, Catallo C, Croce A, Croci R, Cutigni M, Di Placido A, Dinardo S, Federico C, Flamini E, Fois F, Frigeri A, Fuga O, Giacomoni E, Gim Y, Guelfi M, Holt JW, Kofman W, Leuschen CJ,

Marinangeli L, Marras P, Masdea A, Mattei S, Mecozzi R, Milkovich SM, Morlupi A, Mouginot J, Orosei R, Papa C, Paternò T, Persi del Marmo P, Pettinelli E, Pica G, Picardi G, Plaut JJ, Provenziani M, Putzig NE, Russo F, Safaeinili A, Salzillo G, Santovito MR, Smrekar SE, Tattarletti B, Vicari D (2007) Accumulation and erosion of Mars' south polar layered deposits. Science 317:1715. https://doi.org/10.1126/science.1144120

Shinnaka Y, Fougere N, Kawakita H, Kameda S, Combi MR, Ikezawa S, Seki A, Kuwabara M, Sato M, Taguchi M, Yoshikawa I (2017) Imaging observations of the hydrogen coma of comet 67P/Churyumovgerasimenko in 2015 September by the Procyon/Laica. Astron J 153(2):76. https://doi.org/10.3847/1538-3881/153/2/76

Sierks H, Barbieri C, Lamy PL, Rodrigo R, Koschny D, Rickman H, Keller HU, Agarwal J, A'Hearn MF, Angrilli F, Auger AT, Barucci MA, Bertaux JL, Bertini I, Besse S, Bodewits D, Capanna C, Cremonese G, Da Deppo V, Davidsson B, Debei S, De Cecco M, Ferri F, Fornasier S, Fulle M, Gaskell R, Giacomini L, Groussin O, Gutierrez-Marques P, Gutierrez PJ, Guttler C, Hoekzema N, Hviid SF, Ip WH, Jorda L, Knollenberg J, Kovacs G, Kramm JR, Kuhrt E, Kuppers M, La Forgia F, Lara LM, Lazzarin M, Leyrat C, Lopez Moreno JJ, Magrin S, Marchi S, Marzari F, Massironi M, Michalik H, Moissl R, Mottola S, Naletto G, Oklay N, Pajola M, Pertile M, Preusker F, Sabau L, Scholten F, Snodgrass C, Thomas N, Tubiana C, Vincent JB, Wenzel KP, Zaccariotto M, Patzold M (2015) On the nucleus structure and activity of comet 67P/Churyumov-Gerasimenko. Science 347(6220):aaa1044. https://doi.org/10.1126/science.aaa1044

Slade MA, Butler BJ, Muhleman DO (1992) Mercury radar imaging—evidence for polar ice. Science 258:635–640. https://doi.org/10.1126/science.258.5082.635

Snodgrass C, Carry B, Dumas C, Hainaut O (2010a) Characterisation of candidate members of (136108) Haumea's family. Astron Astrophys 511:A72. https://doi.org/10.1051/0004-6361/200913031. arXiv:0912.3171

Snodgrass C, Tubiana C, Vincent JB, Sierks H, Hviid S, Moissi R, Boehnhardt H, Barbieri C, Koschny D, Lamy P, Rickman H, Rodrigo R, Carry B, Lowry SC, Laird RJM, Weissman PR, Fitzsimmons A, Marchi S, Team OSIRIS (2010b) A collision in 2009 as the origin of the debris trail of asteroid P/2010A2. Nature 467:814–816. https://doi.org/10.1038/nature09453. arXiv:1010.2883

Snodgrass C, Jehin E, Manfroid J, Opitom C, Fitzsimmons A, Tozzi GP, Faggi S, Yang B, Knight MM, Conn BC, Lister T, Hainaut O, Bramich DM, Lowry SC, Rozek A, Tubiana C, Guilbert-Lepoutre A (2016) Distant activity of 67P/Churyumov-Gerasimenko in 2014: ground-based results during the Rosetta pre-landing phase. Astron Astrophys 588(67):A80. https://doi.org/10.1051/0004-6361/201527834. arXiv:1602.01493

Snodgrass C, A'Hearn MF, Aceituno F, Afanasiev V, Bagnulo S, Bauer J, Bergond G, Besse S, Biver N, Bodewits D, Boehnhardt H, Bonev BP, Borisov G, Carry B, Casanova V, Cochran A, Conn BC, Davidsson B, Davies JK, de León J, de Mooij E, de Val-Borro M, Delacruz M, DiSanti MA, Drew JE, Duffard R, Edberg NJT, Faggi S, Feaga L, Fitzsimmons A, Fujiwara H, Gibb EL, Gillon M, Green SF, Guijarro A, Guilbert-Lepoutre A, Gutiérrez PJ, Hadamcik E, Hainaut O, Haque S, Hedrosa R, Hines D, Hopp U, Hoyo F, Hutsemékers D, Hyland M, Ivanova O, Jehin E, Jones GH, Keane JV, Kelley MSP, Kiselev N, Kleyna J, Kluge M, Knight MM, Kokotanekova R, Koschny D, Kramer EA, López-Moreno JJ, Lacerda P, Lara LM, Lasue J, Lehto HJ, Levasseur-Regourd AC, Licandro J, Lin ZY, Lister T, Lowry SC, Mainzer A, Manfroid J, Marchant J, McKay AJ, McNeill A, Meech KJ, Micheli M, Mohammed I, Monguió M, Moreno F, Muñoz O, Mumma MJ, Nikolov P, Opitom C, Ortiz JL, Paganini L, Pajuelo M, Pozuelos FJ, Protopapa S, Pursimo T, Rajkumar B, Ramanjooloo Y, Ramos E, Ries C, Riffeser A, Rosenbush V, Rousselot P, Ryan EL, Santos-Sanz P, Schleicher DG, Schmidt M, Schulz R, Sen AK, Somero A, Sota A, Stinson A, Sunshine JM, Thompson A, Tozzi GP, Tubiana C, Villanueva GL, Wang X, Wooden DH, Yagi M, Yang B, Zaprudin B, Zegmott TJ (2017) The 67p/churyumov-gerasimenko observation campaign in support of the rosetta mission. Philos Trans R Soc Lond 375(2097):20160249. https://doi.org/10.1098/rsta.2016.0249

Snodgrass C, Jones G, Boehnhardt H, Gibbings A, Homeister M, et al (2017a) The Castalia mission to main belt comet 133P/Elst-Pizarro. Adv Space Res (**submitted**)

Snodgrass C, Yang B, Fitzsimmons A (2017b) X-shooter search for outgassing from main belt comet P/2012 T1 (Pan-STARRS). Astron Astrophys 605:A56. https://doi.org/10.1051/0004-6361/201731085

Sonnett S, Kleyna J, Jedicke R, Masiero J (2011) Limits on the size and orbit distribution of Main Belt Comets. Icarus 215:534–546. https://doi.org/10.1016/j.icarus.2011.08.001. arXiv:1108.3095

Spinrad H (1982) Observations of the red auroral oxygen lines in nine comets. PASP 94:1008–1016. https://doi.org/10.1086/131101

Spudis PD, Bussey DBJ, Baloga SM, Cahill JTS, Glaze LS, Patterson GW, Raney RK, Thompson TW, Thomson BJ, Ustinov EA (2013) Evidence for water ice on the moon: results for anomalous polar craters from the LRO Mini-RF imaging radar. J Geophys Res (Planets) 118:2016–2029. https://doi.org/10.1002/jgre.20156

Stevenson R, Kramer EA, Bauer JM, Masiero JR, Mainzer AK (2012) Characterization of active main belt object P/2012 F5 (Gibbs): a possible impacted asteroid. Astrophys J 759:142. https://doi.org/10.1088/0004-637X/759/2/142. arXiv:1209.5450

Sunshine JM, A'Hearn MF, Groussin O, Li JY, Belton MJS, Delamere WA, Kissel J, Klaasen KP, McFadden LA, Meech KJ, Melosh HJ, Schultz PH, Thomas PC, Veverka J, Yeomans DK, Busko IC, Desnoyer M, Farnham TL, Feaga LM, Hampton DL, Lindler DJ, Lisse CM, Wellnitz DD (2006) Exposed water ice deposits on the surface of Comet 9P/Tempel 1. Science 311:1453–1455

Sunshine JM, Farnham TL, Feaga LM, Groussin O, Merlin F, Milliken RE, A'Hearn MF (2009) Temporal and spatial variability of lunar hydration as observed by the deep impact spacecraft. Science 326:565

Swings P, Elvey CT, Babcock HW (1941) The spectrum of comet Cunningham, 1940C. Astrophys J 94:320. https://doi.org/10.1086/144336

Takir D, Emery JP (2012) Outer main belt asteroids: identification and distribution of four 3 μm spectral groups. Icarus 219:641–654. https://doi.org/10.1016/j.icarus.2012.02.022

Takir D, Reddy V, Sanchez JA, Shepard MK, Emery JP (2017) Detection of water and/or hydroxyl on asteroid (16) Psyche. Astron J 153:31

Taylor MGGT, Altobelli N, Buratti BJ, Choukroun M (2017) The rosetta mission orbiter science overview: the comet phase. Philos Trans R Soc Lond A 375(2097):20160262. https://doi.org/10.1098/rsta.2016.0262

Tegler SC, Bauer JM, Romanishin W, Peixinho N (2008) Colors of Centaurs. In: Barucci MA, Boehnhardt H, Cruikshank DP, Morbidelli A (eds) The solar system beyond Neptune. University of Arizona press, Tucson

Thomas N, Sierks H, Barbieri C, Lamy PL, Rodrigo R, Rickman H, Koschny D, Keller HU, Agarwal J, A'Hearn MF, Angrilli F, Auger AT, Barucci MA, Bertaux JL, Bertini I, Besse S, Bodewits D, Cremonese G, Da Deppo V, Davidsson B, De Cecco M, Debei S, El-Maarry MR, Ferri F, Fornasier S, Fulle M, Giacomini L, Groussin O, Gutierrez PJ, Güttler C, Hviid SF, Ip WH, Jorda L, Knollenberg J, Kramm JR, Kührt E, Küppers M, La Forgia F, Lara LM, Lazzarin M, Moreno JJL, Magrin S, Marchi S, Marzari F, Massironi M, Michalik H, Moissl R, Mottola S, Naletto G, Oklay N, Pajola M, Pommerol A, Preusker F, Sabau L, Scholten F, Snodgrass C, Tubiana C, Vincent JB, Wenzel KP (2015) The morphological diversity of comet 67P/Churyumov-Gerasimenko. Science 347:aaa0440. https://doi.org/10.1126/science.aaa0440

Thomas PC, Parker JW, McFadden LA, Russell CT, Stern SA, Sykes MV, Young EF (2005) Differentiation of the asteroid Ceres as revealed by its shape. Nature 437:224–226. https://doi.org/10.1038/nature03938

Thomas PC, Burns JA, Helfenstein P, Squyres S, Veverka J, Porco C, Turtle EP, McEwen A, Denk T, Giese B, Roatsch T, Johnson TV, Jacobson RA (2007) Shapes of the saturnian icy satellites and their significance. Icarus 190:573–584. https://doi.org/10.1016/j.icarus.2007.03.012

Toth I (2000) Impact-generated activity period of the asteroid 7968 Elst-Pizarro in 1996: identification of the asteroid 427 galene as the most probable parent body of the impactors. Astron Astrophys 360:375–380

Toth I (2006) Search for comet-like activity in asteroid 7968 Elst-Pizarro and limitation of its rotational pole orientation. Astron Astrophys 446:333–343. https://doi.org/10.1051/0004-6361:20053550

Trilling DE, Benz W, Guillot T, Lunine JI, Hubbard WB, Burrows A (1998) Orbital evolution and migration of giant planets: modeling extrasolar planets. Astrophys J 500:428–439. https://doi.org/10.1086/305711. arXiv:astro-ph/9801292

Trujillo CA, Brown ME, Barkume KM, Schaller EL, Rabinowitz DL (2007) The surface of 2003 el61 in the near-infrared. Astrophys J 655:1172–1178

Trujillo CA, Sheppard SS, Schaller EL (2011) A photometric system for detection of water and methane ices on Kuiper Belt objects. Astrophys J 730(2):105. https://doi.org/10.1088/0004-637X/730/2/105. arXiv:1102.1971

Tubiana C, Snodgrass C, Bertini I, Mottola S, Vincent JB, Lara L, Fornasier S, Knollenberg J, Thomas N, Fulle M, Agarwal J, Bodewits D, Ferri F, Güttler C, Gutierrez PJ, La Forgia F, Lowry S, Magrin S, Oklay N, Pajola M, Rodrigo R, Sierks H, A'Hearn MF, Angrilli F, Barbieri C, Barucci MA, Bertaux JL, Cremonese G, Da Deppo V, Davidsson B, De Cecco M, Debei S, Groussin O, Hviid SF, Ip W, Jorda L, Keller HU, Koschny D, Kramm R, Kührt E, Küppers M, Lazzarin M, Lamy PL, Lopez Moreno JJ, Marzari F, Michalik H, Naletto G, Rickman H, Sabau L, Wenzel KP (2015) 67P/Churyumov-Gerasimenko:

activity between March and June 2014 as observed from Rosetta/OSIRIS. Astron Astrophys 573:A62. https://doi.org/10.1051/0004-6361/201424735
Ulaby FT, Moore RK, Fung AK (1986) Microwave remote sensing: active and passive, vol 3. Addison-Wesley Publishing Company
Vasavada AR, Paige DA, Wood SE (1999) Near-surface temperatures on Mercury and the moon and the stability of polar ice deposits. Icarus 141:179–193. https://doi.org/10.1006/icar.1999.6175
Vilas F, Gaffey MJ (1989) Phyllosilicate absorption features in main-belt and outer-belt asteroid reflectance spectra. Science 246:790–792
Vilas F, Smith BA (1985) Reflectance spectrophotometry (about 0.5–1.0 micron) of outer-belt asteroids—implications for primitive, organic solar system material. Icarus 64:503–516
Vilas F, Hatch EC, Larson SM, Sawyer SR, Gaffey MJ (1993) Ferric iron in primitive asteroids—a 0.43-micron absorption feature. Icarus 102:225–231
Villanueva GL, Mumma MJ, Novak RE, Käufl HU, Hartogh P, Encrenaz T, Tokunaga A, Khayat A, Smith MD (2015) Strong water isotopic anomalies in the martian atmosphere: probing current and ancient reservoirs. Science 348:218–221. https://doi.org/10.1126/science.aaa3630
Walsh KJ, Morbidelli A, Raymond SN, O'Brien DP, Mandell AM (2011) A low mass for Mars from Jupiter's early gas-driven migration. Nature 475:206–209. https://doi.org/10.1038/nature10201. arXiv:1201.5177
Waszczak A, Ofek EO, Aharonson O, Kulkarni SR, Polishook D, Bauer JM, Levitan D, Sesar B, Laher R, Surace J, Team PTF (2013) Main-Belt Comets in the Palomar Transient Factory Survey. I. The search for extendedness. MNRAS 433:3115–3132. https://doi.org/10.1093/mnras/stt951. arXiv:1305.7176
Weaver HA, Feldman PD, McPhate JB, A'Hearn MF, Arpigny C, Smith TE (1994) Detection of CO Cameron band emission in comet P/Hartley 2 (1991 XV) with the hubble space telescope. Astrophys J 422:374–380. https://doi.org/10.1086/173732
Weaver HA, Stern SA, Parker JW (2003) Hubble space telescope STIS observations of comet 19P/Borrelly during the deep space 1 encounter. Astron J 126:444–451. https://doi.org/10.1086/375752
Wells M, Pel JW, Glasse A, Wright GS, Aitink-Kroes G, Azzollini R, Beard S, Brandl BR, Gallie A, Geers VC, Glauser AM, Hastings P, Henning T, Jager R, Justtanont K, Kruizinga B, Lahuis F, Lee D, Martinez-Delgado I, Martínez-Galarza JR, Meijers M, Morrison JE, Müller F, Nakos T, O'Sullivan B, Oudenhuysen A, Parr-Burman P, Pauwels E, Rohloff RR, Schmalzl E, Sykes J, Thelen MP, van Dishoeck EF, Vandenbussche B, Venema LB, Visser H, Waters LBFM, Wright D (2015) The mid-infrared instrument for the James Webb space telescope, VI: the medium resolution spectrometer. PASP 127:646. https://doi.org/10.1086/682281. arXiv:1508.03070
Winn JN, Fabrycky DC (2015) The occurrence and architecture of exoplanetary systems. Ann Rev Astron Astrophys 53:409–447. https://doi.org/10.1146/annurev-astro-082214-122246. arXiv:1410.4199
Wong MH, de Pater I, Showalter MR, Roe HG, Macintosh B, Verbanac G (2006) Ground-based near infrared spectroscopy of Jupiter's ring and moons. Icarus 185:403–415. https://doi.org/10.1016/j.icarus.2006.07.007
Xu S (1994) CCD photometry and spectroscopy of small main—asteroids. PhD Thesis, MIT
Yang B, Hsieh H (2011) Near-infrared observations of comet-like asteroid (596) Scheila. Astrophys J 737:L39. https://doi.org/10.1088/2041-8205/737/2/L39. arXiv:1107.3845
Yang B, Sarid G (2010) Comet P/2010 H2 (Vales). IAU Circ. 9139
Yang B, Jewitt D, Bus SJ (2009) Comet 17P/Holmes in outburst: the near infrared spectrum. Astron J 137:4538–4546
Yang B, Keane J, Meech K, Owen T, Wainscoat R (2014) Multi-wavelength observations of comet C/2011 L4 (Pan-STARRS). Astrophys J 784:L23. https://doi.org/10.1088/2041-8205/784/2/L23